CANADIAN THESES

THÈSES CANADIENNES

NOTICE

The quality of this microfiche is heavily dependent upon the quality of the original thesis submitted for microfilming. Every effort has been made to ensure the highest quality of reproduction possible.

If pages are missing, contact the university which granted the degree.

Some pages may have indistinct print especially if the original pages were typed with a poor typewriter ribbon or if the university sent us an inferior photocopy.

Previously copyrighted materials (journal articles, published tests, etc.) are not filmed.

Reproduction in full or in part of this film is governed by the Canadian Copyright Act, R.S.C. 1970, c. C-30.

AVIS

La qualité de cette microfiche dépend grandement de la qualité de la thèse soumise au microfilmage. Nous avons tout fait pour assurer une qualité supérieure de reproduction.

S'il manque des pages, veuillez communiquer avec l'université qui a conféré le grade.

La qualité d'impression de certaines pages peut laisser à désirer, surtout si les pages originales ont été dactylographiées à l'aide d'un ruban usé ou si l'université nous a fait parvenir une photocopie de qualité inférieure.

Les documents qui font déjà l'objet d'un droit d'auteur (articles de revue, examens publiés, etc.) ne sont pas microfilmés.

La reproduction, même partielle, de ce microfilm est soumise à la Loi canadienne sur le droit d'auteur, SRC 1970, c. C-30.

THIS DISSERTATION
HAS BEEN MICROFILMED
EXACTLY AS RECEIVED

LA THÈSE A ÉTÉ
MICROFILMÉE TELLE QUE
NOUS L'AVONS REÇUE

Canada

PHOTOCONDUCTIVITY AND PHOTOLUMINESCENCE IN $ZnIn_2S_4$

by

David A. Crandles

Thesis submitted to the
School of Graduate Studies
in partial fulfillment of the requirements
for the degree of
Master of Science in Physics

Department of Physics
Faculty of Science and Engineering
University of Ottawa
Ottawa, Canada

1985

ISBN 0-315-30982-2

ABSTRACT

The influence of two impurity levels - an acceptor and a donor - on the recombination processes of electrons excited from the acceptor to the conduction band in $ZnIn_2S_4$ has been studied.

The work can be divided into two sections: (i) sample characterization and (ii) laser excited photoconductivity and photoluminescence.

Four techniques were used to characterize the samples: (i) the measurement of the PC spectra; (b) the low intensity (approximately 1 W/m^2) lux-ampere characteristic (the intensity dependence of PC); (c) Fermi Level Analysis; and (d) the measurement of the absorpton coefficient in the extrinsic region. The presence of an extrinsic peak in the PC spectra allowed the binding energy of the acceptor to be estimated at approximately 0.2 eV. The Fermi Level Analysis allowed the donor density to be mapped from 0.1 to 0.6 eV below the CB. Two significant features appear in the donor density of states distribution: (i) the density of donors decreases exponentially by a factor of 10 per 0.1 eV on the range 0.1 to 0.3 eV below the CB - a feature which has been observed by other workers; (ii) the density of donors increases at around 0.5 eV below the CB. It was assumed that this increase indicates the presence of localized donor 0.6 eV below the CB. The total donor density was determined to be of the order of 10^{18} to 10^{19} cm^{-3}.

After the samples were characterized, photoconductivity and donor-acceptor photoluminescence were studied as a function of excitation intensity up to 500 MW/m^2 for photon energies ($h\nu$ =

2.50 eV) producing electron transitions from the acceptor involved in the donor-acceptor luminescence to the the conduction band. A significant change in the intensity dependence of both photoconductivity and photoluminescence occurs for photoexcitation densites of the order 10^{16} - 10^{17} cm^{-3}. This can be explained by the onset of saturation of the donor-acceptor recombination mechanism.

ACKNOWLEDGEMENTS

First of all, I would like to thank Dr. E. Fortin for suggesting the $ZnIn_2S_4$ project and for his advice throughout my stay at the University of Ottawa. I appreciate the productive and exciting research environment.

Special thanks are due to Alberto Anedda of the University of Cagliari in Italy for supplying the single crystals and for doing much of the groundbreaking work on $ZnIn_2S_4$.

Sincere thanks are due to Sylvain Charbonneau for many (fruitful) arguments, for help in performing the luminescence experiments and for carefully reading the text.

Thanks are also due to Art Buser for constructing the PC detection circuit, to Laura Stewart for help in doing the absorption experiments on the biochemistry department's spectrophotometer and to Gilles Fillion and Jacques Beauvais for deigning to help a computer illerate.

I am very grateful for the financial assistance received from the National Science and Engineering Research Council and the University of Ottawa.

TABLE OF CONTENTS

CONTINUED

TABLE OF CONTENTS CONT'D

LIST OF FIGURES

CONTINUED

LIST OF FIGURES CONT'D

LIST OF TABLES

CHAPTER 1 - INTRODUCTION

1.1 Origin of the Project

$ZnIn_2S_4$ is still a relatively unknown compound. This becomes obvious when one compares the number of papers published on $ZnIn_2S_4$ since it was first synthesized in 1950[1] - about forty - to the thousands published on GaAs in the same time period. The University of Ottawa is one the few places in the world where it has been studied; there is an active group in Greece, one in the U.S.S.R. and a couple in Italy but that is about all.

The reason for the perhaps small but continuing interest in $ZnIn_2S_4$ is the unique electrical and optical properties which it exhibits and which could possibly be utilized in new electronic devices. For example $ZnIn_2S_4$ exhibits photoconductivity[2-6], switching behaviour[7-15] and a bright red luminescence band[3,16-18].

These interesting optoelectronic properties have all been linked to impurity levels but a lot of work remains to be done in elucidating the mechanisms involved. What has been established is that certain types of localized levels appear to be a family characteristic of the AB_2X_4 (A = Zn,Cd; B = In,Ga; X = S,Se,Te) semiconducting compounds. Whereas one is accustomed to the fact that substances with similar lattice structures have similar intrinsic properties, the AB_2X_4 compounds have different lattice structures but similar extrinsic properties! The localized levels mentioned above are not due to substitutional defects, but rather to "intrinsic disorder"[19]. In a recently published review

paper[20], it was shown that many AB_2X_4 ternary compounds contain an exponential distribution of donors (that is, the density of donors decreases exponentially from a maximum at the conduction band edge down to hundreds of meV below) and a shallow acceptor. The density of these two classes of levels is about the same and hence non-intentionally doped AB_2X_4 compounds are well compensated. It was also shown that radiative transitions take place between the exponential distribution of donors - or traps, referred to as 'T' levels - and the shallow acceptors - referred to as 'A' levels. Figure 1 presents a 'band' diagram -- or rather a schematic summary of the defect levels and transitions which are common to the AB_2X_4 compounds.

This work concerns one of these ternary materials ($ZnIn_2S_4$) and the 'three level' system composed of the conduction band (CB) and the "intrinsic disorder" related defects, (T) and (A). Several different types of measurements were employed to study the 'three level' system. To the author's knowledge, laser excited photoconductivity has been performed for the first time on $ZnIn_2S_4$ single crystals and laser excited photoluminescence measurements have been done at higher intensity levels than previously published. Electrons were excited from the 'A' levels to the CB and the photoconductivity and photoluminescence (radiative electron transitions between the 'T' levels and the 'A' levels) were observed as a function of incident intensity.

Before progressing let us introduce some fundamental concepts concerning photoconductivity and donor-acceptor photoluminescence.

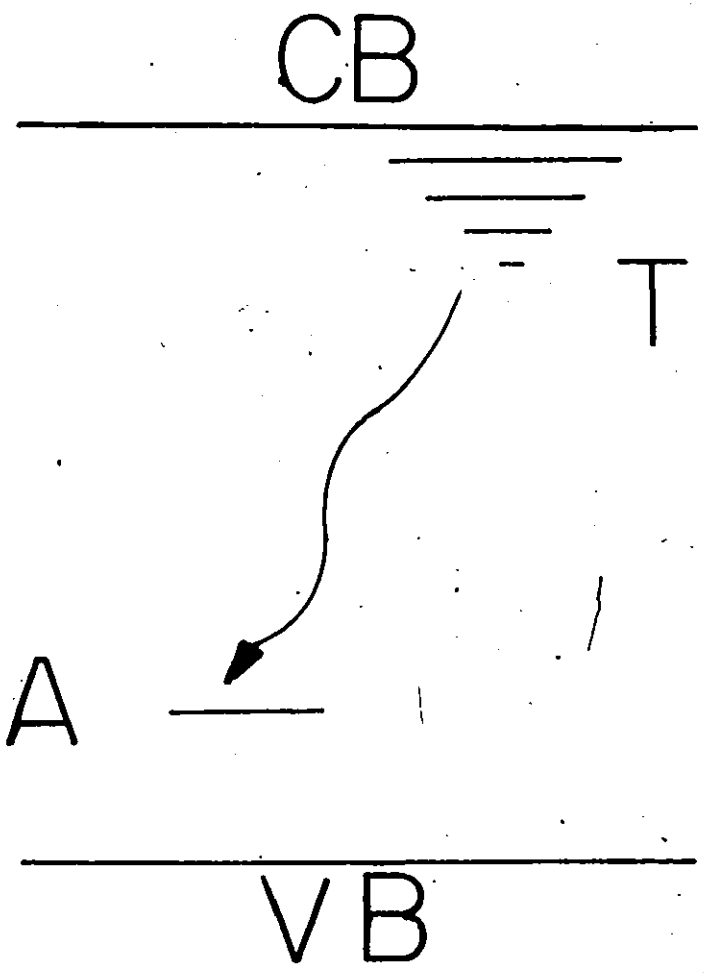

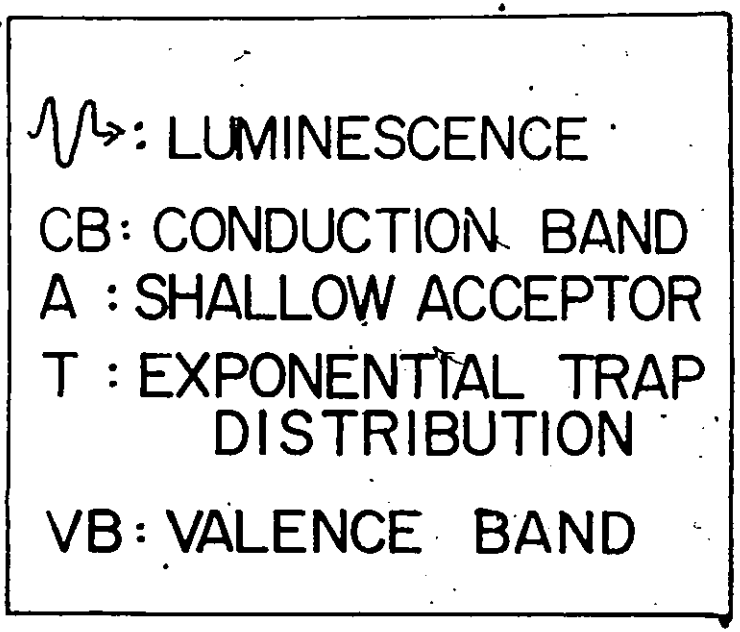

FIGURE 1 - IMPURITY LEVEL DISTRIBUTION COMMON TO THE AB_2X_4 SEMICONDUCTING COMPOUNDS

1.2 Fundamental Concepts

1.2(a) Photoconductivity

When light is shone on a sample and there are photons in the beam whose energy coincides with an energy difference between either the valence band and the conduction band (intrinsic PC) or a localized impurity level in the crystal and the conduction band (extrinsic PC), free carriers will be created. In general, in intrinsic PC both carrier types are created while in extrinsic PC free carriers of only one type are created. One can describe intrinsic PC with the following equation, where 'σ' represents conductivity, 'μ' the mobility, 'n' the density of free electrons and 'p' the density of free holes :

$$\Delta\sigma = \Delta n e\, \mu_n + n e\, \Delta\mu_n + \Delta p e\, \mu_p + p e\, \Delta\mu_p \qquad (1)$$

Holes will be ignored, since all previous research on $ZnIn_2S_4$ indicates n-type photoconductivity[5,7,17] for non-intentionally doped samples. It will also be assumed that the mobility is not affected by changes in the population of the localized levels. This is equivalent to saying that charged impurity scattering is not the dominant scattering mechanism which is a reasonable enough hypothesis in the temperature range (82K - 350K). All the measurements to be reported below were performed on this temperature range.

Hence the above equation can be simplified to:

$$\Delta\sigma = \Delta n e \mu_n \qquad (2)$$

The photoexcited electrons will not remain in the CB forever: they will try to relax back to the lowest energy state via radiative or non-radiative recombination. The study of the processes (band to band recombination, recombination through charged impurities, Auger recombination etc.) and the rate at which electrons recombine is called PC kinetics. Each recombination process is characterized by a lifetime which is the inverse of the probability of recombination via this process. If the free electrons have a number of recombination channels, the free electron lifetime will be an average of the lifetimes characterizing each recombination process. Since the various recombination processes are parallel channels, the effective free electron lifetime (τ_{eff}) is given by:

$$\tau_{eff}^{-1} = \sum_i \tau_i^{-1} \qquad (3)$$

In general, the steady state density of photocreated electrons (n), is equal to the product of the excitation rate per unit volume (f) and the effective free electron lifetime. That is,

$$n = f \tau_{eff} \qquad (4)$$

One final kinetic phenomenon should be discussed: the effect of trapping. In general, one can divide defect levels into two classes, recombination centres and traps. A defect will be a recombination centre for electrons if there is a greater probability for the electron to make a transition from the level to the valence band than to be thermally excited to the conduction band. It will be a trap if the probability for thermal excitation to the conduction band is greater[21]. The most important trapping effect is the production of a difference between the response time and the free carrier lifetime. The response time is the time required for the photocurrent to decay to 1/e of its steady state value following removal of continuous wave excitation. If there are no traps then the response time equals the free carrier lifetime; however, if there are traps then the response time is longer than the free carrier lifetime. These ideas will be developed further in section 1.2(b) below and in chapter 2 of the thesis.

1.2(b) Demarcation and Quasi-Fermi Levels

One could summarize the final two paragraphs of section 1.2(a) ~~with~~ the following quote from Albert Rose's Concepts in Photoconductivity and Allied Problems (p.13):

> (effective) lifetimes are controlled by recombination centers and response times by the combined effects of recombination centers and traps; that the distinction between traps and recombination centers depends in large part on the statistics of recombination and may shift with the temperature and level of excitation

Section 1.2(b) is included to explain Rose's quantitative criterion for determining whether an impurity is a trap or a recombination center -- the demarcation level - and to discuss how states are occupied in the forbidden gap under steady state excitation.

Actually there is not a single demarcation level. If one has two different types of impurity centers (for example centers which have different free electron capture cross sections) then each center will have its own demarcation level[21]. The electron demarcation level (D_n) for the i^{th} center is defined as follows:

$$\nu_n^* \exp\left[\frac{-|D_n, E_c|}{T}\right] = \tau_i^{-1} \qquad (5)$$

Equation 5 expresses equality between the probability of thermal excitation and the probability of recombination. ν_n^* is the product of the highest lattice frequency and a factor less than or equal to one which expresses the probability that an electron thermally excited to the conduction band will actually stay there. After some argument Rose showed that the above equation can be written as follows:

$$|D_n, E_c| = |E_{fn}, E_c| + kT \ln (n_{ri}/p_{ri}) \qquad (6)$$

In equation 6 'E_{fn}' is the quasi-fermi level for electrons, 'E_c' is the conduction band energy, 'n_{ri}' is the number of 'i' type states which are occupied by electrons and 'p_{ri}' is the number of 'i' type states that are occupied by holes. The notation $|E_1, E_2|$ means the absolute value of the difference between the values E_1 and E_2.

The quasi-fermi level is a concept which is an aid in visualizing the relative population of various states. With no photoexcitation, the occupation probability of the states is given by the fermi function centered on the thermal equilibrium fermi level (E_f) which is a chemical potential. However, photoexcitation disturbs the thermal equilibrium population of the states. A new steady state free electron density is established where the occupation probability is given by the fermi function centered on the "quasi-fermi level", E_{fn}. The quasi- fermi level for electrons is defined as follows (where N_c is the effective density of states in the CB).

$$E_{fn} = kT \ln (N_c/n) \qquad (7)$$

Note that there is a single quasi-fermi level for all states in comparison to the fact that each type of state has its own demarcation level. Demarcation levels and quasi fermi levels for holes (D_p and E_{fp} respectively) can be defined analogously by substituting 'E_v' for 'E_c' ,N_v for N_c and 'p' for 'n'. These ideas are summarized in figure 2 below.

Now one can address the question - how are the states occupied? States above the electron demarcation level - D_n - are in thermal equilibrium with the conduction band and the probability of occupation by electrons is given by the fermi function centered on E_{fn}. The occupancy of states between D_n and D_p is <u>independent of energy</u>; the occupation probability is determined by the cross section for capture: states which have a

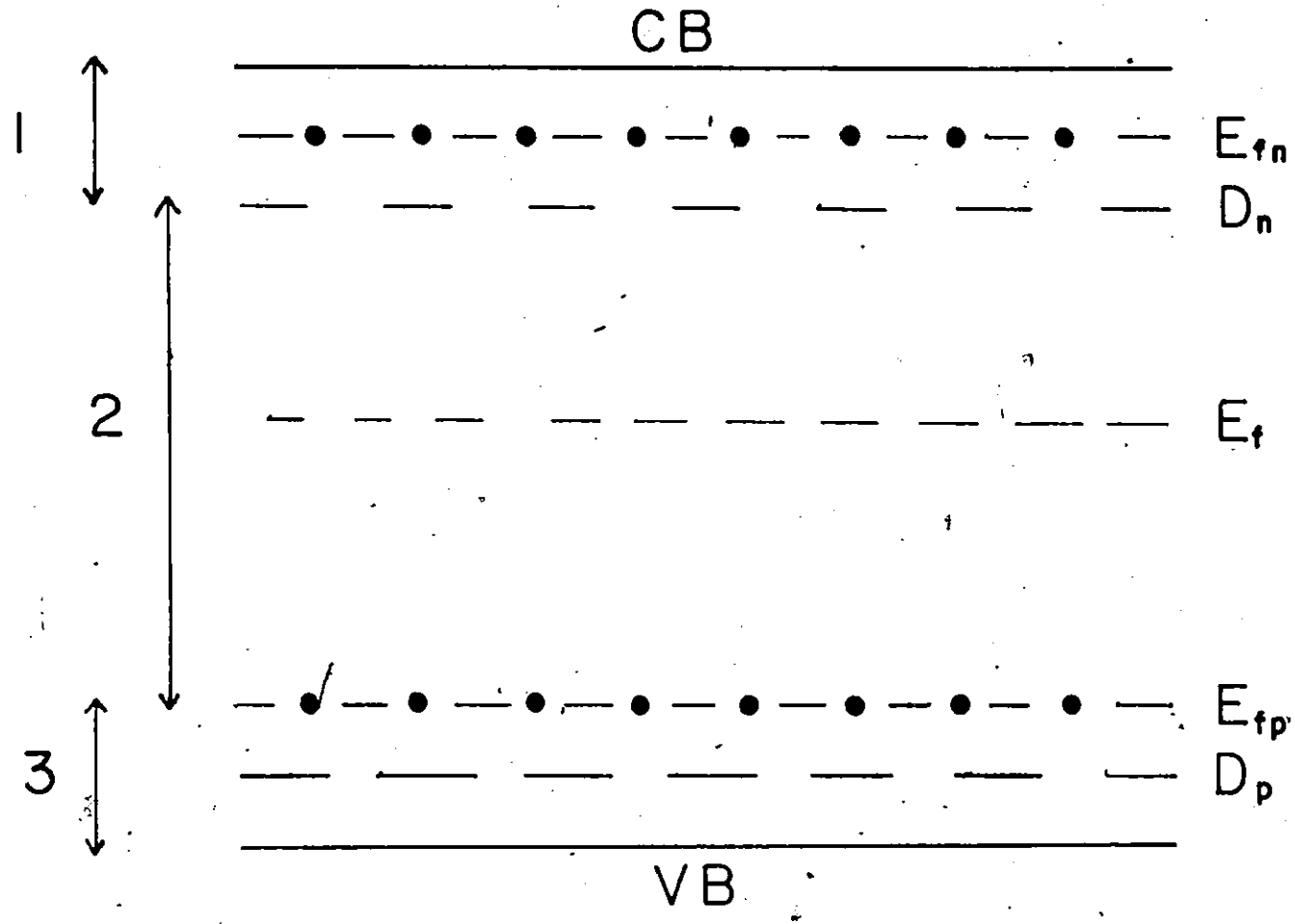

FIGURE 2 - DEMARCATION AND QUASI-FERMI LEVELS

E_{fn} (E_{fp}) - electron (hole) quasi-fermi level

D_n (D_p) - electron (hole) demarcation level

E_f - thermal equilibrium fermi level

large probability for free electron capture will tend to be occupied by electrons and states which have a large free hole capture cross section will tend to be occupied by holes. The probability of occupation by holes of states between D_p and E_v is given by the fermi function centred on the quasi-fermi level for holes (E_{fp}).

We now turn to the other important phenomena to be discussed in the thesis: donor- acceptor luminescence.

1.2(c) Donor-Acceptor Luminescence

Donor-acceptor luminescence is a process whereby excess injected electron-hole pairs can be annihilated. If there is band to band excitation the holes and electrons must first be captured by the acceptor and donor states, respectively (thereby neutralizing them). The second step is the electron transition from the donor to the acceptor accompanied by the emission of a photon. In the measurements to be reported below, electrons are excited directly from the acceptor (the 'A' level) to the CB and so only the electron needs to be captured. The transition photon energy is given by the following equation[22]:

$$h\nu = E_g - E_a - E_d + e^2/\varepsilon r \qquad (8)$$

In the above equation 'ε' is the static dielectric constant, 'r' the spatial separation of the donor and acceptor and E_g, E_a, E_d are the band gap, acceptor binding energy and donor binding energy respectively.

There are a number of experimental tags which indicate the presence of donor-acceptor (d-a) recombination such as the shift of the peak of the luminescence emission spectrum with excitation density, and the shift of the spectrum in time after cessation of excitation. Both these features have been observed in $ZnIn_2S_4$[18]. In $CdIn_2S_4$ a shift of the emission spectrum has been observed in time resolved photoluminescence work[23]. The cause of the spectral shifts has to do with the fact that the transition probability is a function of pair separation[24]. Pairs which are farther apart and which yield lower energy photons are less likely to recombine. As the intensity of excitation increases the more distant pairs are more easily saturated and hence spectrum peak shifts to higher energy.

Another hallmark of donor-acceptor luminescence is that a spectrum of discrete lines is formed. This is easily predicted by the above equation - if the defects are substitutional then 'r' can only take on the discrete values permitted by the lattice. Such line spectra have indeed been seen, but more often in indirect band gap compounds such as GaP[25] than direct gap compounds. A discrete line spectrum has not been seen in $ZnIn_2S_4$ which is a direct gap compound as will be discussed in section 1.3(a).

Now that we have more of an idea of the physical processes involved in the experimental techniques which will be used to study $ZnIn_2S_4$ let us become more familiar with the physical properties of the compound itself.

1.3 Review of the Literature

1.3(a) Intrinsic Properties

$ZnIn_2S_4$ is a yellow-orange coloured layered crystal which cleaves easily. It can form numerous polytypes of which this thesis concerns only the so-called type (III) polytype[12]. Each layer is composed of seven sheets of atoms in the sequence S-In-S-In-S-Zn-S with weak suplhur-sulphur bonds between the layers[26].

$ZnIn_2S_4$ is a direct gap material and different workers have employed many techniques to measure the band gap. The following table I summarizes these measurements. In the table 'α' represents the absorption coefficent. If 'I_o' is the intensity incident on the face of a crystal of thickness 't' and surface reflectivity 'R' and if $R^2\exp(-2\alpha t) << 1$ then the transmitted intensity will be[27]:

$$I_t = I_o (1 - R)^2 \exp(-\alpha t) \qquad (9)$$

UPS is an acronym for ultraviolet photemission spectroscopy.

1.3(b) Transport Properties

Because non-intentionally doped $ZnIn_2S_4$ is such a high resistivity compound - between 10^6 and 10^{14} ohm-cm parallel to the layers[12,33,34] - the measurement of transport properties is extremely difficult. In fact the only detailed measurements of the transport properties of $ZnIn_2S_4$ published so far were performed on poorly compensated low resistivity samples[35].

TABLE I - BAND GAP OF $ZnIn_2S_4$

Reference	E_g(300K)	E_g(77K)	Technique
6	2.50 eV	-	α^2 vs. $h\upsilon$
28	2.86 eV	3.0 eV	a^2 vs. $h\upsilon$
29	2.82 eV		UPS
30	-	2.96 eV	Kramers-Kroenig analysis of reflectivity
31	2.62 eV	2.72 eV	empirical fit of α vs.temperature
32	2.90±.03 eV	-	ellipsometry

The electron mobility parallel to the layers has been measured to be between 10 and 100 $cm^2v^{-1}sec^{-1}$ 34-36.

Because this work is concerned with the three state system composed of the conduction band, the exponential distribuion of donors and the shallow acceptors, a review of previous work on localized levels seems appropriate. The data will be presented in four tables with a short discussion of each.

1.3(c) Exponential Trap Distribution

The exponential trap distribution is characterized by two parameters: the distribution "slope" and the trap density per unit energy at the conduction band edge (N_o). The "slope" is a measure of how quickly the trap density decreases with energy below the conduction band. It is expressed in "m" meV/decade meaning that in "m" meV the trap density per unit energy decreases by a decade. This means that the trap density per unit energy at an energy "E" below the conduction band - $n_t(E)$ - is given by:

$$n_t(E) = N_o \, 10^{-(E/m)} \qquad (10)$$

or where 'β' equals $\ln 10/m$:

$$n_t(E) = N_o \exp(-\beta E) \qquad (11)$$

In work on the AB_2X_4 compounds, many authors refer to the total or integrated trap density. They calculate this quantity by integrating $n_t(E)$ - equation 11 - with respect to energy from the

CB band edge (E=0) to infinity. The total trap density N_t is given by equation 12 where N_o is the density per unit energy at the CB band edge:

$$N_t = N_o/\beta \qquad (12)$$

Previous work on the exponential trap distribution (the T levels of figure 1)is summarized in table II:

The data this table was obtained using a variety of techniques including thermoluminescence[16,19], phosphorescence decay[16,19] pulsed photoconductivity decay and thermally stimulated current[5], space charge limited current[6,37], fermi level analysis and the lux ampere characteristic[6], and optical absorption[36]. There is also one other evaluation of the trap distribution which is not included in the table because an exponential distribution of traps was not found at all. To account for their measurements of current vs. temperature and space charge limited current, Aganostopolcus et al.[38] required a set of three discrete traps located at 69, 119 and 315 meV below the conduction band. The authors offered no explanation for the discrepancy between their work and other published work.

Returning to the table one might note that it is not surprising that there is a wide range of total trap densities measured: the trap distribution is associated with disorder and the degree of disorder is probably very sensitive to the actual crystal growth conditions.

TABLE II - TRAP PARAMETERS

Reference	Position below CB (meV)	Distribution "slope" (meV/decade)	Trap Density at CB band edge(N_o) ($cm^{-3}eV^{-1}$)	Integrated Trap Density (N_t) (cm^{-3})
5	100-400	68±4 74±4	- -	- -
6	0-350	85 90 110	5×10^{18} - -	2×10^{17} - -
16	-	70±6 86±8	- -	- -
18	0-1000	-	-	-
19	200-500	160±20 150±30	-	-
36	-	-	-	10^{20}
37	0-600	111±11	$8 \times 10^{10} < N_o < 2 \times 10^{14}$	$4 \times 10^{9} < N_t < 1 \times 10^{13}$

1.3(d) A Levels

It can be shown that the shallow acceptor (the A level of figure 1), the other localized level related to disorder, is the ground state of the luminescence transition: the sum of the energies required to thermally quench luminescence and the energy required to excite luminescence and photocoductivity is equal to the band gap as table III demonstrates. Table III presents measurements of the binding energy of the shallow acceptor. Three different methods of estimating the binding energy (E_a) are employed.

The first method is to determine the activation energy for thermal quenching of luminescence[4]. One plots the logarithm of the integrated intensity of the luminescence band (L) as a function of 1/T. Below a certain 1/T value log(L) is a linear function of 1/T with slope $E_a{}^1$. Equation 13 expresses the thermal quenching relation.

$$L \propto \exp(E_a{}^1/kT) \qquad (13)$$

To understand thermal quenching of luminescence note that at low temperatures the 'A' levels have a low probability of being occupied. As the temperature increases the thermal occupation probability for electrons in the 'A' levels increases making radiative transitions from the 'T' levels to the 'A' levels more difficult.

In the second and third methods for estimating E_a involve measureing the difference between E_g, the energy gap, and E_{ph} and E_{le} which are the peaks in the photoconductivity and

TABLE III
BINDING ENERGY OF THE SHALLOW ACCEPTOR

Reference	E_a^1	E_a^2	E_a^3
3	-	-	200 meV
4	85 meV	-	-
	-	-	160 meV
5	-	310 meV	-
17	300 meV	-	-
	=	-	210 meV
18	92 meV	-	-

Notes: (1)these are room temperature results
(2)E_a^1 is determined from equation 13
(3)E_a^2 is determined from equation 14
(4)E_a^3 is determined from equation 15

photoluminescence excitation spectra corresponding to transitions between the acceptor level and the conduction band, respectively. Equations 14 and 15 refer to these methods of determining E_a.

$$E_a^{\,2} = E_g - E_{ph} \qquad (14)$$

$$E_a^{\,3} = E_g - E_{\ell e} \qquad (15)$$

One further observation about the 'A' levels is that the peak in the PC spectrum corresponding to electron transitions from the 'A' levels to the CB shifts towards the UV with decreasing temperature[5].

1.3(e) Luminescence Band

It was not until quite recently (1983) that the luminescence band in $ZnIn_2S_4$ was identified with donor acceptor transitions. The last entry in the table IV is one indication that donor-acceptor (d-a) transitions are the source of luminescence: one of the hallmarks of a d-a band is the shift of the peak of the band with increasing excitation density[22]. This was discussed in section 1.2(c) above.

One should make note of a curious feature of the three level system in the ternary compounds: there is a discrepancy between the predicted donor-acceptor photon energy (E_1^{theo}) calculated using equation (5) and the measured peak of the luminescence band (E_1^{exp}). The initial state of the most probable donor acceptor transitions must lie close to the conduction band since the trap

TABLE IV
LUMINESCENCE BAND PARAMETERS

Reference	band peak (300K)	band peak (77K)	half width (300K)	half width (77K)
3	1.58 eV	1.73 eV	0.43 eV	0.33 eV
4	1.50 eV	1.70 eV	0.60 eV	0.44 eV
18	1.60 eV[a] 1.85 eV[b]	1.74 eV[a] 1.93 eV[b]	0.62 eV[a] 0.65 eV[b]	-

Note: (a) low excitation intensity 10^{17} photons $cm^{-2}sec^{-1}$
(b) high excitation intensity 10^{22} photons $cm^{-2}sec^{-1}$

TABLE V
THE PL ANOMALY

Compound	E_g	E_a	E_1^{exp}	E_1^{theo}
$CdIn_2Se_4$	1.61	0.14	1.20	1.48
$ZnIn_2Se_4$	1.93	0.14	1.29	1.80
$CdIn_2S_4$	2.45	0.28	1.61	2.18
$ZnIn_2S_4$	2.96	0.30	1.73	2.67

(1) Data refers to 77 K
(2) E_g, E_1^{exp}, E_a taken from reference R19
(3) All table entries are in eV.

density per unit energy is greatest there (see equation 10 or 11). This means that the effective sum of the donor and acceptor binding energies ($E_d + E_a$) is approximately equal to E_a. The discrepancy between the theoretical predictions of equation 5 (where a reasonable value for $e^2/\varepsilon r = 0.01$ eV[39] is used) and E_1^{exp} is listed for various AB_2X_4 compounds in table V.

Measurements of the actual trap density in the $ZnIn_2S_4$ samples studied to be reported in chapter 2 provide more information on the anomaly.

1.3(f) Non-Radiative Recombination

It should be mentioned that a non-radiative recombination process has been observed in many of the AB_2X_4 compounds[5,17,20]. In a non-radiative process an electron is captured by a centre with the emission of phonons rather than the emission of a photon. The non-radiative process common to the AB_2X_4 ternaries is associated with yet another centre (different from the 'A' and 'T' levels) in the forbidden gap. In $ZnIn_2S_4$ this centre has been seen by other workers in both photoconductivity and photoconductivity quenching spectra[5]. (A photoconductivity quenching experiment is one where the sample is excited with two beams of different wavelength - see reference 5). The structures which were associated with the non-radiative centre in the PC and PC quenching spectra of Serpi[5] were not observed in the samples studied.

Sections 1.3(a)-(f) have been included to give some numbers to figure 1. It has shown how the quantitative details of the three level system vary from sample to sample, emphasizing the need to characterize one's own samples in order to make an informed interpretation of the measurements. Two experimental tools will be used to study the three level system in $ZnIn_2S_4$: photoconductivity (PC) and photoluminescence (PL). As we conclude chapter 1 in the next section we will discuss what these techniques will allow us to learn about the the recombination kinetics of electrons in the A, T and CB levels.

1.4 Structure of the Thesis

We can divide the measurements to be reported below into two classes. Low intensity PC work will be used to characterize the samples. As discussed in section 1.2(a), free electrons will be created if the incident photons are of the correct energy to excite transitions between a localized level in the forbidden gap and the conduction band. Thus the measurements of the PC spectra are an ideal tool to see whether the shallow acceptor is present in the sample.

The fact that the presence of traps causes the PC response time to be different from the free carrier lifetime - see section 1.2(a) is the basis of 'Fermi Level Analysis', the technique which will be employed to measure the trap distribution.

Measurements of PC vs. Intensity at low intensity provide another means of characterizing the trap distribution. As will be seen in chapter 2, there must be at least two different types of

levels in the forbidden gap to account for the superlinear intensity dependence PC which is observed at low intensity for some temperatures.

After characterizing the samples with these tools, we will have a basis with which to interpret measurements of PC and PL as a function of intensity at very high excitation levels. The laser photons will be of the correct energy to induce electron transitions from the A levels to the conduction band. By studying the PC transients - the time variation of the PC pulse - we will be able to monitor the electrons in the conduction band. Supplementing these are measurements of PL vs. intensity, with which we will be able to monitor the radiative transition.

The thesis will be composed of three more chapters. Chapter two, entitled 'Sample Characterization', will present the theory, experimental techniques and a discussion of the results of the low intensity work. Chapter three, entitled 'Laser Excited Photoconductivity and Photoluminescence' will present the theory, experimental techniques and a discussion of the results of the high intensity laser work. The fourth and final chapter will consist of the conclusions drawn from the measurements and suggestions for future work on $ZnIn_2S_4$.

CHAPTER 2 - SAMPLE CHARACTERIZATION

2.1 Introductory Remarks

In this work, four samples were studied. In section 1.1 of the last chapter was mentioned the goal of the thesis: to study the extrinsic properties, particularly the effect of the 'A' and 'T' levels on recombination kinetics by subjecting $ZnIn_2S_4$ to very high excitation intensity. Since it is obvious that the defect density should vary from sample to sample, it would be helpful to have as good an idea as possible of what defects are present and what the densities are.

Three techniques were employed to characterize the samples: (i) measurement of the PC spectra; (ii) Fermi Level Analysis and (iii) the intensity dependence of PC. The PC spectra were measured to detect the presence of 'A' levels, since a peak corresponding to electron transitions between the 'A' levels and the conduction band has been observed by other workers[5]. Fermi Level Analysis, or rather one version of it, was used to measure the trap density as a function of energy below the conduction band. The Fermi Level Analysis suggested the presence of a discrete donor 600 meV below the CB as well as the exponential trap distribution measured by other workers. The intensity dependence of PC allowed us to identify two types of levels in the forbidden gap and supported the idea that the '600 meV' donor exists. Since the traps play an important role in photoconductivity kinetics and because the radiative donor-acceptor transition takes place between the traps and a shallow acceptor level[19] quantitative knowledge of the trap distribution

will be an aid to the interpretation of the high intensity photoconductivity and photoluminescence measurements.

2.2 Theory Required for Data Analysis

2.2(a) PC Spectra

Many factors combine to determine the shape of a PC spectrum; the spectrum of PC response does not necessarily follow the same variation with wavelength as does the absorption coefficient (defined in section 1.3(a)). This is because PC is proportional to the product of the creation rate and the effective free electron lifetime (recall equation 10). For example, discrepancies between the PC spectrum and the absorption coefficient spectrum arise from the DeVore effect.

DeVore[40] modeled the shape of the "intrinsic" PC spectrum for very pure semiconductors with constant bulk free electron lifetimes. In the long wavelength region of the typical "intrinsic" PC spectrum the PC equals 0. Moving towards shorter wavelengths the PC begins to increase with the onset of intrinsic excitation and reaches a maximum value. With still shorter wavelengths it decreases and finally reaches an asymptotic value which is different from zero. Thus, there is a peak in the PC spectrum which does not exist in the spectrum of the absorption coefficient. DeVore showed that the peak in the high absorption region occured only when surface recombination was prominent. He also showed that the actual position and shape of the peak depended on the ratio of the surface to volume recombination rate, the carrier diffusion length and the

thickness of the sample. One of the main results of the DeVore theory is that for constant surface to volume recombination ratio, the 'peak' in the high absorption region becomes broader for thinner samples.

When impurities are present the PC spectrum often shows peaks corresponding to electron transitions between the impurity level and the conduction band. Discerning whether the peak in the PC spectrum corresponds to an impurity or to the DeVore effect mentioned above is usually simple when the band gap is known.

2.2(b) Intensity Dependence of Photoconductivity (low intensity)

The intensity dependence of photoconductivity is another tool for probing the distribution of impurity states in the forbidden gap. As a matter of fact, the intensity dependence of PC which was first explained over thirty years ago by Rose[41], is still being used today to probe the density of states in the forbidden gap of amorphous silicon[42].

To begin to understand the intensity dependence of PC recall equation 4. Let us assume as we did in equation 2 that the photoconductivity is due only to the change in free electron density. In equation 4, 'f' and 'τ_{eff}' are the creation rate and the effective free electron lifetime respectively. A linear dependence of photosignal occurs when 'τ_{eff}' is independent of excitation intensity. However, when 'τ_{eff}' is intensity dependent, both sublinear and superlinear dependence of photocurrent are conceivable. The effective lifetime is

determined using equation 3 where 'τ_i', the lifetime of the i^{th} recombination channel, is given by the following expression:

$$\tau_i^{-1} = p_{ri}\ \sigma_{ni}\ V \qquad (16)$$

In equation 16, 'p_{ri}' is the density of i^{th} centers which are occupied by holes, 'σ_{ni}' is the free electron capture cross section of these centers, and 'v' is the electron velocity[21]. One can see how changing the population of various impurity centers can change 'τ_{eff}'.

Models for sublinear and superlinear intensity dependent photoconductivity will be discussed in the remainder of section 2.2(b).

2.2(b)-(i) Sublinearity: Model for PC α f^k; 1/2 < k < 1 (taken from Rose's Concepts in Photoconductivity and Allied Problems, pp.38-43)

For sublinearity to occur, 'τ_{eff}' must decrease with intensity. The distribution of impurity states assumed in this model is shown in figure 3. One assumes that the trapping centers are exponentially distributed as follows:

$$N_t(E) = A \exp\left(\frac{-|E_c, E|}{kT_1}\right) \qquad (17)$$

Secondly, one assumes that the 'r' (for recombination - see figure 3) states are fully occupied in the dark. A third assumption is that the total density of 'r' states (N_r) satisies the following relation:

$$N_r > \int_{E_f}^{E_c} N_t(E)\, dE \qquad (18)$$

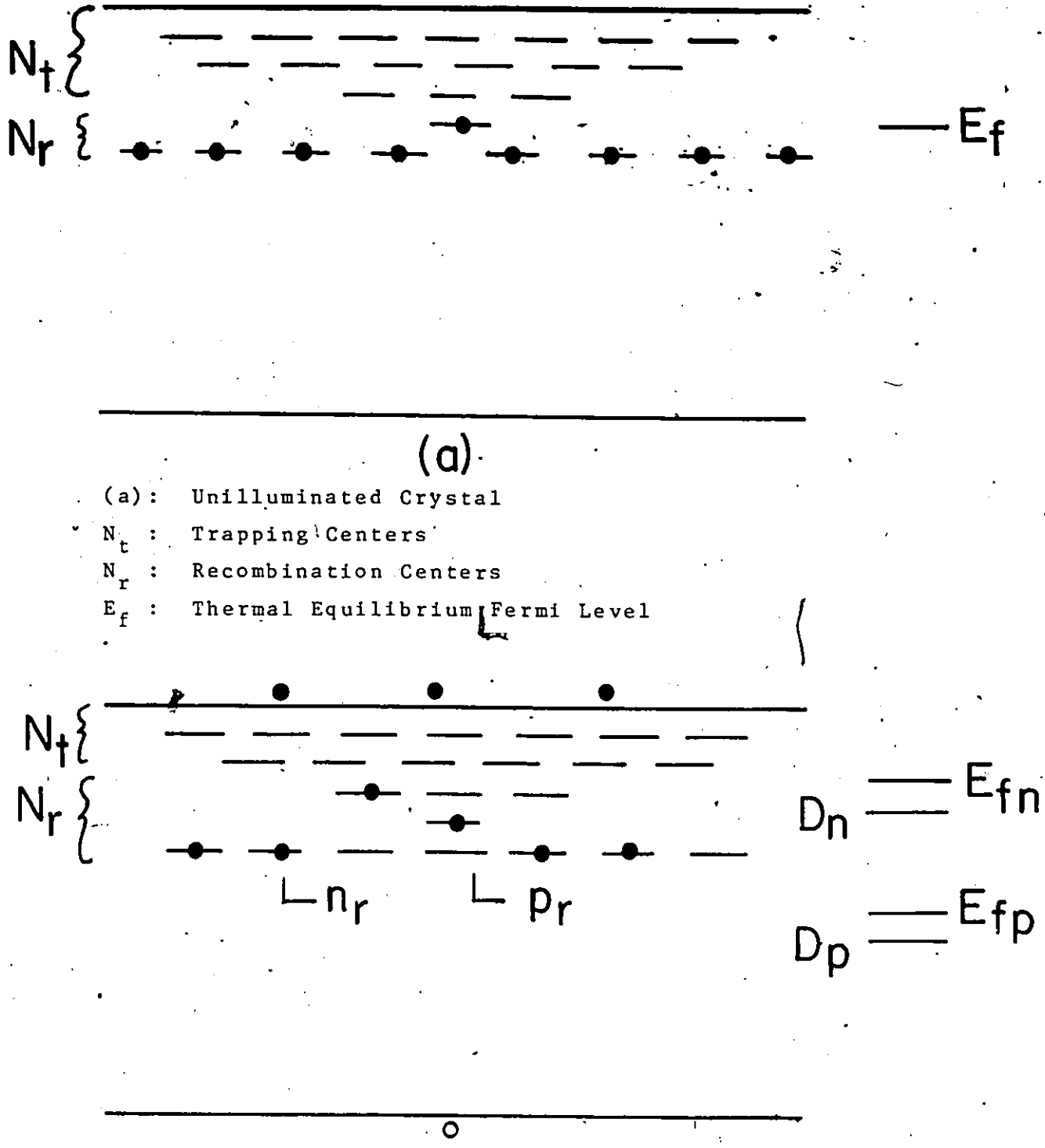

(a): Unilluminated Crystal

N_t : Trapping Centers

N_r : Recombination Centers

E_f : Thermal Equilibrium Fermi Level

(b) : Illuminated Crystal

D_n (D_p) : electron (hole) demarcation level

E_{fp} (E_{fp}) : electron (hole) quasi-fermi level

n_r (p_r) : occupied (unoccupied) recombination centers

FIGURE 3

IMPURITY LEVEL DISTRIBUTION PRODUCING SUBLINEARITY

It is also assumed that both the 'r' and the 't' (for trapping) states have the same free electron capture cross section. As the state or quasi-fermi level rises, more and more of the 't' states are converted into recombination states as indicated in figure 3(b). The number of 'p_r' states is given to a good approximation by the number of 't' states lying betwen the dark Fermi level and the steady state quasi-fermi level. That is,

$$P_r = A \int_{E_f}^{E_{fn}} \exp \frac{-|E_c, E|}{kT_1} dE \doteq kT_1 N_t(E_{fn}) \qquad (19)$$

Hence, one can rewrite equation 4 using equations 16,17 and 19:

$$n = f \tau_{eff} = f \frac{1}{kT_1 A \exp -(\frac{|E_c, E_{fn}|}{kT_1}) \sigma_n V} \qquad (20)$$

By definition - see equation 7 - the free electron density (n) satisfies the following relation:

$$n = N_c \exp (\frac{-|E_c, E_{fn}|}{kT}) \qquad (21)$$

Using equation 21 one can write:

$$\exp (\frac{-|E_c, E_{fn}|}{kT_1}) = (\frac{n}{N_c})^{T/T_1} \qquad (22)$$

Substituting equation 22 in equation 20 one obtains:

$$n = C(T) f^{\frac{T_1}{T + T_1}} \qquad (23)$$

Hence 'n' (thus the PC) is proportional to f^k where $1/2 < k < 1$. Battacharya and Narasimhan[42] have shown that a sublinear power law intensity dependence does not necessarily imply an

exponential distribution of states; any continuous distribution will do that produces an increasing number of recombination states with rising quasi-fermi level.

2.2(b)-(ii) Superlinearity: Model for PC α f^k; $k \geq 1$ (taken from Rose's Concepts in Photoconductivity and Allied Problems, ppl 48-51)

Let us restrict our discussion to n-type photoconductivity. For superlinearity of n-type PC to occur, the effective free electron lifetime must increase with intensity. It has been rigourously demonstrated that superlinearity cannot occur when only one type of impurity exists in the forbiden gap[43]. There must be at least two types of centres which have different free electron capture cross sections. A distribution of states which can give rise to superlinearity appears in figure 4.

One assumes that the one type of centers (called class II centers) has a smaller free electron capture cross section than the other type of center (called class I centers). Class I centers have equal free hole and free electron capture cross sections of about 10^{-15} cm^{-2} at room temperature. Class II centers are coulomb repulsive centers which have cross sections for free electrons of about 10^{-20} cm^{-2} and larger cross sections for free holes at room temperature[21]. As was discussed in section 1.2(b), under photoexcitation, only the states above the electron quasi-fermi level (E_{fn}) are in thermal equilibrium with the conduction band. To a first approximation, states between E_{fn}

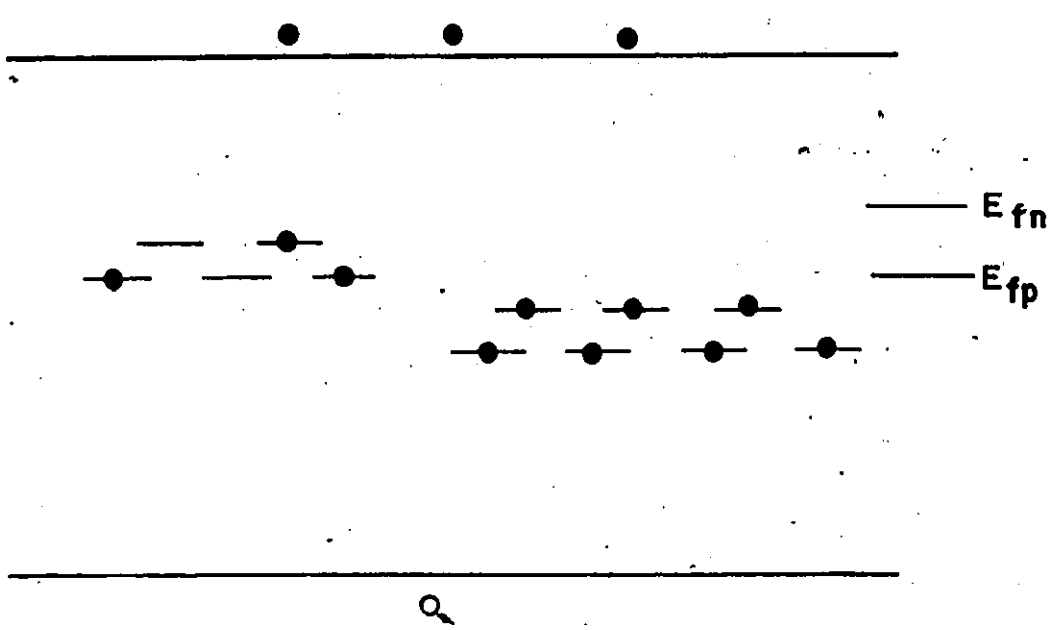

(a)

(a) low light level

E_{fn} (E_{fp}): electron (hole) quasi-fermi level

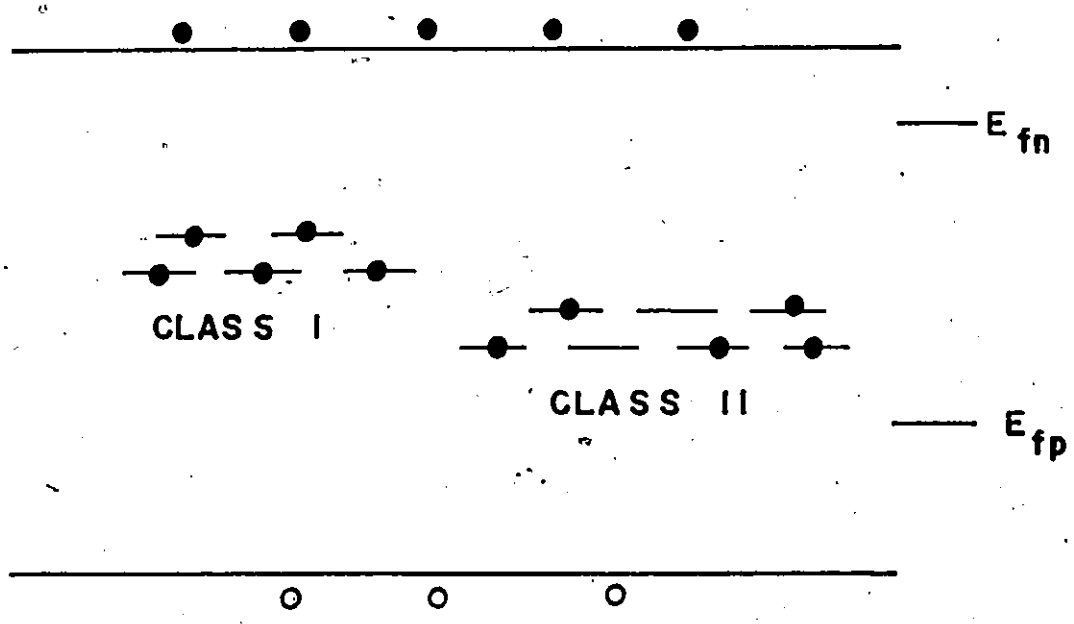

(b)

(b) : high light level

class I : centers with equal electron and hole capture cross sections

class II: centers with larger hole than electron capture cross sections

FIGURE 4

IMPURITY LEVEL DISTRIBUTION PRODUCING SUPERLINEARITY

and the hole quasi-fermi level are not distributed thermally. The occupation of these states is governed by the relative magnitudes of the capture cross-sections. This means that as the fermi level rises (which is equivalent to saying the intensity increases) the class I centers will tend to be filled while the class II centers will tend to be empty. Hence from equations 3 and 16, one can see the effective free electron lifetime increase.

2.2(c) Fermi Level Analysis

There are very many ways to measure the density of traps as a function of the energy below the conduction band[44]. One of the methods is the so-called "Fermi Level Analysis". Before any further remarks are made we state that we will ignore holes to make the discussion simpler and because all previous research on $ZnIn_2S_4$ indicates n-type photoconductivity in non-intentionally doped samples. At the root of this technique lies the understanding that there is a difference between the response time and the effective free carrier lifetime. If there are no traps then the response time equals the free carrier lifetime; however, if there are traps then they are different. Rose first introduced this distinction because of "the fact that the measured photocurrents are often as much as eight orders of magnitude smaller than one would compute from the known rate of excitation and the observed time constant (speed of response). It is clear that the speed of response is not a good measure of the lifetime of an electron in the free states."[41] In summary,

in samples where the hole conductivity can be ignored (as it can be for extrinsic excitation in $ZnIn_2S_4$) and where traps exist the magnitude of the steady state photocurrent is governed by the effective free carrier lifetime (τ_{eff}) but the photoconductivity kinetics are governed by the response time.

The response time (τ_r) and the effective free carrier lifetime (τ_{eff}) are related quantitatively as follows (where 'n_t' represents the density of electrons trapped within an energy 'kT' of the Fermi level and 'n' represents the density of electrons in the conduction band[44]:

$$\tau_r = \tau_{eff} (1 + n_t/n) \qquad (24)$$

The basic technique of a Fermi-Level analysis of the trap distribution is to measure the time it takes the photocurrent to decay to 1/e of its steady state value as a function of steady state photocurrent. In other words one measures 'τ_r' as a function of the quasi-fermi Level (E_{fn}), the steady state photocurrent being related to the E_{fn} through equation 7. Equation 24 is the key to understanding: if we know the position of the E_{fn} and the corresponding response time, one can determine the trap density per unit energy range at E_{fn}. By changing E_{fn} one can measure the trap density per unit energy range as a function of energy below the conduction band. There are two techniques for controlling the position of E_{fn} (or the steady state PC): increasing the temperature lowers E_{fn} while

increasing the incident intensity raises it[21].

The experiments are run as follows: One keeps the wavelength of the exciting beam constant for the whole experiment. Then for a known temperature (T) and incident intensity (I_o) one allows the photocurrent to reach its steady state value (PC). Then the light is removed and 'τ_r' is measured. 'τ_r' is the time required for the PC to reach 1/e times its steady state value. So, the experimental data will consist of quadruplets: (T, I_o, PC, τ_r). From these data quadruplets one has to determine the position of E_{fn} and the trap density per unit energy (n_t'). Note that (n_t) of equation 24 equals (kTn_t').

2.2(c)-(i) Determination of $n_t'(E_{fn})$

If we assume that $n_t >> n$ then equation 24 becomes:

$$\tau_r = n_t/n\, \tau_{eff} \qquad (25)$$

Using equation 4 and the definition $n_t = kTn_t'$, we can rewrite equation 25 as follows:

$$n_t'(E_{fn}) = \frac{f\,\tau_r}{kT} \qquad (26)$$

In equation 26, 'τ_r' and 'T' are experimentally determined quantities while the calculation of 'f', the creation rate of free carriers, is rather involved. To calculate 'f', we first note that the intensity (I_o) is proportional to the number of photons arriving per unit time per unit area and:

$$I_o = I_r + I_t + I_a \qquad (27)$$

In the above equation 'I_o' is the incident intensity, 'I_r', the reflected intensity; 'I_t', the transmitted intensity; 'I_a', is the energy absorbed per unit area per unit time. The transmitted intensity is given by equation 9. The reflected intensity is given by (assuming $R^2\exp(-2\alpha t) << 1$)[27]:

$$I_r = I_o R [1 - \exp(-2\alpha t)] \qquad (28)$$

To find the number of photons absorbed per unit volume (which is equal to 'f' if one assumes a quantum efficiency of unity) we just substitute equations 9 and 28 in equation 27 and divide by 't', the thickness of the crystal and '$h\nu$', the photon energy:

$$f = \frac{I_o}{(t)(h\nu)} [1 - (1-R^2) \exp(-\alpha t) - R(1 - \exp(-2\alpha t)] \qquad (29)$$

One should note that as the absorption is non-uniform, equation 29 gives the average free carrier creation rate per unit volume.

One can calculate 'R', for use in equation 29, if one knows 'N', the index of refraction. The following equation is good if $\alpha\lambda/4\pi << N$ ('λ' = excitation wavelength; 'α' = absorption coefficient):

$$R = \left(\frac{N - 1}{N + 1}\right)^2 \qquad (30)$$

'N' has the value 2.7 at 495 nm (which is the excitation wavelength as will be discussed below) independent of temperature[30] and hence R = 0.21.

We still do not have all the information one requires to calculate 'f' - equation 29. The absorption coefficient is itself temperature dependent. 'α (T)' was not measured but rather was calculated using data published by other workers. Figure 5

is a compilation of data from other published works for a wavelength of 495 nm, the wavelength of excitation for the measurements as will be discussed below. As one can see, in the temperature range 77-350K the majority of measurements follow an approximately linear relation between 'α' and 'T'. A least squares fit resulted in the following equation for (T):

$$\alpha = 0.34\ T + 16\ cm^{-1} \qquad (31)$$

In summary, to calculate the trap density per unit energy at E_{fn} (n_t') one uses equation 26 where 'f' is determined using equations 29 and 31.

2.2(c)-(ii) Determination of E_{fn}

To find the quasi-fermi Level which corresponds to the trap density calculated using the method of section 2.2(c)-(i), one uses equation 7. 'n' is calculated using the following formula where 'PC' is the experimentally determined steady state photocurrent; 'V' is the voltage between the electrodes; 'w','l' and 't' are sample dimensions (see figure 6); 'e' is the fundamental charge unit; and 'μ' is the electron mobility (which is a function of temperature):

$$n = \frac{PC\ l}{Vwte\mu} \qquad (32)$$

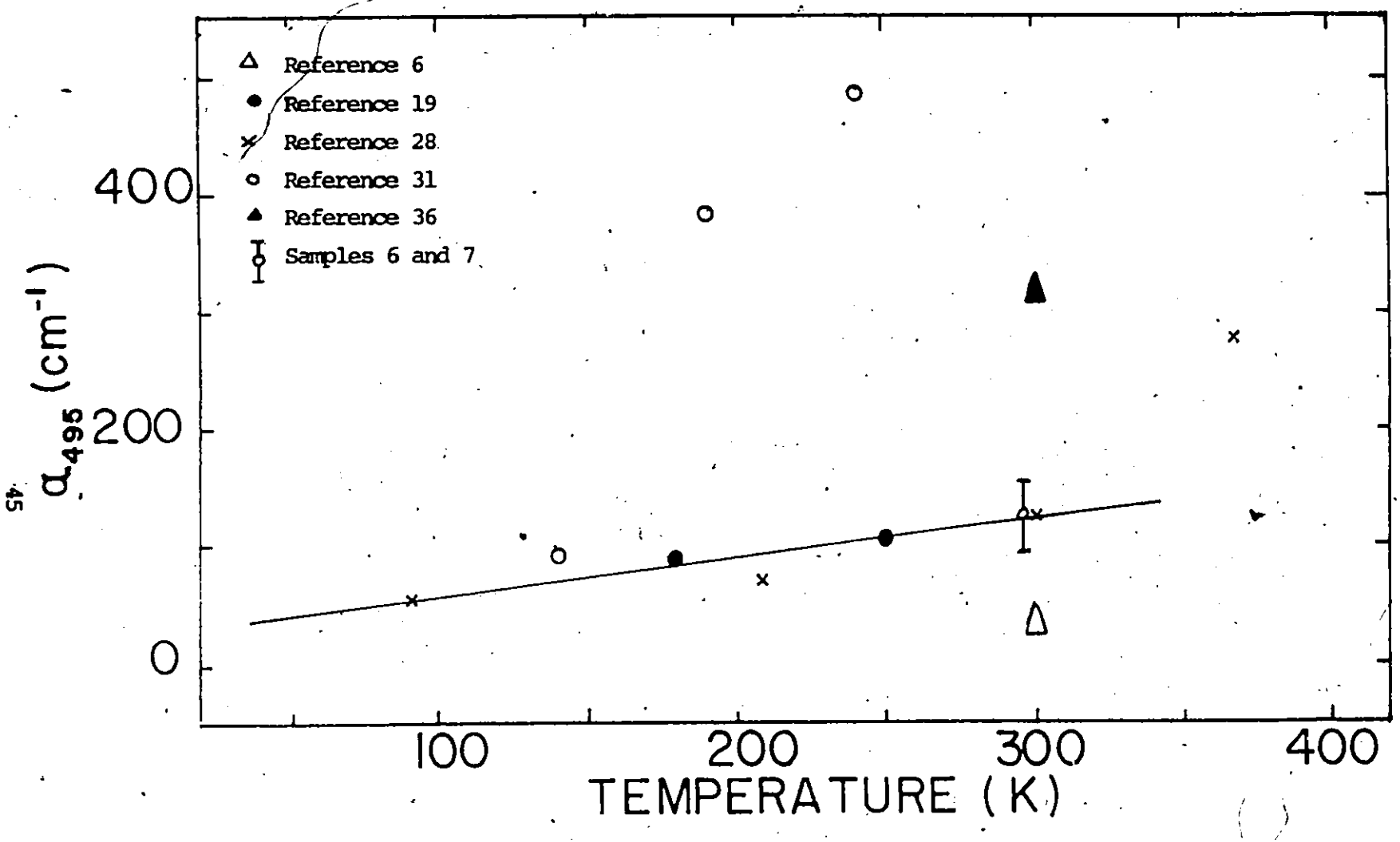

FIGURE 5

TEMPERATURE DEPENDENCE OF THE ABSORPTION COEFFICIENT OF $ZnIn_2S_4$ FOR 495 nm

When Bube[43] and others use the technique of Fermi Level analysis to determine the trap distribution in a compound they usually have the advantage of knowing the dominant scattering mechanism in the compound and hence being able to know the temperature dependence of the electron mobility. However $ZnIn_2S_4$, as has been previously discussed, is a very high resistivity compound making measurement of the transport properties difficult; hence we have assume a mobility model. The calculation will be performed assuming 'μ' equals 50 $cm^2/Vsec$ at 300 K (see section 1.3(b)) for two different mobility models (acoustic phonon scattering dominant and optical phonon scattering dominant). If acoustic phonon scattering is dominant then[45]:

$$\mu = 50\ (T/300k)^{-3/2} \qquad (33)$$

The second model for the temperature dependence of electron mobility is taken from Fivaz and Mooser's theory for transport in layered compounds[46]. They showed that in certain layered compounds, optical phonon scattering dominates and:

$$\mu = 50\ (T/300k)^{-2.5} \qquad (34)$$

$N_c(T)$ must also be known in order to calculate E_{fn} using equation 7. For $ZnIn_2S_4$, one assumes that $N_c = 10^{19}\ cm^{-3}$ at 300 K[6]. The usual temperature dependence of the effective density of states is assumed[47]. That is:

$$N_c = 10^{19}\ (T/300)^{-3/2} \qquad (35)$$

SAMPLE DIMENSIONS

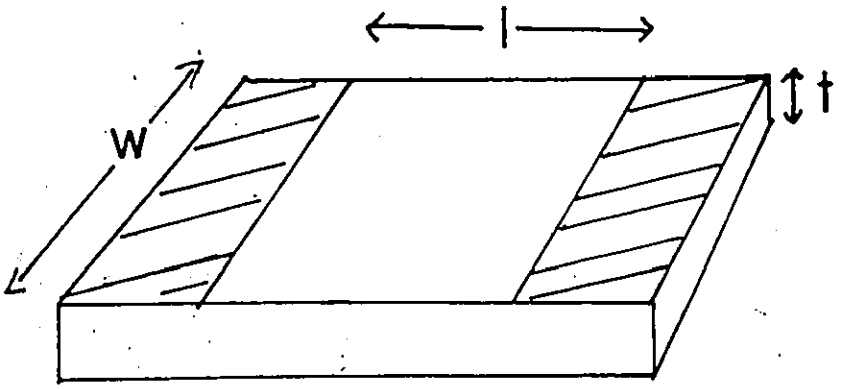

sample	1	5	6	7	ε
w (mm)	1.7	3.0	1.8	1.5	± 0.1
l (mm)	1.6	1.6	1.6	1.6	± 0.1
t (μ)	180	50	170	56	± 5

 In CONTACT

FIGURE 6

SAMPLE DIMENSIONS AND CONTACT GEOMETRY

In summary to calculate E_f corresponding to the $n_t'(E_f)$ found using the method of section 2.2(c)-(i), we use equation 7. 'n' is calculated using equations 32 and 33 or 34 and N_c is calculated using equation 35.

2.3 Experimental Details

2.3(a) Sample Preparation

$ZnIn_2S_4$ single crystals were obtained from the Solid State Physics group at the University of Cagliari, Italy where they were grown by the method of chemical vapour transport. $ZnIn_2S_4$, being a layered compound is fairly easy to cleave but is also quite soft. The following method was used to cleave the samples to achieve good surfaces on which to make electrical contacts: Put a crystal on a piece of scotch tape (the regular kind not magic tape) and then fold the scotch tape over such that both sides of the crystal are stuck to the tape. Carefully pulling the tape apart cleaves the crystal. To remove the tape dissolve the glue in n-Butyl Acetate. n-Butyl Acetate will partially dissolve the magic tape itself leaving a gue which is extremely difficult to remove. With regular scotch tape only the glue dissolves and the tape falls off. To dissolve residual traces of glue put the crystal in toluene for about ten minutes then wash in acetone and finally in methanol.

Two indium contacts (approximately 3000 angstroms thick) were then evaporated onto the same face of the crystal about 1.5 mm apart in the manner shown in figure 6 - see section 2.3(c)-

mm apart in the manner shown in figure 6 - see section 2.3(c)-(ii). The sample dimensions, measured with a micrometer, are also presented in figure 6. The single crystals were then placed on specially prepared sapphire plates and held there with Wakefield thermal compound, a good thermal conductor. The sapphire plates had two copper contacts evaporated onto them. The sample on top of the sapphire plate was then placed on the cold finger of an MMR technologies model R2101 refrigerator inside a model D2101 optical vacuum chamber (the model R2101 and the model D2101 together make up the optical minicryostat). Electrical contact was made from outside the cryostat to the inside by means of two pairs of wires. The first pair went from outside the cryostat to the copper contacts on the sapphire plate. The second set were very short and went from the copper contacts to the indium contacts on the sample. The wires were held to both the copper and indium contacts with silver paint. The silver paint contacts on the copper were then covered with GE brand 'glyptal cement'. The glue covered silver paint contacts are very durable. With this mounting procedure the sample could be cooled down to liquid nitrogen temperaure many more times than if wires were connected directly to the sample without the sapphire plate at all.

2.3(b) Minicryostat Operation

The model R2101 refrigerator operates using the Joule-Thompson throttling principle. With proper care, it can cool samples down to between 82K and 84K within 20 minutes. Temperatures were measured by means of an Omega model 199P1

platinum resistance thermometer. The transducer was a platelet which could also be mounted on the cold finger of the R2101 refrigerator.

Before the vacuum chamber (model D2101) is evacuated, the refrigerator should be purged with ultrapure dry N_2 gas (approximately 400 lbs/in^2) for a couple of minutes. The chamber is then evacuated to less then one millitorr and high pressure (1600-1800lbs/in^2) ultrapure N_2 allowed to flow through the refrigerator. The N_2 is not allowed to flow directly from the cylinder but is further purified via molecular sieves in the model F2101 filter. The powdered chemicals which form the molecular sieves should be changed every 3 or 4 cylinders of N_2. In the course of the experiments it was found that the model D2101 sprang a leak at the place where the high pressure N_2 line entered the vacuum chamber. This was successfully repaired using epoxy resin.

The lowest temperature obtained - approximately 83 K - could be maintained for hours. Unfortunately, there is no direct correlation between gas flow pressure and temperature. The device is constructed in an "all or nothing" fashion: with pressures above a certain level - about 1600 lbs/in^2 - the device tended towards 84 K. With pressures below this level, the device tended toward room temperature. However, by playing with the gas flow - alternately increasing and decreasing it - a short term steady state (a couple of minutes) could be maintained for many temperatures between room temperature and 84 K. One could obtain a target temperature to within ± 5 K.

Temperatures up to 20 K above room temperature could be obtained by using a blow dryer on the cryostat. One must be careful not to heat the glass refrigerator above 70 degrees celcius (353 K) for fear of damaging it.

2.3(c)Experimental Apparatus and Method

The basic experimental set-up for both the measurement of PC spectra and the Fermi Level Analysis is shown in figure 7. The excitation source was a Bausch and Lomb monochromator (BL) which produces an approximately 1 W/m^2 output intensity for a linewidth of about 6nm. The intensity of excitation was controlled by a set of Balzers neutral density filters (NF).

The electronics were very simple: The sample (S) was connected in series with a power supply (PS) and a Keithley 602 electrometer (K). An output proportional to the photocurrent measured by the Keithley was recorded by an XY recorder (XY).

The PC spectra were measured as a function of wavelength for constant temperature and intensity.

For the Fermi Level analysis, 495 nm was chosen for excitation because the absorption coefficient at this wavelength was large enough to ensure a photocurrent much greater than the dark current, yet small enough to enable approximately uniform free carrier creation throughout the whole volume of the crystal.

As discussed in section 2.2(c), Fermi Level Analysis requires measurement of the response time as a function of the Fermi Level. A Keithley model 602 electrometer, in the fast

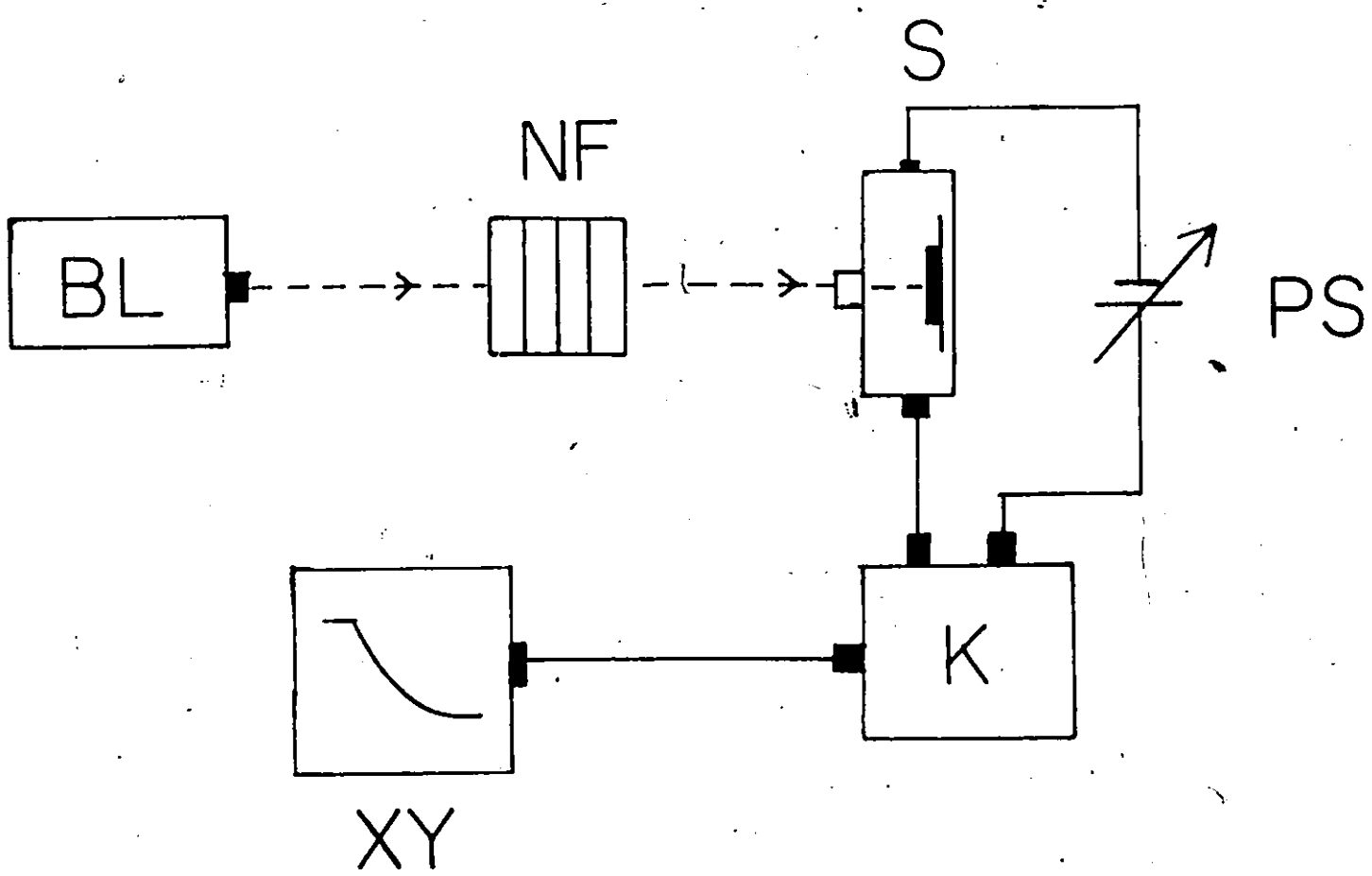

FIGURE 7
EXPERIMENTAL APPARATUS FOR MEASUREMENT OF
PC SPECTRA AND FERMI LEVEL ANALYSIS

BL: Bausch and Lomb Monochromator

NF: Neutral Density Filters

S : Sample Mounted in cryostat

PS: Power Supply

K: Keithley 602 Electrometer

XY : XY Recorder

mode was employed to measure the response times. Response times were measured using the XY recorder, the y axis corresponding to the magnitude of the photocurrent, the x axis corresponding to time. The response time of the coupled electrometer and chart recorder was measured to be no more than 75 ms (by shorting the leads of the power supply). This was adequate for measuring response times in $ZnIn_2S_4$ since they proved to be much greater than 75 ms - up to hundreds of thousands of milliseconds.

The experiment ran as follows: Response times were measured for several intensities (thus data for a study of the intensity dependence of PC was also collected) per temperature at approximately 20 K intervals between 83 K and 300 K.

2.3(d) Absorption Coefficient

For the Fermi Level Analysis, it was necessary to know the absorption coefficient. Measurements were made of 'α' as a function of wavelength at 300 K using the Phillps Pye Unicam SP8-500 spectrophotometer in the biochemistry department in the university of Ottawa. What the spectrophotometer does is to compare the amount of light transmitted through a sample on a holder (which were copper plates with small holes drilled in them over which the sample was held in place by a small quantity of grease which could be easily removed with an appropriate organic solvent) with the amount of light transmitted through an empty control sample holder. The results for 495 nm for samples 6 and 7 are shown in figure 5. One can see that they agree within experimental error to the least squares fit discussed in section 2.2(c).

2.4 Results and Discussion

2.4(a) PC Spectra

Figure 8 presents typical PC spectra (normalized to the black body output of the monochromator) for both 82 K and 300 K. The PC spectra differed widely in shape, a reflection of the fact that many factors combine to produce the shape, but they share a couple of features.

The first thing to notice in figure 8 is the presence of two peaks, one at about 400nm at both temperatures - called the 'intrinsic' peak since the exciting photon energy was greater than the band gap energy (2.86 eV) - and the other at around 470 nm in the 300K spectra (450 nm at 82 K) - labelled the 'extrinsic' peak since the exciting photon energy was less than 2.86 eV. The position of the two peaks for various samples is listed in table VI below.

The wavelength attributed to the 'intrinsic' and 'extrinsic' peaks should be taken with caution because of the difficulty in normalization. This difficulty is due to the non-linear intensity dependence of PC which will be discussed in section 2.4(c). At 84K and 300K the photocurrent is a sublinear function of intensity. For example in sample number 6, at 495 nm, the photocurrent varies as $I^{0.8}$ at 300 K. If the data was normalized assuming the photocurent manifested the same intensity dependence at all wavelengths (which is not true), the "intrinsic peak" of sample number 6 would shift from 410 to 420 nm. The intensity dependence of steady state PC depends quite strongly on the types

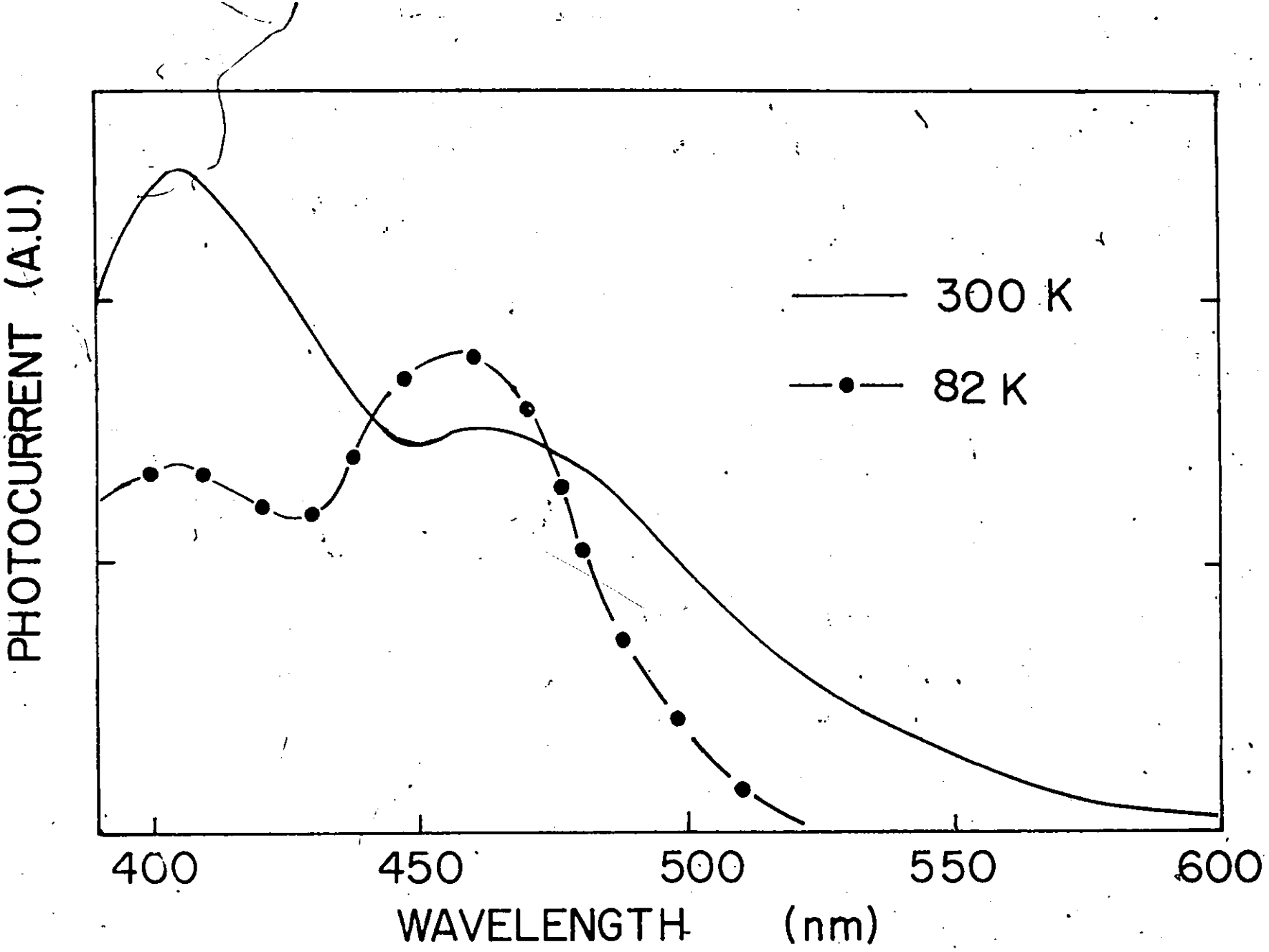

FIGURE 8
TYPICAL PC SPECTRA (NORMALIZED)

TABLE VI
INTERSAMPLE COMPARISON OF
PC SPECTRA

	sample 1	sample 2	sample 6	sample 7
intrinsic peak (300 K)	410 nm	400 nm	410 nm	405 nm
intrinsic peak (84 K)	-	-	does not exist	405 nm
extrinsic peak (300 K)	495 nm	470 nm	unresolved	470 nm
extrinsic peak (84 K)	-	-	450 nm	450 nm
$E_g - E_{ph}$ (300K)	360 meV	220 meV	does not exist	220 meV
$E_g - E_{ph}$ (84 K)	-	-	210 meV	210 meV

The reason for the nul entries for 84 K for samples 1 and 5 is that the samples were ruined before low temperature PC spectra could be performed.

and distribution of defects levels in the forbidden gap[21] as was discussed in section 2.2(b). Hence it varies not only from wavelength to wavelength but from sample to sample. Such difficulties in normalization might explain why the extrinsic peak in the 300 K spectrum of sample 1 is at 495 nm while it appears at 470 nm in samples 5 and 7.

The 'intrinsic' peaks at around 400 nm (see table VI) are due to the DeVore effect discussed in section 2.2(a).

The 'extrinsic' peaks are due to electron transitions from the A levels to the conduction band[5] (see figure 1). The energy difference between the conduction band and the A levels (E_{ph}) is given roughly by energy corresponding to the wavelength where the extrinsic peak appears in the spectrum.

The difference between the band gap energy (E_g) and E_{ph} is also listed in table VI. '$E_g - E_{ph}$' is a very rough measure of the binding energy of the acceptor (E_a) as was discussed in section 1.2(d). Note that most of the acceptor binding energy estimates listed in table VI agree with the 'E_a' values determined by other workers - see section 1.3(d).

The shift of the extrinsic peak in the spectrum of sample 7 towards the UV with decreasing temperature agrees with previous observations[5].

The extrinsic peak is listed as unresolved in the 300 K spectrum of sample 6 for two reasons. First, the DeVore theory predicts that the intrinsic peak tends to be broader in thinner samples. While sample 6 is at least three times thicker than samples 5 and 7 (see figure 5) a comparison between the PC

spectra of samples 5, 6 and 7 showed that the "intrinsic peak" of sample 6 is broader than that of samples 5 and 7. The presence of an unresolved peak could account for this discrepancy. The second reason is that the 84 K spectra of samples 6 and 7 both exhibit a peak at 450 nm.

As has been mentioned several times, the whole point of doing the PC spectra was to ascertain whether 'A' levels were present in the samples. The presence of the extrinsic peaks is good evidence that 'A' levels exist in all four samples studied. We now turn to a study of the trap distribution by Fermi Level Analysis.

2.4(b) Fermi Level Analysis

Some typical data from a Fermi Level Analysis experiment is shown in figure 6. One should note a couple of features:

(i) As I_o increases, the steady state PC (PC before the decay begins) increases and accordingly 'n', the free electron density increases. Hence the difference in energy between E_f and the CB - given by equation 7 - becomes smaller. In summary, increasing the intensity (I_o) moves the Fermi Level (E_f) towards the conduction band (CB).

(ii) The response time (τ_r) changes with the I_o. As was noted above, increasing I_o moves E_f towards the CB. Hence one can see 'τ_r' change with E_f in figure 9. Also note that the response time is much greater than 75 msec which is the measuring system response time.

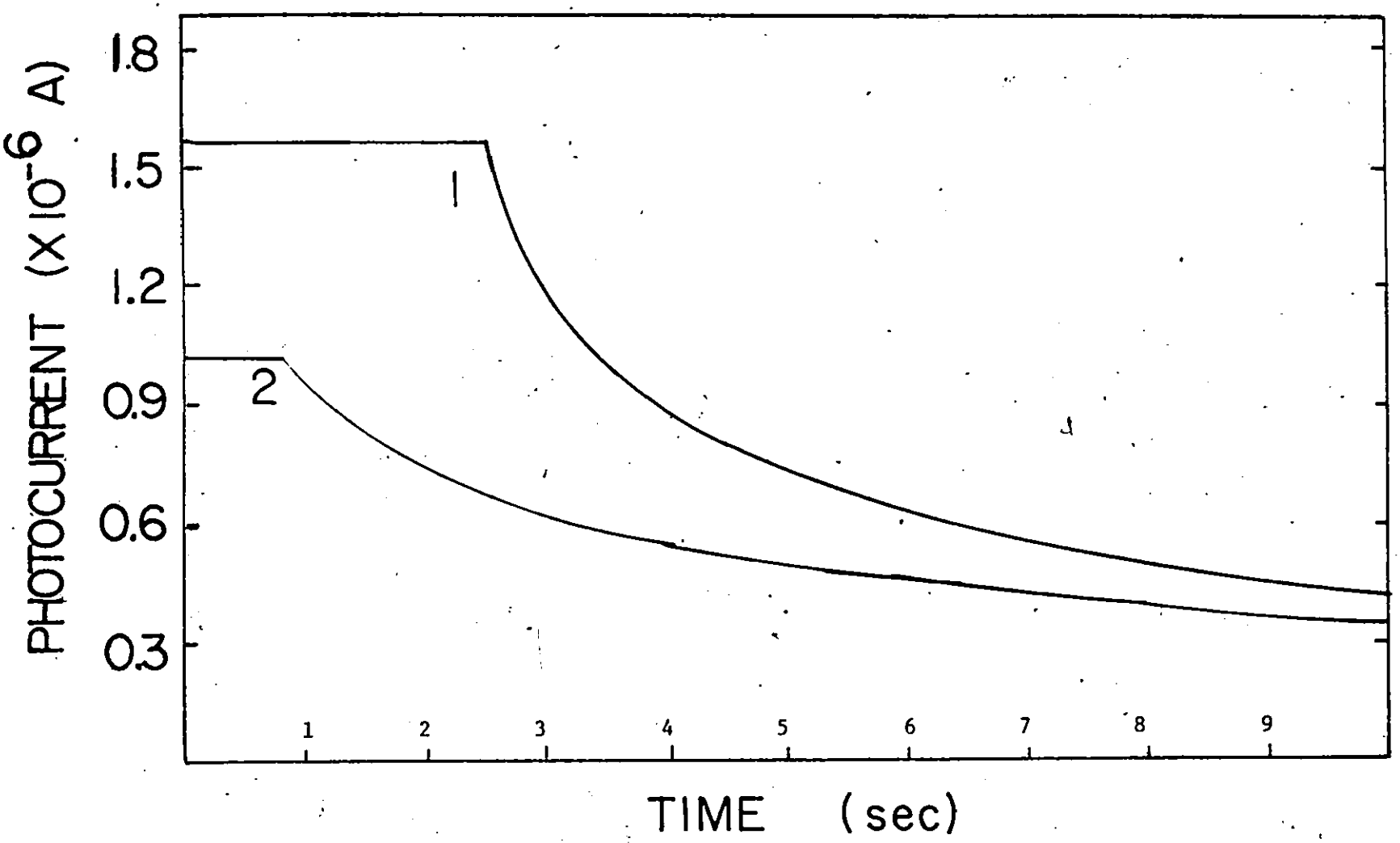

FIGURE 9
TYPICAL DATA FROM FERMI LEVEL ANALYSIS EXPERIMENT

V : interelectrode voltage (14V)
1 : incident intensity (0.95 W/m^2); response time (4.8 seconds)
hν: incident photon energy (2.5 eV)
T: samplé temperature (84K)
2: incident intensity (0.48 W/m^2) response time (8.3 seconds)

Each decay curve corresponds to one of the quadruplets (T, I_o, PC, τ_r) mentioned in section 2.2(c). The result of subjecting 40 or so decay curves (approximately 4 per temperature at about 10 temperatures) to the theory of section 2.2(c) resulted in figures such as 10 and 11. These figures assume the optical phonon scattering model (equation 34). A least squares 6^{th} degree polynomial fit appears with the data. The curve fitting was performed in anticipation of the numerical integration required for total trap density determination to be discussed below. The standard error of the fit is about 20 per cent while the uncertainty in the individual experimental points - the combined uncertainty of the response time and the free carrier creation rate per unit volume - is about 25 to 30 per cent.

In general terms, one sees in figures 10 and 11 that the trap density decreases exponentially from the CB band edge with a "slope" of approximately 100 meV per decade for several hundred meV, reaches a minimum at a trap depth of about 400 meV and then increases again. In the discussion to follow we assume the trap distribution to be composed of two parts: an exponential distribuiton - the trap distribution discussed in section 1.3(d) - and a localized donor which will be called the '600 meV' donor because of the increase in trap density near 600 meV below the CB. A summary of the measured trap parameters appears in table VII. The slope and trap density per unit energy at the CB band edge (N_o) in table VII refer to the exponential part of the trap distribution (0.1 to 0.3 eV for sample number 6 - see figure 10)

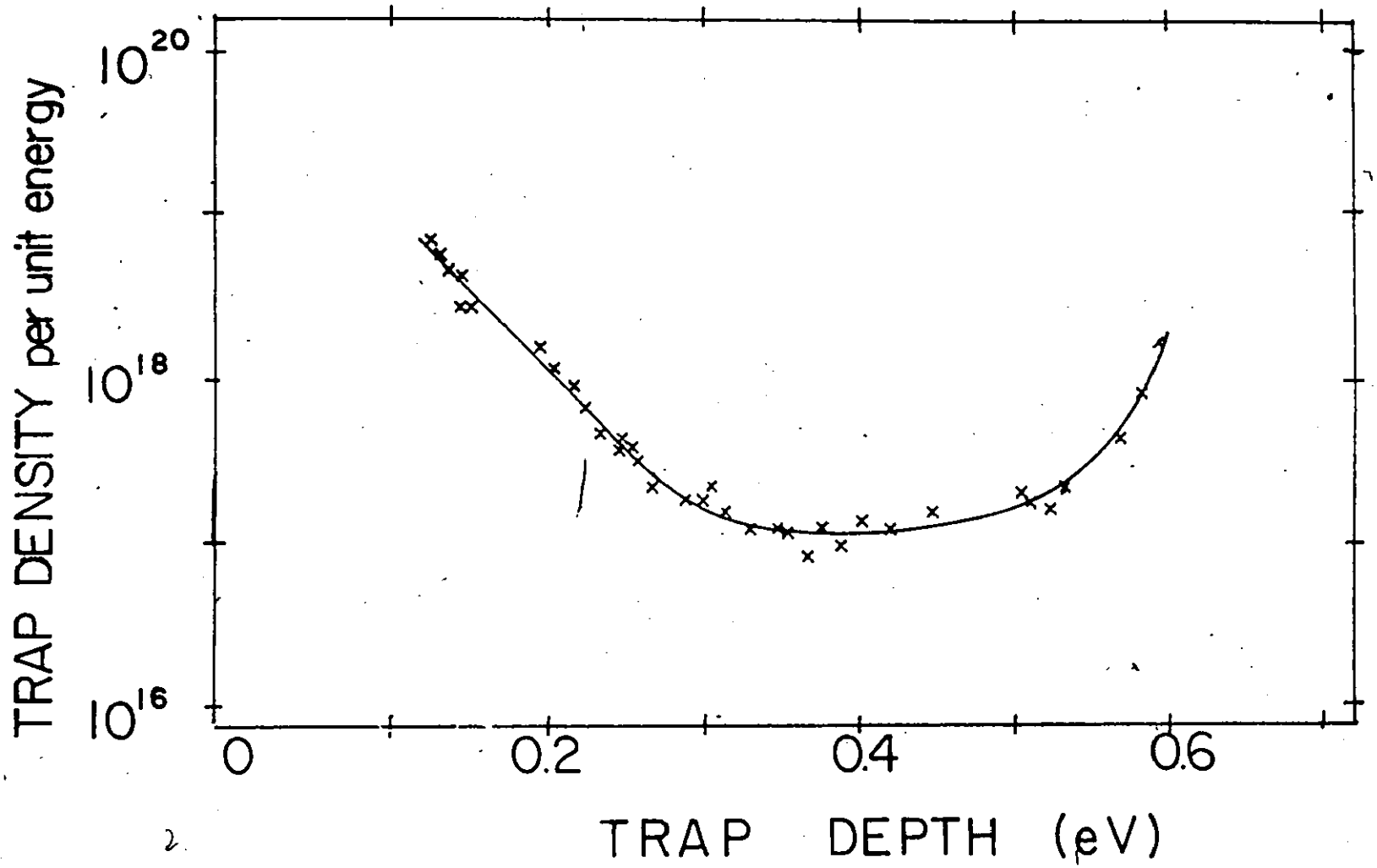

FIGURE 10
TRAP DENSITY DISTRIBUTION FOR SAMPLE 6
ASSUMING OPTICAL PHONON SCATTERING DOMINANT

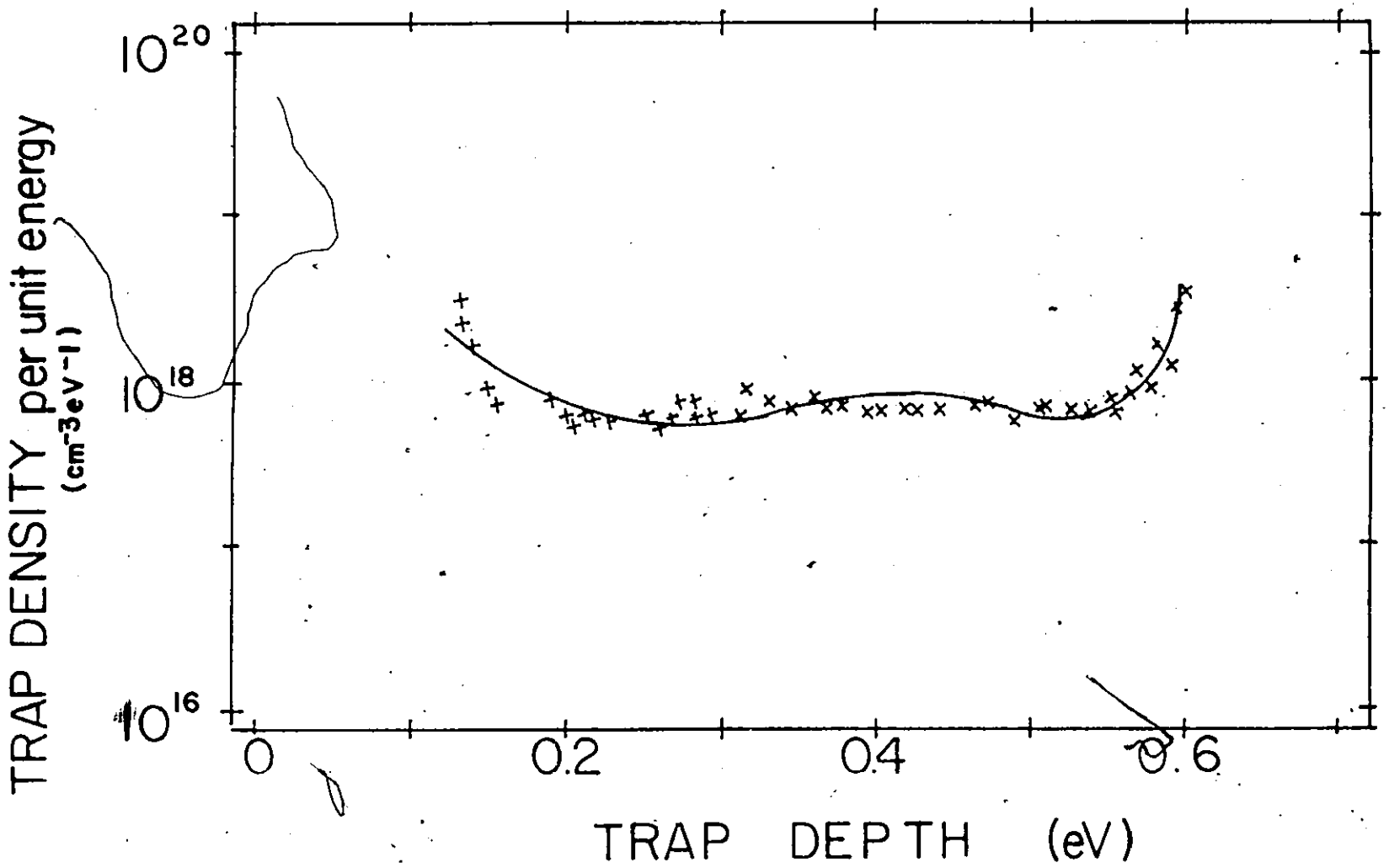

FIGURE 11
TRAP DENSITY DISTRIBUTION FOR SAMPLE 7
ASSUMING OPTICAL PHONON SCATTERING DOMINANT

TABLE VII

SUMMARY OF
MEASURED TRAP PARAMETERS

sample	Range of exponential region (meV)	slope (meV/ decade)	trap density at CB band edge N_o (cm^{-3}/eV)	integrated trap density N_t (cm^{-3})
6*	100-300	106±4	$7.31\pm0.07\ \bar{X}10^{19}$	$3.2\pm0.4X10^{18}$
6**	100-300	104±2	$9.5\pm0.1\ \bar{X}10^{19}$	$4.3\pm0.3X10^{18}$
7*	100-200	140±50	$1.3\pm1.2\ \bar{X}10^{19}$	$1.2\pm0.2X10^{20}$
7**	100-200	150±50	$1.2\pm1.1\ \bar{X}10^{19}$	$1.0\pm0.2X10^{18}$

* assumes acoustic phonon scattering dominant and the temperature variation of the mobility is given by equation 33.

** assumes optical phonon scattering dominant and the temperature variation of the mobility is given by equation 34.

were obtained by performing a least squares linear fit of the logarithm of trap density versus energy for the range over which the trap density varied exponentially. The Fermi Level Analysis was performed only on samples 6 and 7.

The error in the "slope" and the trap density at the band edge are proportional to the standard error of the fit (which is the square root of the sum of the differences between the trap densities predicted by the fit and the measured trap densities divided by the number of points minus 2)[48].

In table VII note that the measured trap distribution "slope" for both samples 6 and 7 and both mobility models agree reasonably well with the "slopes" measured by other workers - see table II. The choice of mobility model does not significantly influence the "slope".

It is curious that the error in the slopes and trap density at band edge is so much bigger for sample 7 than for sample 6. Assuming all the points have equal weight, it is partially due to the fact that in sample 7 the energy range over which $N_t(E)$ varies exponentially was 100-200 meV while the range was 100-300 meV in sample 6 (compare figures 10 and 11); there were thus fewer points for the fit.

One should also note that the integrated trap density in the table was not calculated in the same manner as other workers have calculated it (equation 12 in section 1.3(c)). This is because a purely exponential trap distribution was not measured. Instead the integrated trap density was calculated in two parts. The total trap density on the range 0 to 0.15 eV below the CB was

determined by integrating equation 11 (with parameters from table VII) from 0 to 0.15 eV. The error in this part of the total trap density was taken as the standard error of the linear fits to the exponential part of the trap distribution discussed above. The total trap density on the range 0.15 to 0.6 eV below the CB was determined by numerically integrating the least square 6th degree polynomial fits shown in figures 10 and 11 using Simpson's rule and a 2.5 meV integration step. It is reasonable that the truncation error in the numerical integration was smaller than standard error of the polynomial fit and hence the latter was taken as the error in integrated trap density on the range 0.15 to 0.6 eV below the CB.

The origin of this exponential trap distribution is still unclear. For $CdIn_2S_4$, Anedda et al.[49] suggested Cd-In antisite defects as the origin of both the exponential trap distribution and the shallow acceptor. This is a reasonable hypothesis since the most important criterion for the formation of an antisite defect is ionic size rather than valence[50]. (The ionic radii of Zn^{2+}, Cd^{2+}, and In^{3+} respectively are 0.74, 0.97, and 0.81 angstroms respectively[50].) This suggestion raises the further question of why the donors are spread exponentially in energy while the acceptors are discrete. To explain this Anedda et al.[49] invoked the effective mass theory for shallow impurity states. In this theory, the radius of the impurity state is inversely proportional to the effective mass of the nearest band minimum[51]. Since, in general, the effective mass of electrons is smaller than that of holes, the acceptors are more localized

and hence a high defect density broadens acceptor states less than donor states. An objection can be raised since the effective mass theory may not be applicable. Antisite defects can form deep levels. For example they have been suggested to be the origin of the deep EL2 state in semi-insulating GaAs[52]. For deep levels the effective mass theory is not appropriate. The wave functions of deep levels in semiconductors and insulators are likely to contain contributions from all over the Brillouin zone and not only near the nearest band minimum[53].

The other interesting feature of the measured trap distributions is the observed increase in trap density at around 600 meV below the conduction band which we assume indicates the presence of a localized level called the '600 meV' donor. Further work should be done to map the density of states function for this level. Thermally stimulated current or deep level transient spectroscopy may be useful in this regard. Further evidence will be presented in section 2.4(c) below for the increase in trap density at around 600 meV below the CB. But let us assume for the time being that the trap density really does increase beginning at about 500 meV below the CB and has a maximum near 600 meV. Then it is part of the solution to the PL anomaly discussed in section 1.2(e). The discrepancy between the predicted and observed donor-acceptor photon energy is reduced from 0.96 eV (see table V) to 0.36eV. The rest of the discrepancy could be made up by the electron making transitions to excited states of the acceptor rather than the ground state.

There are of course other possible explanations for the

discrepancy such as the possibility that the donor-acceptor transition is really a "two electron" process - an Auger process in which some of the donor-acceptor binding energy is transferred to a third body[54] - but this seems rather ad hoc.

2.4(c) Intensity Dependence of PC

It was stressed in section 2.2(b) that the intensity dependence of PC is another sensitive probe of the distribution of impurity levels in the forbidden gap. As will be seen presently, a study of the intensity dependence of PC in $ZnIn_2S_4$ permits identification of different kinds of states in the forbidden gap according to the relative size of their free electron capture cross section.

The intensity dependence of PC is characterized by the parameter 'k' where $PC \alpha I^k$.

As was mentioned in section 2.3(c), separate data was not collected for the study of 'k'. The data was contained within the Fermi level analysis since the steady state PC was noted for several intensities per temperature - see figure 9.

Also recall that the position of the quasi fermi levels can be controlled by changing the temperature and incident intensity. In figure 12, the electron quasi-fermi level is shown as a function of temperature for two different incident intensities. The quasi-fermi level (E_{fn}) was determined using the method of section 2.3(c)-(ii). One sees in figure 12 that decreasing the temperature moves E_{fn} closer to the CB. One can also see that increasing the intensity moves E_{fn} closer to the CB. One might

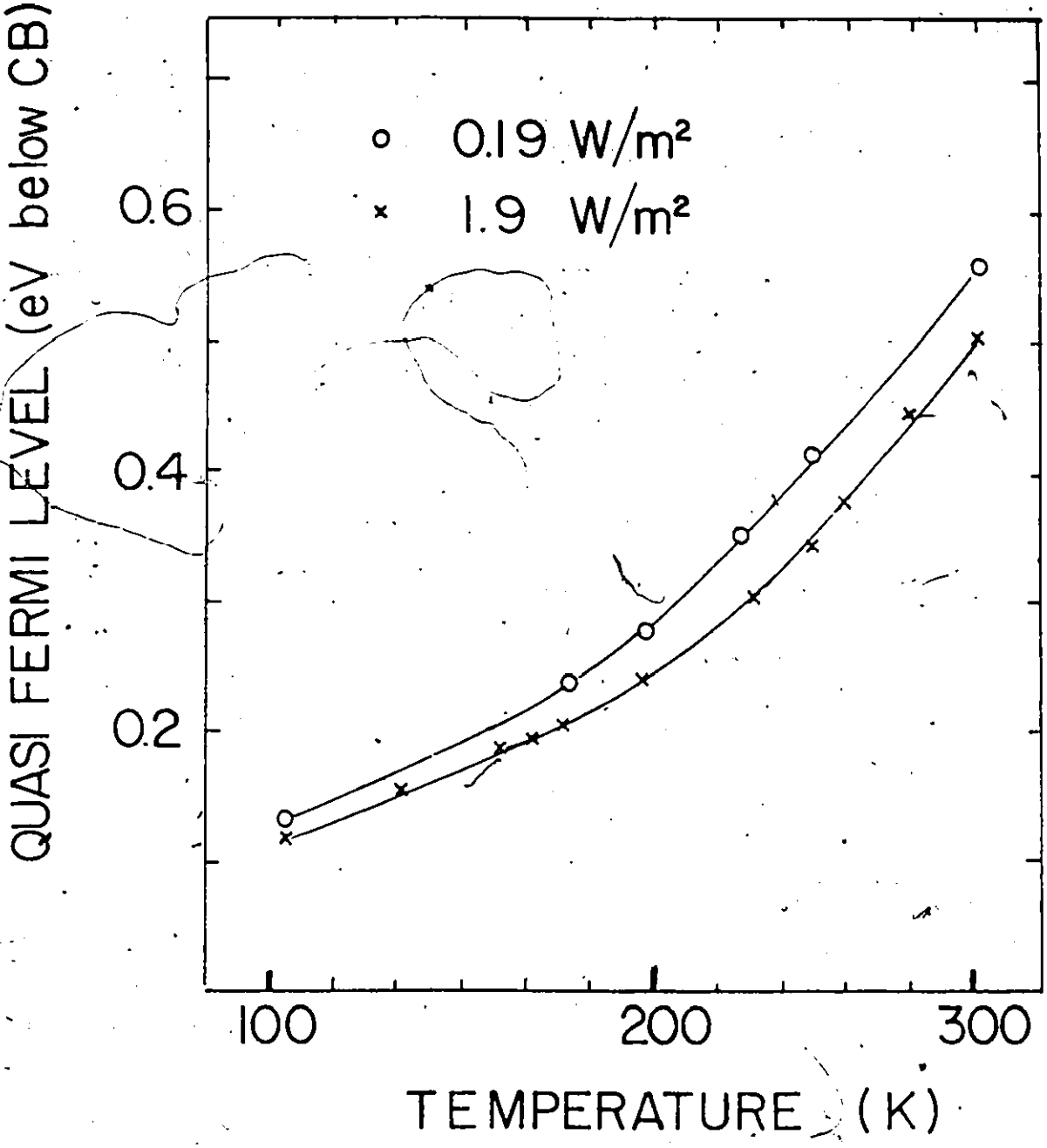

FIGURE 12

QUASI-FERMI LEVEL VS. TEMPERATURE

also add that although it is not shown, the hole quasi fermi level (E_{fp}) has moved closer to the VB.

The intensity dependence of PC was studied for intensities on the small range 0.19 to 1.94 W/m^2 at several temperatures at .495 nm. As one can interpolate from figure 12, 'k' can be studied as a function of E_{fn}. The results of this analysis are shown in figure 13. There are at least three important features in figure 13 to explain. One must account for the fact that $k < 1$ for E_{fn} between 450 and 600 meV below the CB and between 100 and 300 meV below the CB. Secondly one must explain why $k > 1$ for E_{fn} between 300 and 450 meV below the CB. To do so we have the models of sections 2.2(b) to guide us. One might also add that similar data (that is for a fixed intensity range, $k < 1$ for temperatures near 84K; $k < 1$ near 300K; $k > 1$ for temperatures between 84 and 300K) have been observed in GaAs and CdS[55].

Let us first try to explain why $k < 1$ on the range 100 to 300 meV below the CB. We can use the Rose model of section 2.2(b)-(i). The trap distributions of figures 10 and 11 correspond neatly to the defect distributions producing k between 0.5 and 1 if the 'r' states of figure 3 correspond to the increase in trap density at about 600 meV below the CB shown in figures 10 and 11. Then as E_{fn} moves towards the CB more of the 600 meV states become recombination centers causing 'τ_{eff}' to decrease. This is a reasonable explanation for $k < 1$. However, the Rose model does not correctly predict the actual value of 'k'. As can be seen in equation 23, 'k' equals $T_1/(T + T_1)$ where 'T' is the temperature of the sample and 'T_1' is related to the

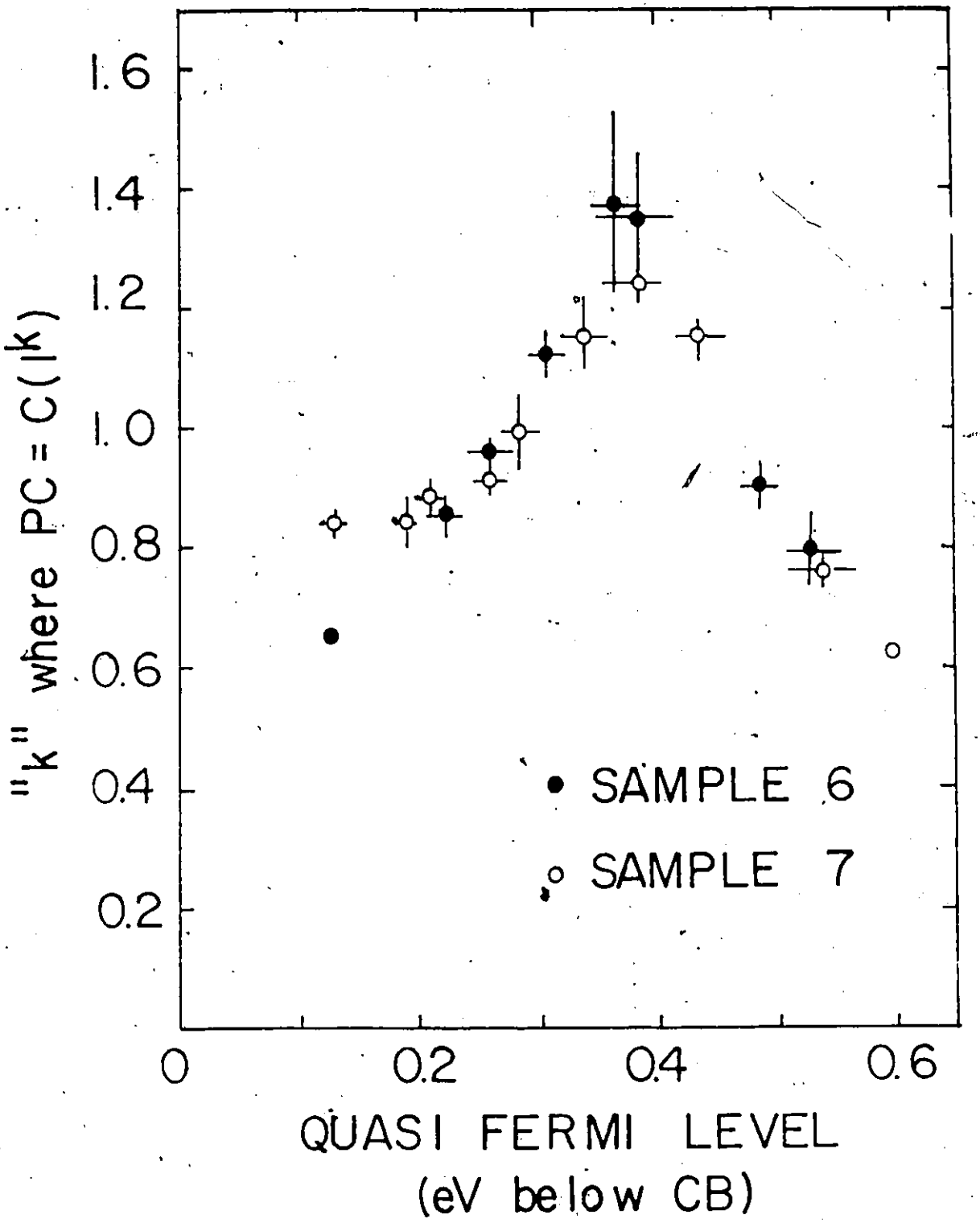

FIGURE 13
INTENSITY DEPENDENCE PARAMETER 'k'
VERSUS QUASI-FERMI LEVEL

"slope" of the trap distribution (equations 10, 11 and 17). Table VIII compares the observed values of 'k' with the predictions of the Rose model for sample 6 for E_{fn} on the range 0 to 300 meV below the CB. Table IX compares the observed and predicted values for sample 7 for E_{fn} on the range 0 to about 200 meV below the CB. One can see that the agreement is not very good but it is probably because the model presented in section 2.3(b)-(i) is too simple for the actual recombination kinetics in $ZnIn_2S_4$.

An assumption implicit in all of Rose's work is that electrons cannot make transitions directly between discrete states[56] whereas in reality, electrons in $ZnIn_2S_4$ make donor-acceptor transitions. Whether a donor state which can be involved in a donor-acceptor transition is acting as a trap depends on the occupation of the acceptor states. It is easy to see this in equation 5. Since we are exciting electrons from the 'A' levels of figure 1 to the CB one can see that the right hand side of equation 5 increases with intensity: the density of ionized donors and acceptors increases with intensity. Accordingly, the average d-a pair separation decreases and the transition probability increases since d-a transitions are more likely for closer pairs.

We can now try to explain why $k < 1$ for 'E_{fn} between 450 and 600 meV below the CB. The Rose model of section 2.3(b)-(i) predicts that 'k' should equal 1 for 'E_{fn}' between 450 and 600 meV below the CB since trap distribution actually decreases towards the CB on this energy range (see figures 10 and 11)[21].

TABLE VIII

COMPARISON OF EXPERIMENTAL 'k' VALUES AND ROSE MODEL PREDICTIONS SAMPLE 6

Temp (K)	E_{fn}(meV)	k_{theo}	k_{exp}
84	125	0.97	0.65±.02
173	220	0.94	0.85±.03
193	260	0.94	0.96±.02

TABLE IX

COMPARISON OF EXPERIMENTAL 'k' VALUES AND ROSE MODEL PREDICTIONS SAMPLE 7

Temp (K)	E_{fn}(meV)	k_{theo}	k_{exp}
84	130	0.98±.01	0.84±.02
132	190	0.97±.01	0.84±.04
150	208	0.96±.01	0.88±.03

This makes sense since there are then less and less trapping levels which can be filled and the population transfer from 'r' levels to 't' levels shown in figure 3 should not occur. Hence, 'τ_{eff}' should be constant. However, the states at 600 meV below the CB continue to be turned into recombination states; as the intensity increases, the density of ionized donors and acceptors increases and the average donor-acceptor pair separation is decreasing and hence the lifetime of an electron 600 meV below the CB is decreasing.

The fact that $k > 1$ for E_{fn} between 300 and 450 meV below the CB cannot be accounted for if just the 'T' and 'A' levels of figure 1 exist in the forbidden gap. However it can be explained qualitatively using the ideas presented in section 2.3(b)-(ii). According to this scheme there must exist two different kinds of states (class I states with large electron capture cross sections and class II states with small free electron capture cross sections) between E_{fn} and the hole quasi-fermi level (E_{fp}). We do not know the precise position of E_{fp} but know that it must be closer to the VB than E_{fn}.

The class I center is obviously the donor state at 600 meV below the CB. The class II center was not directly seen in any of the measurements, however other workers[5,17] have identified a class II center at 1.4 eV below the CB. The superlinearity is produced by transfer of electrons from the class II states to the 600 meV donor.

In summary, the presence of the exponential trap distribution and the 'A' levels has been confirmed. Secondly, the possibility of a localized center around 600 meV below the CB which is the center involved with the d-a transitions has been raised.

Let us now turn to a discussion of laser excited photoluminescence and photoconductivity in $ZnIn_2S_4$.

CHAPTER 3 - LASER EXCITED PHOTOCONDUCTIVITY AND PHOTOLUMINESCENCE

3.1 Introduction

The basic idea behind these experiments was to excite electrons from the A level to the conduction band and then look at what happens to them by examining how the height and time dependence of the PC and PL transients vary as a function of pumping intensity.

To the author's knowledge, measurements of laser excited PC versus intensity in $ZnIn_2S_4$ have never been reported before. Measurements of PL versus pumping intensity have been previously published[16,17] but for a continuous wave Ar^+ laser at much lower excitation levels (the highest excitation intensity was approximately 17 KW/m^2 compared to 500 MW/m^2 in the present work). The measurements and interpretation to be reported below have been accepted for publication in Solid State Communications.

To help us understand the high intensity measurements let us review previous studies of the intensity dependence of laser excited PC and PL in compounds other than $ZnIn_2S_4$.

3.2 Survey of High Intensity Laser Effects

Figures 14 (a) and (b) present two possible ways for the photosignal, either PL or PC, to vary as a function of excitation intensity. Let us call figure 14 (a) a type (a) characteristic

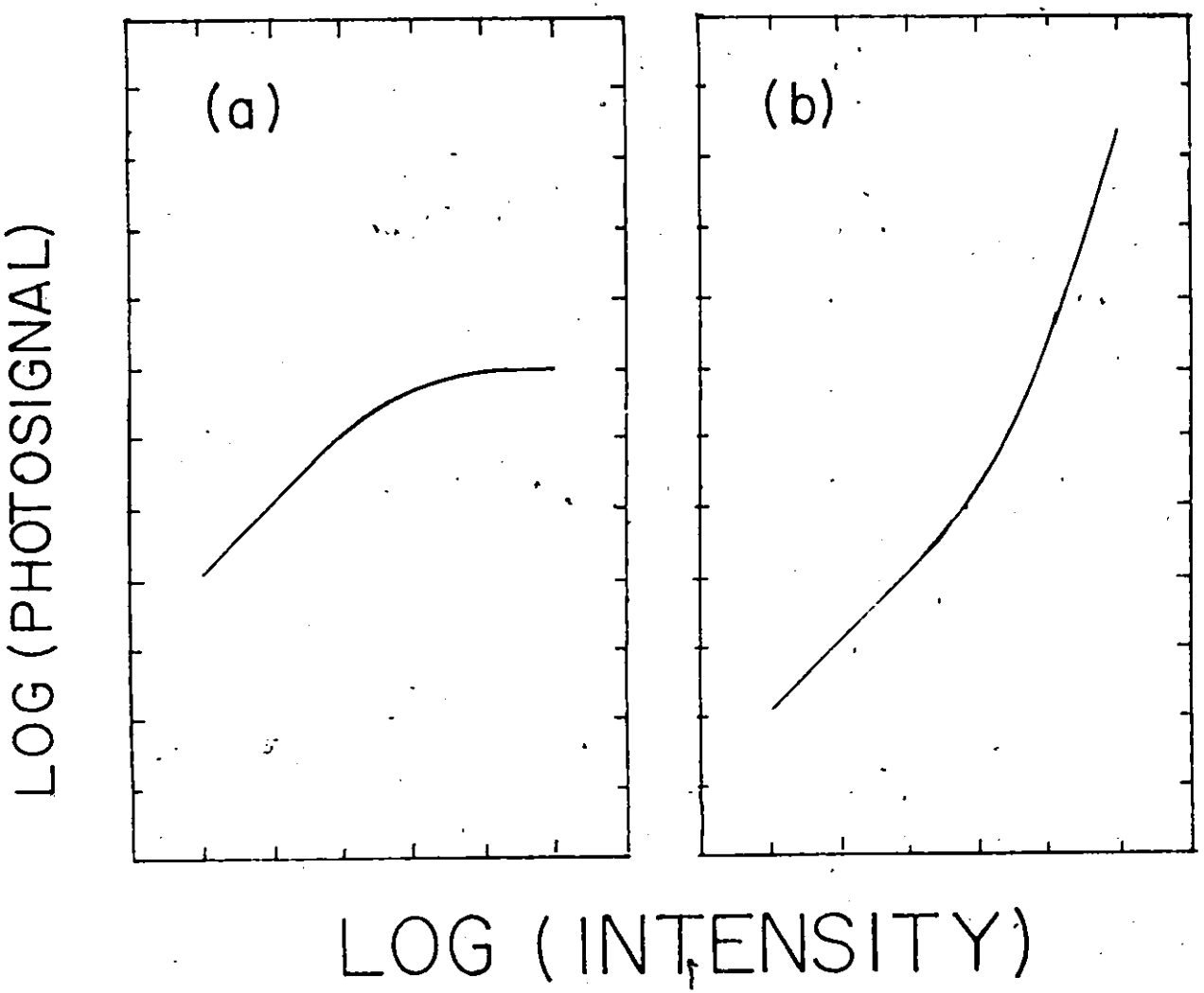

FIGURE 14

PHOTOSIGNAL VS. INTENSITY CLASSIFICATION SCHEME

and figure 14 (b) a type (b) characteristic. Type (a) and type (b) characteristics have been seen in both PC and PL in compounds other than $ZnIn_2S_4$. The mechanisms that have been used to explain type (a) and type (b) characteristics can be classified into two groups: kinetic non-linearities and quantum mechanical non-linearities.

Kinetic non-linearities are effects which depend on the relative population of electron states. Stimulated emission - which is due to population inversion - is a kinetic effect which results in the type (b) PL characteristic seen in CdS[57,58]. At low excitation intensities spontaneous emission is dominant and PL varies linearly with intensity. But as the pumping intensity increases, stimulated emission begins to occur and PL versus I characteristic becomes superlinear. As wil be seen below there is yet another kinetic effect which can lead to a type (b) PC characteristic.

A kinetic effect which can result in either a type (a) or a type (b) PC characteristic is when the effective free carrier lifetime is a function of excitation intensity. This was discussed in detail in section 2.2(b). Although this low intensity analysis was developed before the invention of the laser, it has been used to analyze a sublinear laser produced PC vs. I characteristic in GaAs[59].

PC saturation, or type (a) behaviour has been observed in $CdS_{0.5}Se_{0.5}$[60], n-GaAs[61] and GaSe[62]. In these measurements, the samples contained only one type of impurity centre and capture by these centres was also the primary recombination mechanism.

Extrinsic PC was produced by exciting electron transitions from the impurity centres to the conduction band. PC saturation is then due to the two fold effect of simultaneously decreasing the creation rate 'f' and the effective free carrier lifetime 'τ_{eff}'. Increasing the excitation intensity tends to empty the impurity states of electrons which makes electron transitions from the impurity state to the conduction band less probable but makes the reverse transition more probable.

An intensity dependent lifetime is an explanation for a type (b) PL characteristic which is not due to stimulated emission. Fouqet et al.[63] performed time resolved PL work on a GaAs/$Al_xGa_{1-x}As$ multiple quantum well structure, plotted the time integrated PL vs. intensity, noted a type (b) characteristic and correlated it an with an increasing lifetime for the upper state of the radiative transition. One should note that although PL intensity would decrease if the radiative lifetime increased, the integrated intensity increases. The cause of the increase of the radiative lifetime with excitation intensity was saturation of a trapping mechanism. In these multiple quantum well devices, band to band radiative recombination was the source of the luminescence. But this recombination route is not the most efficient. The most important route was the trapping mechanism. When this mechanism becomes saturated, that is the trapping states become filled with electrons, the electrons must decay via other less efficient routes producing an effective lifetime increase.

Type (a) characteristics in PL have been seen in donor-

acceptor luminescence. They have to do with the fact that the donor-acceptor emission intensity cannot increase indefinitely; once the donors and acceptors involved become completely non-ionized, the emmision intensity saturates. A type (a) behaviour in donor-acceptor luminescence has been recently observed in InSe[64]. The shift of donor-acceptor emission band peak towards higher energy with increasing intensity (which was discussed in section 1.3 (b)) is an indirect manifestation of this effect.

There is one more type of laser produced kinetic effect which results in a type (a) characteristic. This is when the creation rate decreases but the lifetime remains constant. This can happen when the exciting light is so intense that it empties the initial state of electrons but the population of the states involved in the dominant recombination routes are not perturbed greatly. This type of effect has been seen in $CdIn_2S_4$[65].

And so we see that type (a) and type (b) PL characteristics and type (a) PC characteristics have in the past been interpreted by kinetic non-linearities. This is not true for type (b) PC characteristics. Type (b) PC characteristics in GaAs[59], InP[66], $CdIn_2S_4$[67] and GaSe[68] have been attributed to a quantum mechanical non-linearity, two photon absorption. Quantum mechanical non-linearetiea can happen when the incident electric fields - which are proportional to the square root of the incident intensity - approach the magnitude of the crystal field (approximately 10^{10} V/m). Then the incident electric field can no longer be considered a small perturbation and non-linearities can occur. In the case of single photon absorption - where 'I' is the intensity in the bulk of the solid, 'α' is the

absorption coefficient and 'x' is the direction of propagation of the light,

$$\frac{dI}{dx} = -\alpha t \qquad (36)$$

The solution of the above differential equation is the familiar Beer's law.

On the other hand, in the case of two photon absorption,

$$\frac{dI}{dx} = -(\alpha I + \beta I^2) \qquad (37)$$

where 'β' is the coefficient for two photon absorption. A review of measurements of 'β' in various semiconductors by Gibson et al.[69] revealed 'β' in the range 0.02 cm/MW for GaAs to 16±2 cm/MW for InSb. However, Gibson et al. criticized the latter value as being nearly two orders of magnitude too high.

To the writer of this thesis, for two photon absorption to be a convincing interpretation of a type (b) PC characteristic, proof that the free carrier lifetime is independent of intensity should be given as theoretical studies of two photon PC assume constant 'τ_{eff}'[70]. In all of the work referred to above[59,66-68], the PC versus intensity characteristic is linear or sub-linear at low excitation intensity. This means that impurity states must exist in the forbidden gap because the exciting photon energy is less than the forbidden gap and because pure two-photon PC varies as the square of the intensity. Hence it is imperative for a convincing proof of two photon PC that the intensity independence of 'τ_{eff}' be demonstrated. However, in none of the references mentioned above was a study of the PC transients as a function of

intensity mentioned. In measurements of PC versus intensity on $ZnIn_2S_4$ to be reported below, a type (b) characteristic was observed. But it can be correlated with an intensity dependent effective free electron lifetime, as was the type (b) PL characteristic reported by Fouqet et al.[63].

For easy reference when it comes time to interpret the measurements of the intensity dependence of PC and PL in $ZnIn_2S_4$ we summarize the above review of high intensity laser effects in Table X below.

Before discussing the measurements themselves, let us become familiar with the apparatus used in making the measurements.

TABLE X

SUMMARY OF PHOTOSIGNAL VERSUS INTENSITY EFFECTS

type (a) PC:	-two fold effect of decreasing 'f','τ_{eff}' with intensity; seen in $CdS_{0.5}Se_{0.5}$, n-GaAs and GaSe.
	-saturation of the creation rate 'f' only; seen in $CdIn_2S_4$.
type (b) PC:	-two photon PC; seen in GaAs, InP, $CdIn_2S_4$ and GaSe.
type (a) PL:	- saturation of donor-acceptor luminescence; seen in InSe.
type (b) PL:	-saturation of trapping mechanism (intensity dependent 'τ'); seen in a $GaAs/Al_xGa_{1-x}As$ multiple quantum well device.
	-stimulated emission; seen in CdS.

3.3 Experimental Details

3.3(a) Summary of the Apparatus

For the laser work, the $ZnIn_2S_4$ samples were mounted in the manner described in section 2.3 (a). Figures 15 and 16 present the basic experimental set-ups for PC and PL, respectively. In general terms, both set-ups can be broken down into three sections: (i) excitation of the PC and PL photsignals; (ii) detection of the photosignals; and (iii) recording of the photosignal.

(i)Excitation of the Photosignal:

A CMX-4 pulse dye laser (DL) was the excitation source. A small fraction of the laser beam to be used as an optical trigger was obtained using a beam splitter (BS). The incident intensity was controlled by a set of neutral density filters (NF) and lenses (L1,L2).

(ii) Detection of the Photosignal:

In the case of PC, the sample was placed in series with a variable resistor and a power supply forming a simple voltage divider type circuit (C). The photocurrent produced a change in voltage across the resistor in series with the sample. Due to the possibility of a spurious photovoltage being produced, the following test was performed: If the signal disappeared when the power supply voltage was turned off then one was ensured that a photocurrent was being observed.

In the case of PL, the PL transients were

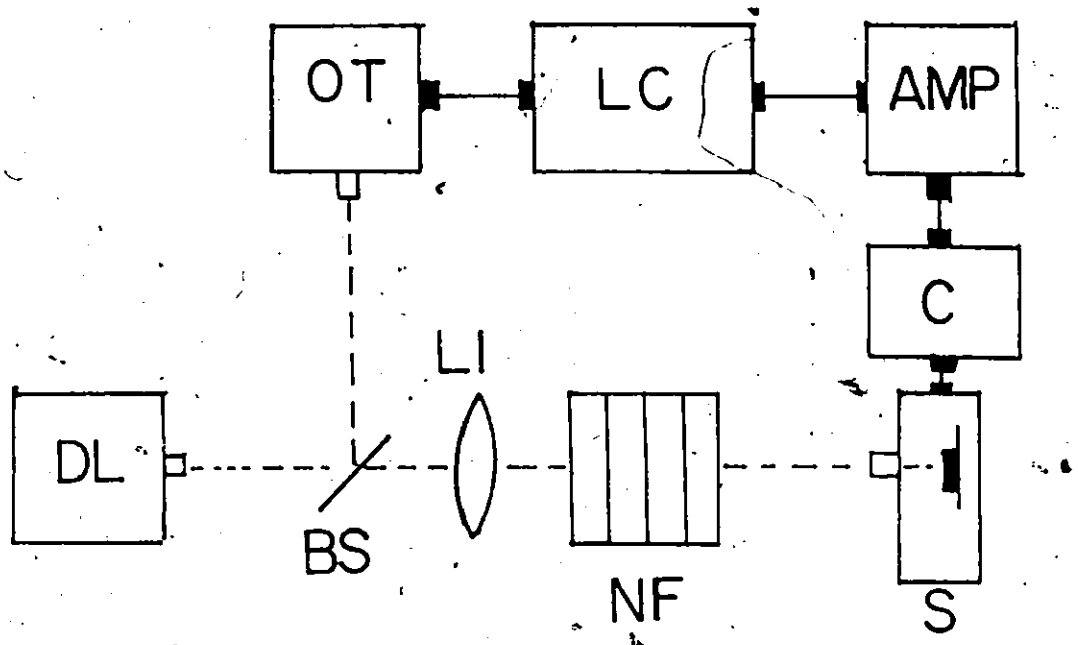

FIGURE. 15
EXPERIMENTAL APPARATUS FOR LASER EXCITED PHOTOCONDUCTIVITY EXPERIMENTS

DL: CMX-4 Dye Laser
BS: Beam Splitter
OT: Optical Trigger
Ll: Lens
NF: Neutral Density Filters
S: Sample mounted in cryostat
C: PC detection circuit
AMP: Tektronix 5A45 Amplifier
LC : LeCroy 3500 Transient Signal Averager

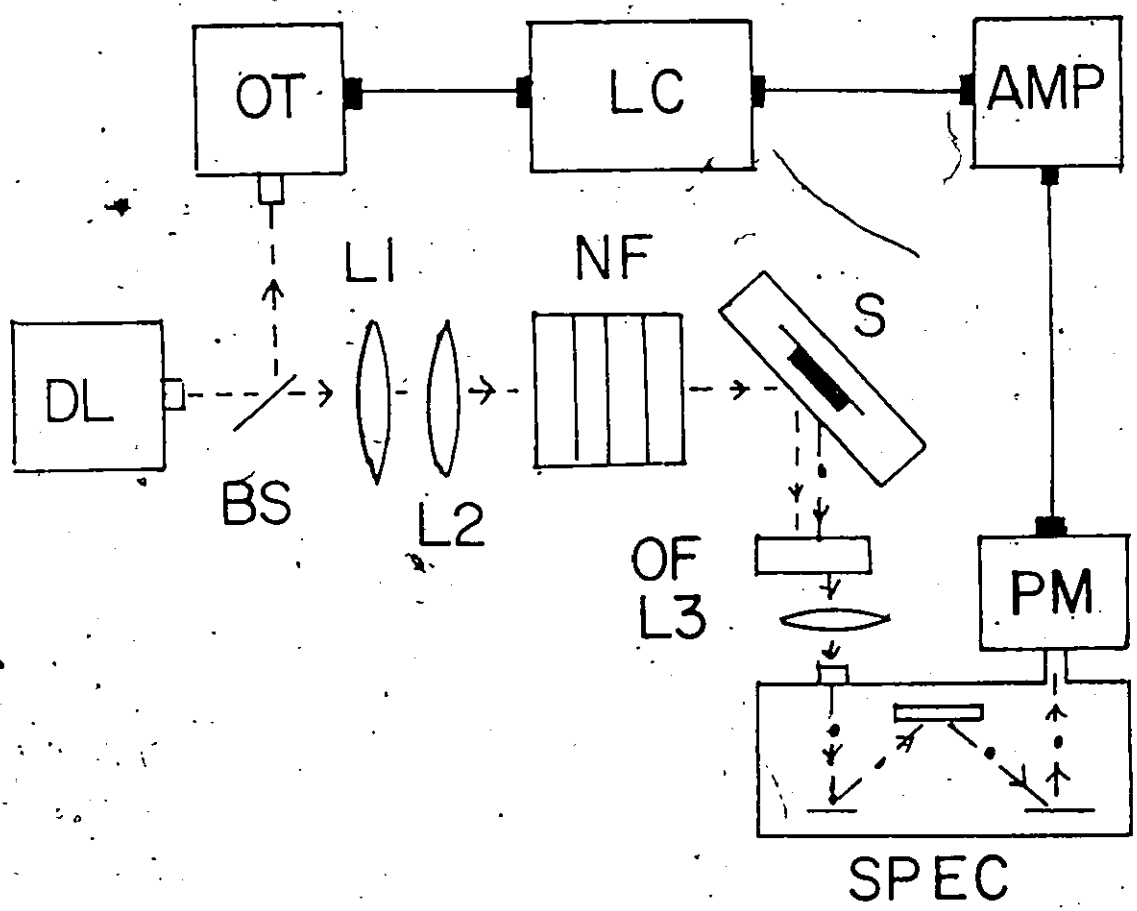

FIGURE 16
EXPERIMENTAL APPARATUS FOR LASER EXCITED PHOTOLUMINESCENCE EXPERIMENTS

DL: CMX-4 Dye Laser
BS: Beam Splitter
OT: Optical Trigger
L1,L2,L3: Lenses
NF: Neutral Density Filters
S: Sample mounted in cryostat
OF: Optical Band Pass Filters
SPEC: Spectrometer
PM: Photomultiplier.
AMP: Tektronix 5A45 Amplifier
LC: Lecroy 350C Transient Signal Averager

focussed (L3) on the entrance slit of a spectrometer (SPEC) which selected the emission wavelength observed. The emitted PL pulses were then picked up by a photomultiplier (PM). To ensure that the PL pulse was being monitored and not stray laser light two optical filters (OF) were used: a red filter which passed all wavelengths above 600 nm and a blue filter which passed all wavelengths below 600 nm. The red filter was kept in front of the entrance slit of the spectrometer at all times in order to remove as much stray laser light as possible. Two scans of the PL transient were collected, the first with only the red filter in front of the spectrometer and the second with both filters in front. As will be discussed in more detail below, 495 nm was the wavelength of the exciting laser light while the PL emission was monitored at 700 nm. Hence, in the first scan - the "signal" scan - the PL signal plus noise was monitored. In the second scan - the "noise" scan - the PL signal was removed by the blue filter, while any stray laser light still making its way beyond the red filter would be recorded. This noise scan was subsequently subtracted from the signal scan.

(iii) Recording of the Photosignal:

The signals had to be passed through an amplifier (AMP), and recorded by LeCroy 3500 transient signal averager(LC) which was optically triggered (OT).

The individual components of the apparatus will now be discussed in more detail.

3.3 (b) CMX-4 Dye Laser

The pulse width of the CMX-4 dye laser is approximately 2 μsec. Fortuitously, in the case of $ZnIn_2S_4$, even with 2 μsec pulses one is able to see a variation in the shape of the PC transient with excitation intensity. On the other hand, these wide pulses are ideal for producing saturation type effects which depend on the total number of photons absorbed.

Since the measurements were performed as a function of intensity and the excitation source is a pulsed dye laser it is important to define just what is meant by intensity. In this work the intensity scales refer to nominal peak intensity rather than average intensity. The following equation is the definition of nominal peak intensity (NPI):

$$NPI = \left(\frac{\text{average power}}{\text{repetition rate}}\right)\left(\frac{1\text{ second}}{2\ \mu\text{sec}}\right)\left(\frac{1}{\text{spot size}}\right) \qquad (38)$$

The average power was measured with a Scientech Model 361 power meter while the repetition rate was 10 pulses per second for all the experiments.

The spot sizes were calibrated by drawing the spot on a piece of graph paper as a function of distance from the lens directly in front of the sample for the experiment in question. Referring to figure 15, this means lens L1 for the PC experiments; referring to figure 16 this means lens L2 for the PL

experiments. The spot size at the sample could then be interpolated from the calibration curves if the distance from the lens were known.

One should be careful when using lenses to focus coherent laser beams. Two samples were burned by assuming that the narrowest beam waist occurs at the focus of the lens. Actually, the position of the narrowest part of the beam is a function of the focal length of the lens and the divergence of the incoming beam[71].

The appropriate dye for exciting electrons from the A level to the conduction band in $ZnIn_2S_4$ is Coumarin 102 (or equivalently Exciton dye LD-490). This dye exhibits maximum intensity at 496 nm. By a lucky coincidence, it is the second most powerful dye after Rhodamine 6G and is the most stable of the Coumarins (which are in general unstable dyes). LD-490 lasts to within a factor of two in intensity for around 100,000 pulses. The pulse to pulse amplitude stability is roughly $\pm$10 % at the beginning of the dye's life worsening to $\pm$50 % as the dye ages.

As the CMX-4 can provide an electrical trigger, one might wonder why an optical trigger is used. It is because of the jitter ($\pm$ 100 ns) between the electrical trigger and the appearance of the light pulse. The optical trigger was a photodiode which was reversed biased to reduce the junction capacitance and make it faster. The optical trigger had no jitter since the trigger pulse follows the light pulse itself.

3.3 (c) 'Neutral' Density Filters

The final thing to consider in this section on excitation of PC and PL is the transmission spectrum of the Fisch-Shurmann 'neutral' density filters since they are not really neutral. Figure 17 presents the spectrum for a filter whose nominal optical density is 0.3 measured using the method of section 2.3(d). Optical density (OD) is defined as follows, where I is the transmitted intensity and I_o is the incident intensity:

$$OD = \log_{10}(I_o/I) \qquad (39)$$

A table of values can be found in the laser manual in the laboratory.

3.3 (d) Circuit for PC Detection

In this and the next section we explore the characteristics of the detectors in order to establish whether the effects which are to be reported below are due to limitations in the instrumentation, or whether they are true physical effects.

The samples were electrically connected via evaporated indium contacts into the circuit of figure 18. A simplified version of this circuit - the voltage divider - appears in the inset. The ohmicity of the contacts in the low intensity regime was discussed in section 2.3. To establish whether the contacts were acting ohmically in the high intensity regime, the height of the PC transient was monitored as a function of V_o. It turned out that in the voltage range 0-30 V, the PC transient height was

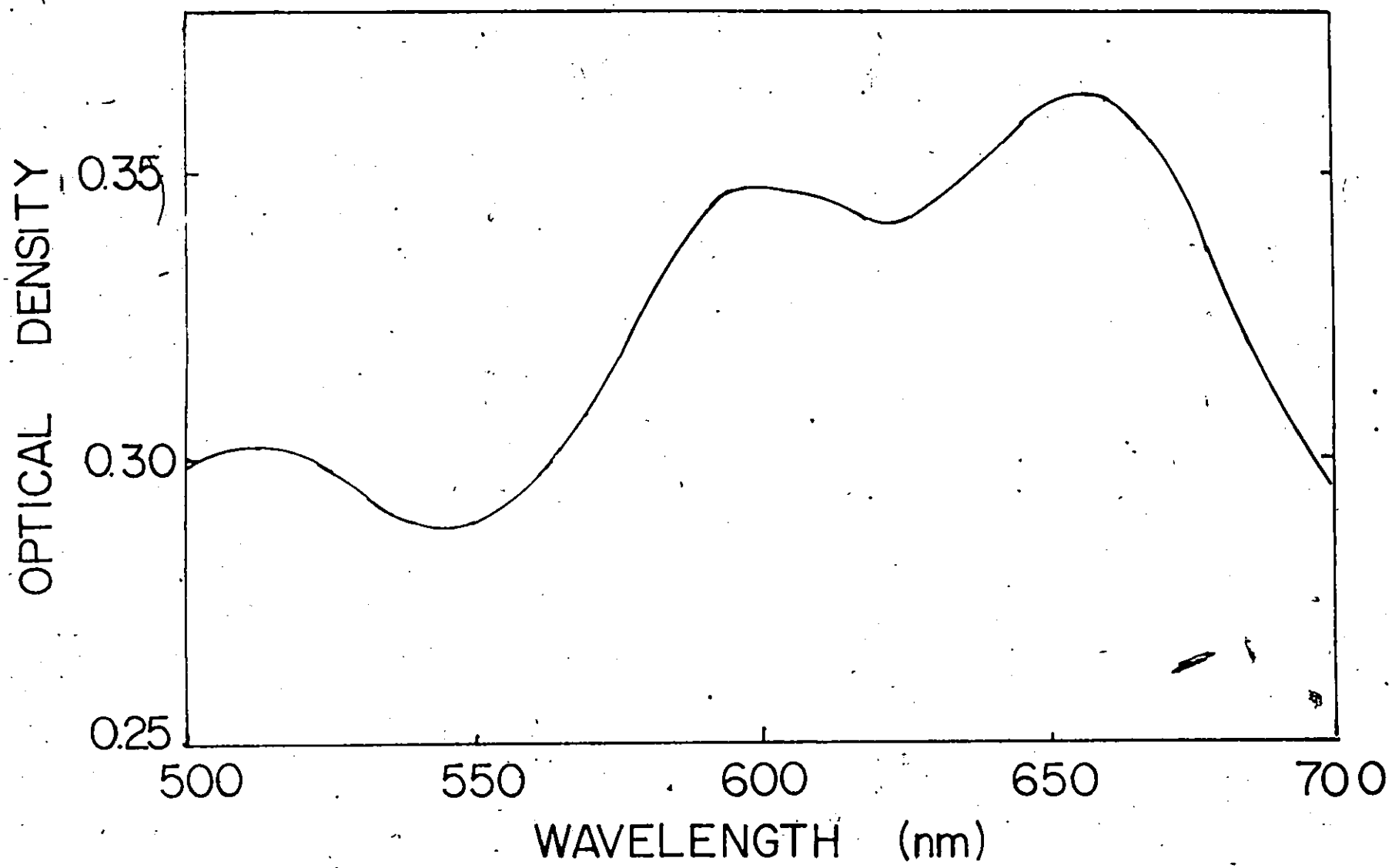

FIGURE 17
FISCH-SCHURMANN 'NEUTRAL' DENSITY FILTER CALIBRATION

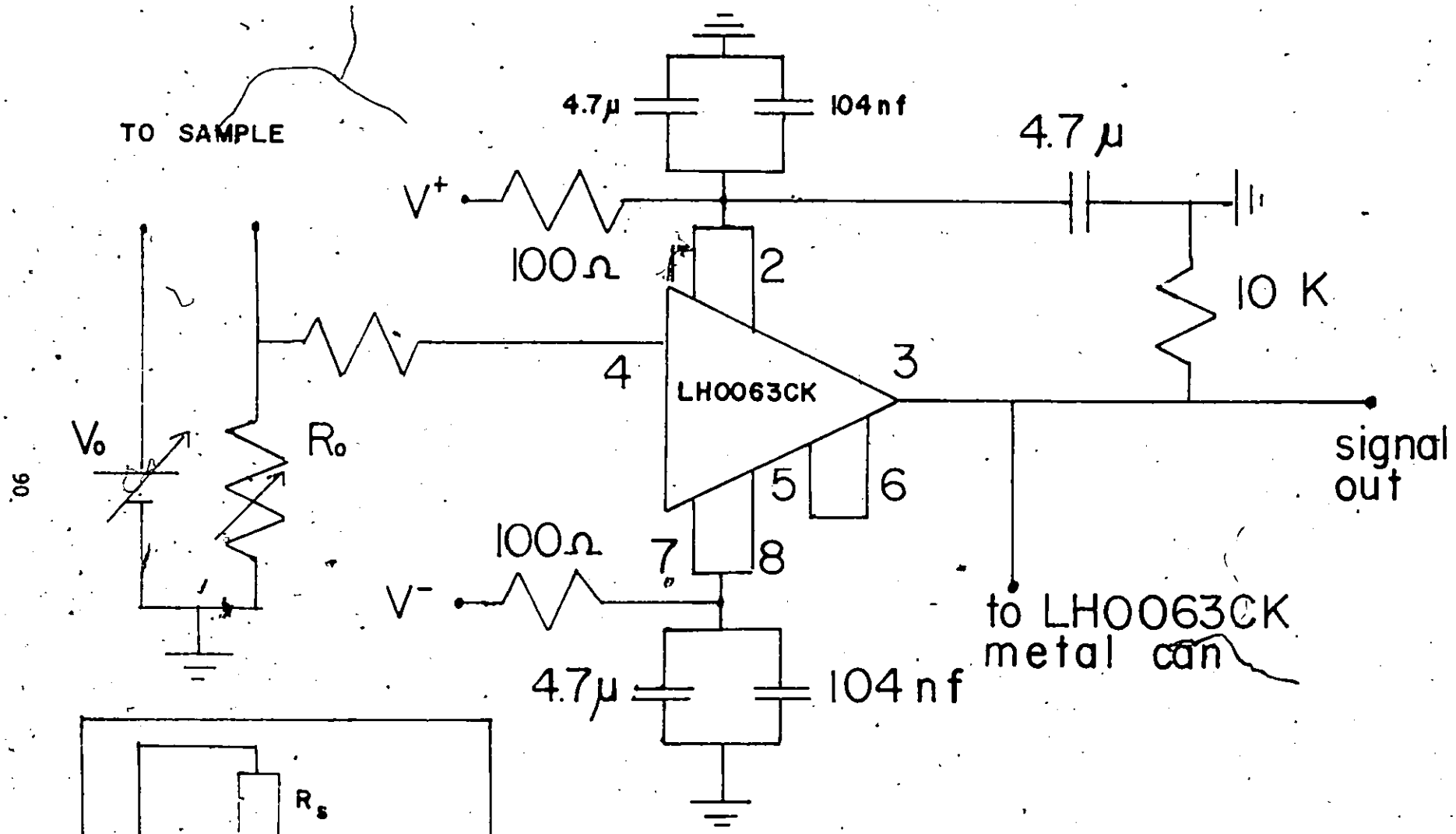

FIGURE 18
PC DETECTION CIRCUIT

Inset: Simplified Circuit

proportional to V_o.

The LH0063CK integrated circuit is the so-called 'Damn-Fast Buffer', which in this particular circuit is acting as an impedance transformer. Specifications indicate a slew rate of 2000V/sec, a 200 MHz bandwidth and a rise time of 1.2 nsec. All these indicate that the chip will easily follow PC transients of the order of μsec wide.

The other important thing to establish is whether the voltage transient is truly proportional to the change in conductivity of the sample. Appendix 1 presents the details of a circuit analysis whose fundamental results are that for proportionality between the voltage transient and conductivity,

$$R_o/R_s < .01 \qquad (40)$$

$$R_o/R_s < 0.01\, R_s'/R_s \qquad (41)$$

In the above equations, R_o is the resistance in series with the sample in the voltage divider circuit, R_s is the sample resistance between pulses, R_s' is the sample resistance at the peak of the PC transient. R_s was estimated by using the Keithley 602 electrometer in series with the sample and the power supply. This instrument could in no way keep up with the fast PC pulses, but gave a measure of the average PC. One could also estimate R_s' by determining the absolute value of the PC transient. In this way one could ensure that the above two conditions were met.

3.3(e) Hammamatsu R446 Photomultiplier

The photomultiplier (PM) used in the experiments was a

Hammamatsu model R446. This is a side-on model with a multialkali dynode material which can be used in the visible region extending up to perhaps 800 nm in wavelength. The manufacturers' specifications indicate a rise time of 2.2 ns (measured by exciting the PM with a pulsed light source whose rise was 70 ps). This is quite adequate for transients in the μsec range.

The other characteristic that one had to be aware of is at what peak current does the PM saturate under pulsed excitation. This was determined by exciting PM with green light from a strobe light with an approximately 2 μsec pulse width. The calibration curve appears in figure 19. One sees that the saturation current is about 10 mA which is consistent 10K resistors between the 10 dynodes and for 1100 V between the anode and the cathode.

3.3 (f) Tektronix 5A45 Amplifier

As the LeCroy 3500 has eight bit resolution and a maximum signal input of 512 mV amplication or de-amplification was necessary. At low intensities, the signals had to be made larger while at high excitation intensity, in some cases, the signal had to be made smaller.

The amplifier used was the Tektronix 5A45 which has a bandwidth which depends on the gain. For amplification of 12.5 or 25, the bandwidth was 25 MHz whereas for gain in the range 0.05 to 5, the bandwidth was 60 MHz. In any case, the bandwidth was enough to reproduce signals of the order of a μsec wide without distortion.

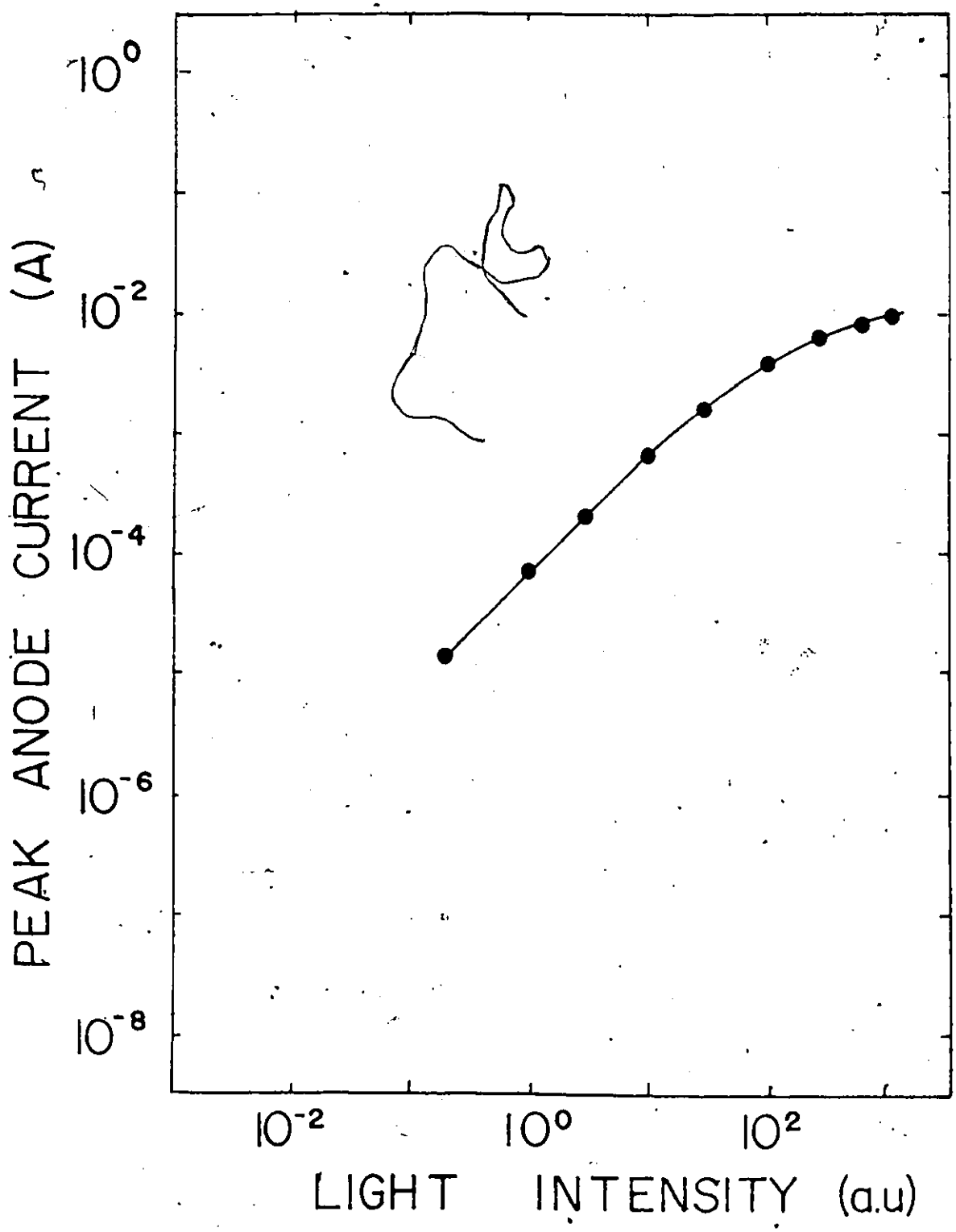

FIGURE 19
HAMMAMATSU R446 PHOTOMULTIPLIER LINEARITY TEST
Anode-Cathode Voltage: 1100V; 10K between each dynode

3.3 (g) LeCroy 3500 Transient Signal Averager

The LeCroy 3500 Transient Signal Averager is an instrument which can digitize an analog signal, store it and analyze it. It has a range of time resolutions, depending on the requirements of the signal. The time resolution is set by a parameter called the dwell time per sample, which is the inverse of the sampling frequency. For example a 20 ns dwell time means a digitizing rate of 50 MHz.

The transient recorders continuously digitize the input signal and store the results sequentially. When it comes to the end of the dedicated memory it goes back to the beginning of the of the memory and overwrites previously stored data. This process continues until the stop triggering signal is received. The stop trigger is the optical trigger mentioned above. The machine knows how many more samples to digitize after the stop trigger is reached based on the record length and the pretrigger. For example if there is a 2K record length and no pretrigger, the the transient recorder will digitize a further 2K samples to be stored and then will continue the digitizing cycle. If the record length is 4K with a 1K pretrigger, the transient recorder will digitize 3K samples after the stop trigger and store the 1K samples previous to and the 3K samples after the stop trigger as the 4K record. Hence the pretriggering mechanism is not a delay circuit as might have been thought.

As mentioned above, the LeCroy has 8 bit resolution with a 512 mV maximum input signal. This means that, for calibration purposes, each count per channel represents 2 mV. The magnitude

of a voltage transient (ΔV_m) is determined by multiplying the peak count (the number of counts in the channel with the maximum number of counts) by 2 mV and then dividing by the gain of the electronics before the input of the LeCroy times the number of scans. That is,

$$\Delta V_m = \left(\frac{\text{peak count}}{\text{\# of scans}}\right) \times \left(\frac{2\text{ mV}}{\text{Gain}}\right) \qquad (42)$$

The horizontal time scale is calibrated by multiplying the scan length times the dwell time.

A sample PC transient collected by the LeCroy 3500 is shown in figure 20. For the signal averaging, a dwell time of 40 ns was used. One hundred 1K scans (1024 channels) were made and hence the time scale from 0 to 40920 nsec. The gain of the Tektronix amplifiers was 25. Hence the peak of this PC transient was 4.35 mV.

3.3(h) Triggering

Before turning to a presentation and discussion of the measurements let us discuss the triggering mechanism of the LeCroy in relation to the optical trigger. There are two triggering options which can be selected by a jumper switch inside the TR8818 transient recorder unit, TTL logic and ECL logic. An acceptable stop trigger in the TTL mode must be the positive going edge of a 4V (minimum) voltage pulse which is at least 8ns wide. With Rhodamine 6G dye and Coumarin 102, the optical trigger satisfies these requirements. However, it will

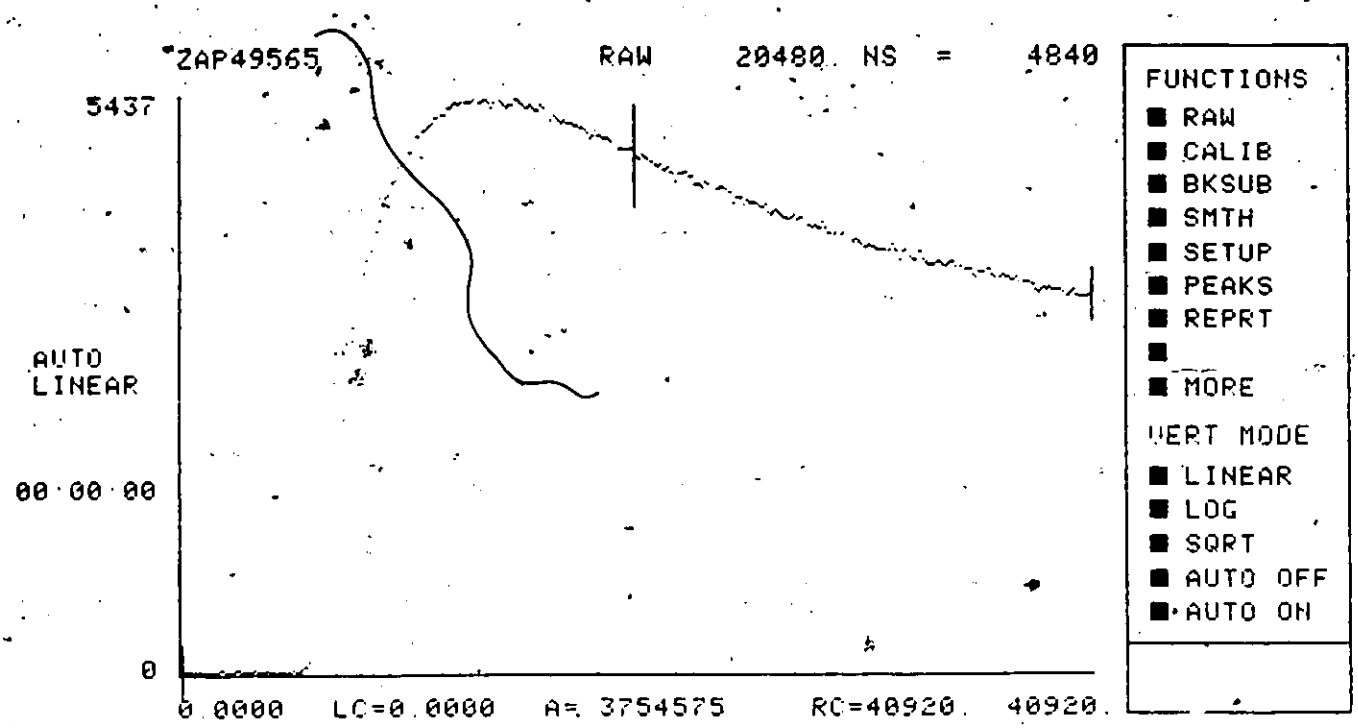

FIGURE 20

SAMPLE DATA COLLECTED BY LECROY 3500

be noticed that the optical trigger response - that is, signal size - markedly decreases towards the blue end of the visible spectrum. This is because the PV cell used is covered with a dielectric coating which becomes optically opaque towards the blue end of the optical spectrum. One will find that with Coumarin 2 dye, whose spectral maximum occurs at 450 nm , the signal produced is too small to be used as the trigger. In this case one has the option of using the model 6102 trigger generator which takes a small trigger signal and produces a uniform 5 V pulse 10 ns wide. However, when using this instrument one has to be very careful about matching impedances because cable reflections and noise can produce spurious trigger signals.

3.4 Results and Discussion

3.4(a) 300 K Results: type (a) PL characteristic / type(b)PC characteristic

Figure 21 presents the relation between the peak of the photosignal transients and exciting intensity at 300 K. One notices immediately that one can classify the photoluminescence relation as type (a) and the photoconductivity relation as type (b) in the scheme of figure 14. All four samples studied exhibited type (b) PC curves and type (a) PL curves at 300 K. Let the intensity where the slope changes in the PC curve be called the PC breakpoint intensity (PCBI). In all samples, the slope of the log(PC) versus log(I) curve for intensities lower than PCBI - (m_1) - is approximately equal to 1, which is a linear dependence of PC on intensity. On the other hand for intensities greater than PCBI the slope (m_2) greater than 1. With regard to the PL curves all four samples manifested an evolution from a superlinear dependence at low intensity - characterized by slope m_3 - to sublinear dependence at high intensity. Let the intensity where the slope of the secant joining two experimental points on the PL curve first becomes less than 1 be called the PL breakpoint intensity (PLBI).

In view of section 3.3(e), one had to ascertain whether the type (a) characteristic was due to a physical effect in $ZnIn_2S_4$, or whether it was due to saturation of the PM. The absolute height of the PL transient could be calibrated and it was

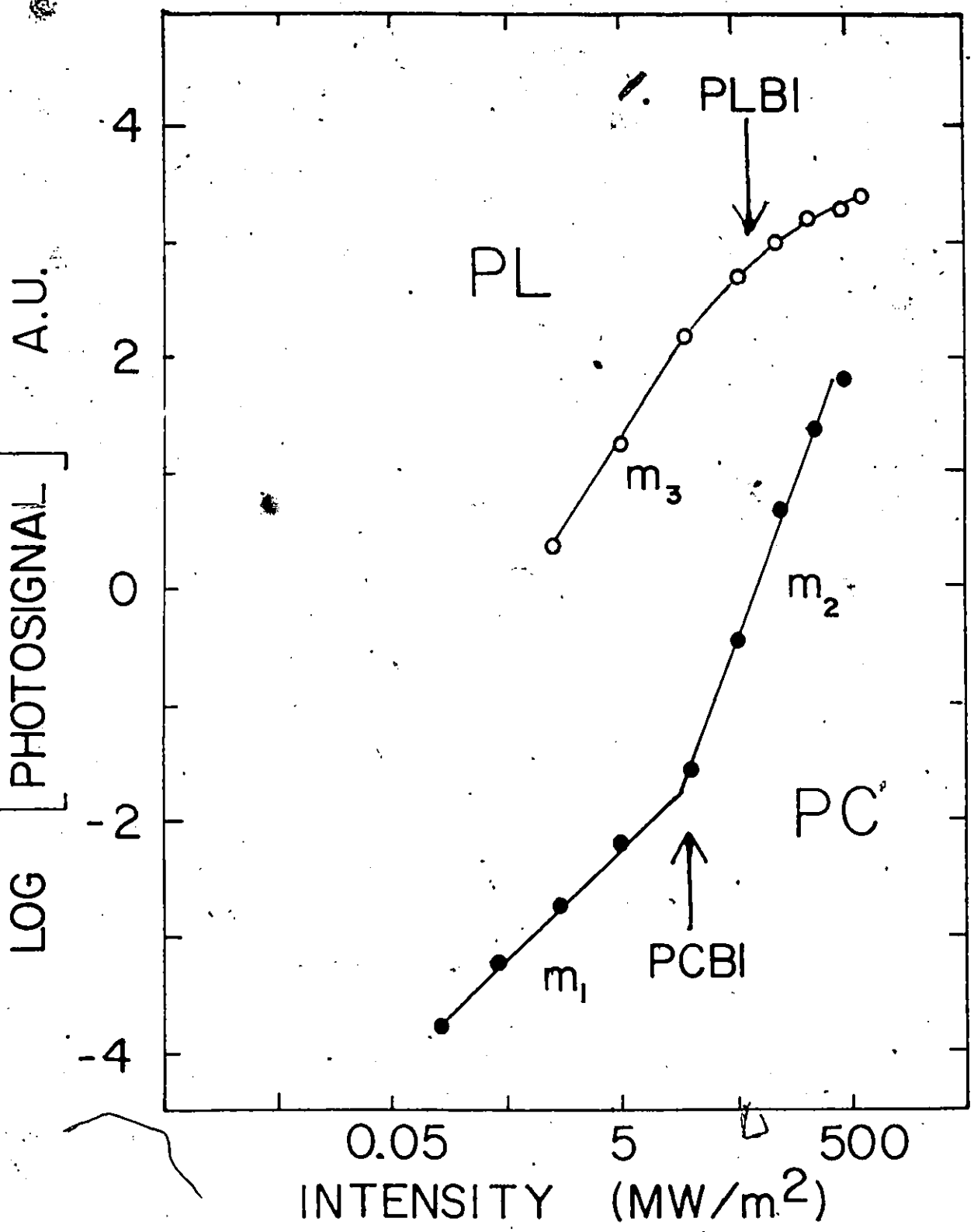

FIGURE 21
PHOTOLUMINESCENCE AND PHOTOCONDUCTIVITY TRANSIENT PEAK HEIGHT AS A FUNCTION OF EXCITATION INTENSITY

Temperature: 300K; PCBI: breakpoint intensity of PC vs. I curve; PLBI: breakpoint intensity of PL vs. I curve; m_1: slope of PC vs. I for I less than PCBI; m_2: slope of PC vs. I for I greater than PCBI; m_3: slope of PL vs. I for lowest Intensities

TABLE XI
INTERSAMPLE COMPARISON OF
PHOTOSIGNAL VS. INTENSITY RELATIONS
(300K)

Sample:	1	5	6	7
BC m_1:	1.08±.03	1.07±.06	1.06±.02	1.01±.03
PC m_2:	2.01±.08	2.7 ±0.3	1.9 ±0.3	1.88±.07
PL m_3:	1.31±.03	1.66±.04	1.4 ±0.1	1.22±.08
PCBI:	*8 MW/m^2	*8 MW/m^2	0.5 MW/m^2	0.15 MW/m^2
PLBI:	*100 MW/m^2	*60 MW/m^2	5 MW/m^2	80 MW/m^2

* ± a factor of 10 because the intensity was not carefully monitored during these experiments.

determined that the PL vs. I curves begin to flatten out for PM currents of the order of 0.1 mA which are easily in the linear response region of the PM as figure 19 shows. Hence it is certain that the type (a) PL characteristic is a physical effect.

Table XI summarizes the details of the slopes m_1, m_2 and m_3 as well as the approximate break point intensities (PCBI and PLBI).

3.4(b) Does Two Photon Absorption Occur?

Table X provides a basis with which to begin our interpretation of the type (b) PC characteristic. In it one sees that type (b) PC characteristics have been traditionally explained by the mechanism of two photon absorption. However it is easy to show that this cannot be the explanation for the type (b) PC versus I characteristic in $ZnIn_2S_4$. It was noted in section 3.2 that 'β' the coefficient for two photon absorption is of the order of 0.02 cm/MW in several semiconductors. Let us assume that 'β' has about the same value in $ZnIn_2S_4$. The product of 'β' and the PCBI, if two photon absorption is beginning to dominate at the PCBI, should be approaching the same order of magnitude as the one photon absorption coefficient, 'β'. However the product of 0.02 cm/MW and the largest PCBI is 1.6×10^{-5} cm^{-1} whereas the one photon absorption coefficient is approximately 120 cm^{-1}. (see section 2.3 (d)). Invoking the two photon aborption mechanism is patently invalid since any two photon effects would be totally masked by one photon absorption.

3.4 (c) The Saturation Hypothesis

Does Table X then offer any guidance in explaining the type (b) PC characteristic? It does after studying the shape of the PC transient as a function of intensity. PC transients for intensities both lesser than and greater than the PCBI are presented along with the laser pulse in figure 22. We see that the PC transient is longer for intensities greater than the PCBI than for intensities lesser than the PCBI. One can demonstrate semi-quantitatively that an effective free electron lifetime increase is seen indirectly in figure 22. The PC transients shown in figure 22 are actually governed by response times (τ_r) and not 'τ_{eff}'. Recall equation 24, the definition of 'τ_r'. One sees in equation 24 that, if $n_t >> n$, then 'τ_r' is proportional to the product of 'τ_{eff}' and n_t/n where n_t is the density of traps within kT of the quasi-fermi level and 'n' is the free electron density.

One can determine the ratio n_t/n as follows: for a given intensity to absolutely determines the peak PC and then the peak free electron density (n), using equation 32.Then one determines the peak quasi-fermi level using equation 7 and interpolates from figures 10 and 11 the trap density per unit energy at the peak quasi-fermi level. Repeating this procedure gives n_t/n as a function of intensity. It turns out that n_t/n actually decreases as a function of intensity. Hence, for the PC transient to increase in length, 'τ_{eff}' must increase as a function of intensity.

Because it is 'τ_r' and not 'τ_{eff}' which is seen in figure 22

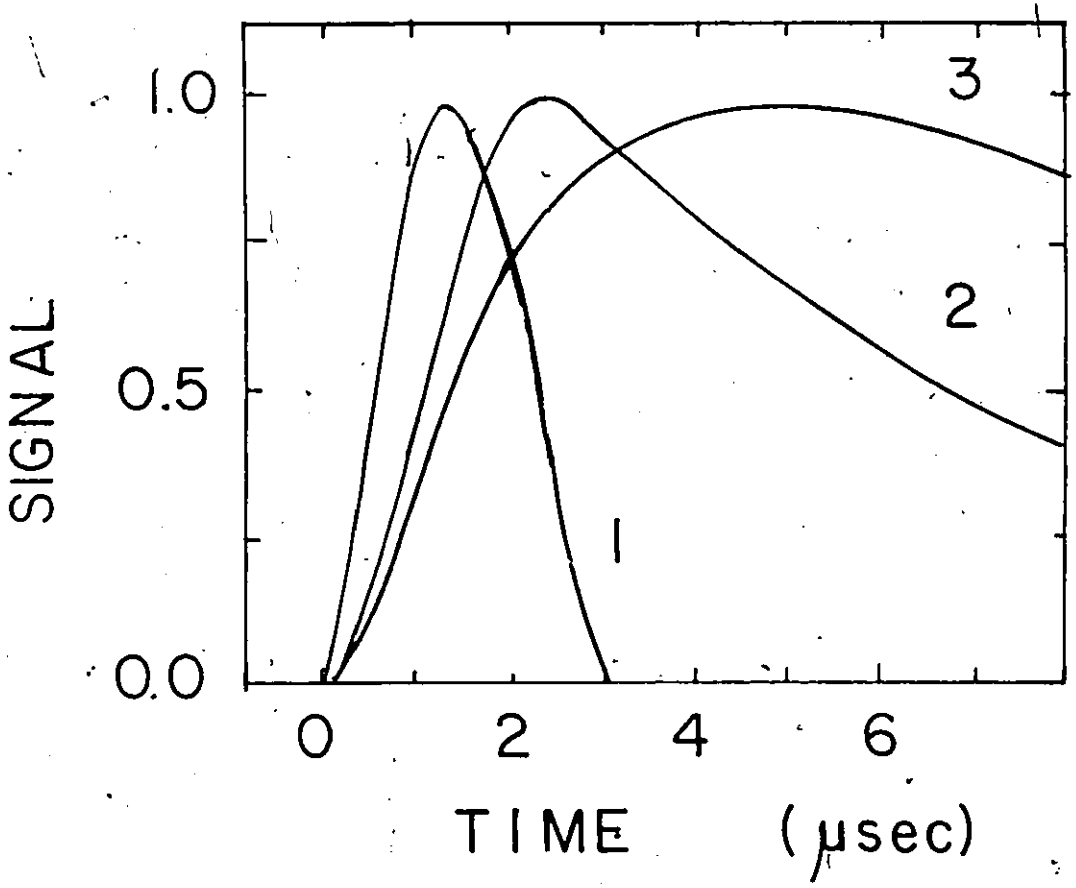

FIGURE 22
COMPARISON OF PC TRANSIENTS WITH THE LASER PULSE

1: laser pulse
2: PC transient for I less than PCBI
3: PC transient for I greater than PCBI

one can explain the fact that the increase in PC transient length seems too small to account for the dramatic break in the intensity dependence of PC shown in figure 21.

A correlation between the type (a) PC relation and 'τ_{eff}' has been found and now one must find the physical mechanism behind the 'τ_{eff}' increase. In table X one sees that a type (b) integrated PL versus intensity curve can be explained by a lifetime that increases with intensity. The time integrated PL is analagous to PC in that it increases when the decay lifetime is longer. In section 3.2 it was explained that the cause of the lifetime increase in the case of the type (b) PL characteristic is saturation of a trapping mechanism. A similar cause is conceivable for the type (b) PC characteristic in $ZnIn_2S_4$: Let one assume that the route whereby free electrons are trapped by the T levels (or perhaps the '600 meV' donor) and then subsequently make radiative transitions to the A levels is an important recombination route. If the T levels become saturated, that is filled with electrons then the effective free electron lifetime (τ_{eff}) can increase.

The type (a) PL characteristic shown in figure 21 is consistent with this saturation mechanism. In section 3.2 it was mentioned that a type (a) donor - acceptor PL characteristic has been seen in InSe[60] and can be explained by the fact that once the donors and acceptors become completely non-ionized the PL emission intensity can increase no further. The superlinearity of PL at low intensity - see table XI (slope m_3) - is not surprising since donor-acceptor pair luminescence intensity is

proportional to the product of the non-ionized donor and the non-ionized acceptor concentration. Since photoexcitation certainly produces a non-ionized acceptor and possibly a non-ionized donor there is an upper limit on the slope of the log PL vs. log I curve of 2. It is seen in table XI that the slopes of the log PL vs. log I curves at lower intensities - m_3 - lie in the range 1.22-1.66. That the exponents are less than 2 is merely a reflection of the fact that not every photoexcited electron will be captured by one of those particular donor-aceptor pairs which yield a photon energy of 1.7 eV (the observed emission energy) upon recombination; there is a whole band of emission energies. The intensity of donor-acceptor luminescence cannot, however, increase indefinitely. Once the donors and acceptors involved become completely non-ionized the emission intensity saturates which explains the slope decrease in the log PL vs. log I curve of figure 21.

Previous measurements of PL vs. pumping intensity in $ZnIn_2S_4$ showed a superlinear to linear evolution when exciting with 2.71 eV photons from a CW Ar^+ laser and monitoring luminescence at 1.5 eV. However, since the maximum excitation intensity was four orders of magnitude lower than in the present work saturation was not observed.

3.4(d) 84 K Results: Type (a) PL Characteristic/ Type (b) PC Characteristic/ Long PC Transient

Figure 23 presents the logarithm of the peak of the photosignal versus the logarithm of intensity at 84 K. The same basic behaviour is seen, a type (a) PL characteristic and a type (b) PC characteristic. Table XII summarizes the slope and break point data (same definitions for m_2, PLBI etc. as at 300K). A complete set of laser data is not available since samples 1 and 5 were ruined before PC vs. I could be measured at 84K and sample 7 was burned during the 300K photoluminescence experiment and hence data for the 84K PL vs. I experiment could not be trusted.

The same saturation interpretation can be used to explain the type (b) PC characteristic and the type (a) PL characteristic observed at 84K as was used for 300 K. There is however a great difference between the PC transients at liquid nitrogen temperature and the PC transient at room temperature. Figure 24 presents a typical PC transient at 84 K for high and low intensity. They are both much longer than the PC transients at 300K (see figure 22). On this time scale the laser pulse would be almost a delta function. Moreover, the PC transient appeared to become faster after the break point which seems to contradict the trap saturation/free electron lifetime increase explanation. What is happening at 84K is that although the 'τ_{eff}' increase is happening, the decrease with intensity of n_t/n completely masks it.

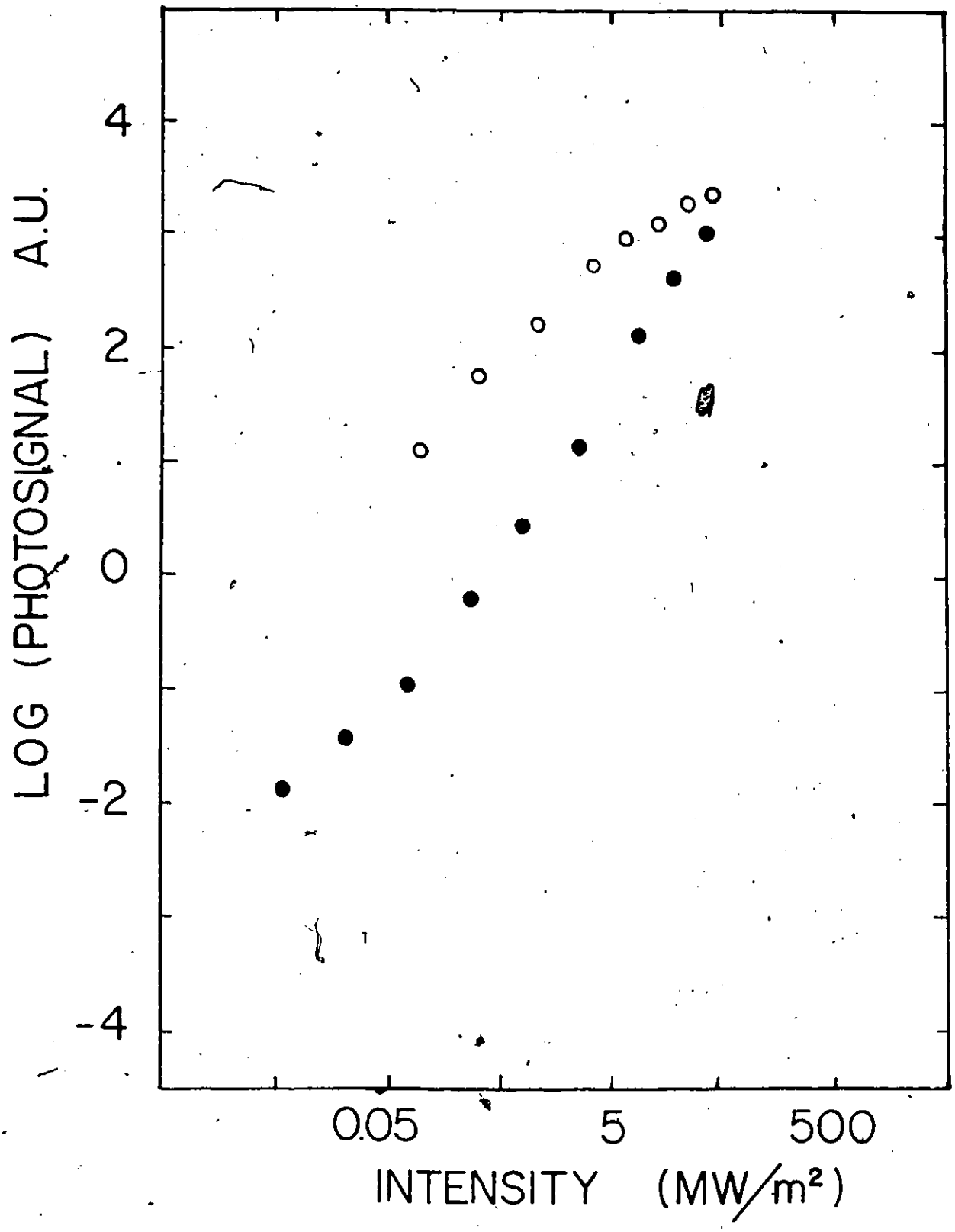

FIGURE 23
PHOTOLUMINESCENCE AND PHOTOCONDUCTIVITY TRANSIENT PEAK HEIGHT
AS FUNCTION OF INTENSITY AT 84K

TABLE XII
SUMMARY OF
PHOTOSIGNAL VERSUS INTENSITY RELATIONS
(84K)

sample:	1	5	6	7
PC m_1	-	-	$0.87 \pm .06$	1.0 ± 0.1
PC m_2	-	-	$1.87 \pm .14$	2.2 ± 0.1
PL m_3	$1.33 \pm .01$	$1.20 \pm .07$	1.3	-
PCBI	-	-	0.16 MW/m^2	0.5 MW/m^2
PLBI	12 MW/m^2	12 MW/m^2	5 MW/m^2	-

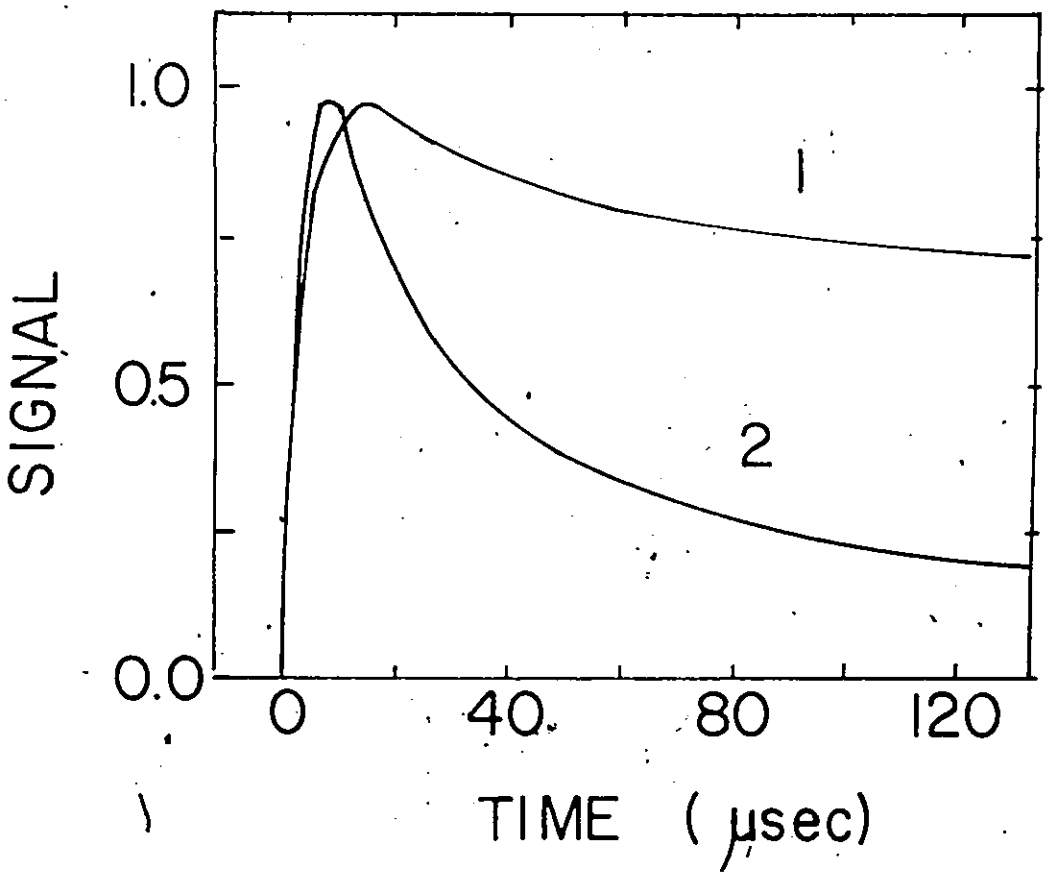

FIGURE 24
SAMPLE PC TRANSIENTS AT 84K

1: PC transient for 0.36 MW/m^2

2: PC transient for 90 MW/m^2

3.4(e) Efficiencies of Various Recombination Processes in $ZnIn_2S_4$

After the electrons have been excited into the conduction band, a number of possibilities arise. First they can stay in the conduction band and contribute to the photocurrent. Secondly they can be trapped by the 'T' levels. Thirdly, they can be captured by a donor and subsequently make a donor-acceptor radiative transition. Lastly they can make a non-radiative transition. One can summarize the situation at the end of the laser pulse in equation 43. Let $N_{h\nu}$ be the total density of electrons excited from the 'A' levels to the CB during the laser pulse. As usual, let 'n' be the density of photoexcited electrons that remain in the CB at the end of the laser pulse. Let n_t denote the density of electrons that are in the 'T' levels of figure 1 at the end of the laser pulse. Let N_{da} and N_{nr} be the number of electrons per unit volume that have made d-a transitions and non-radiative transitions, respectively, during the laser pulse. The non-radiative process is not associated with any center in figure 1. It is included since a non-radiative process has been postulated by other workers[5,17].

$$N_{h\nu} = n + n_t + N_{da} + N_{nr} \qquad (43)$$

Estimates of $N_{h\nu}$ were made by multiplying the photocreation rate (equation 29) by the laser pulse width (2 μsec) and using the nominal peak intensity (NPI defined in equation 38) for I_o. Estimates of 'n' were made by determining the peak PC and using equation 32.

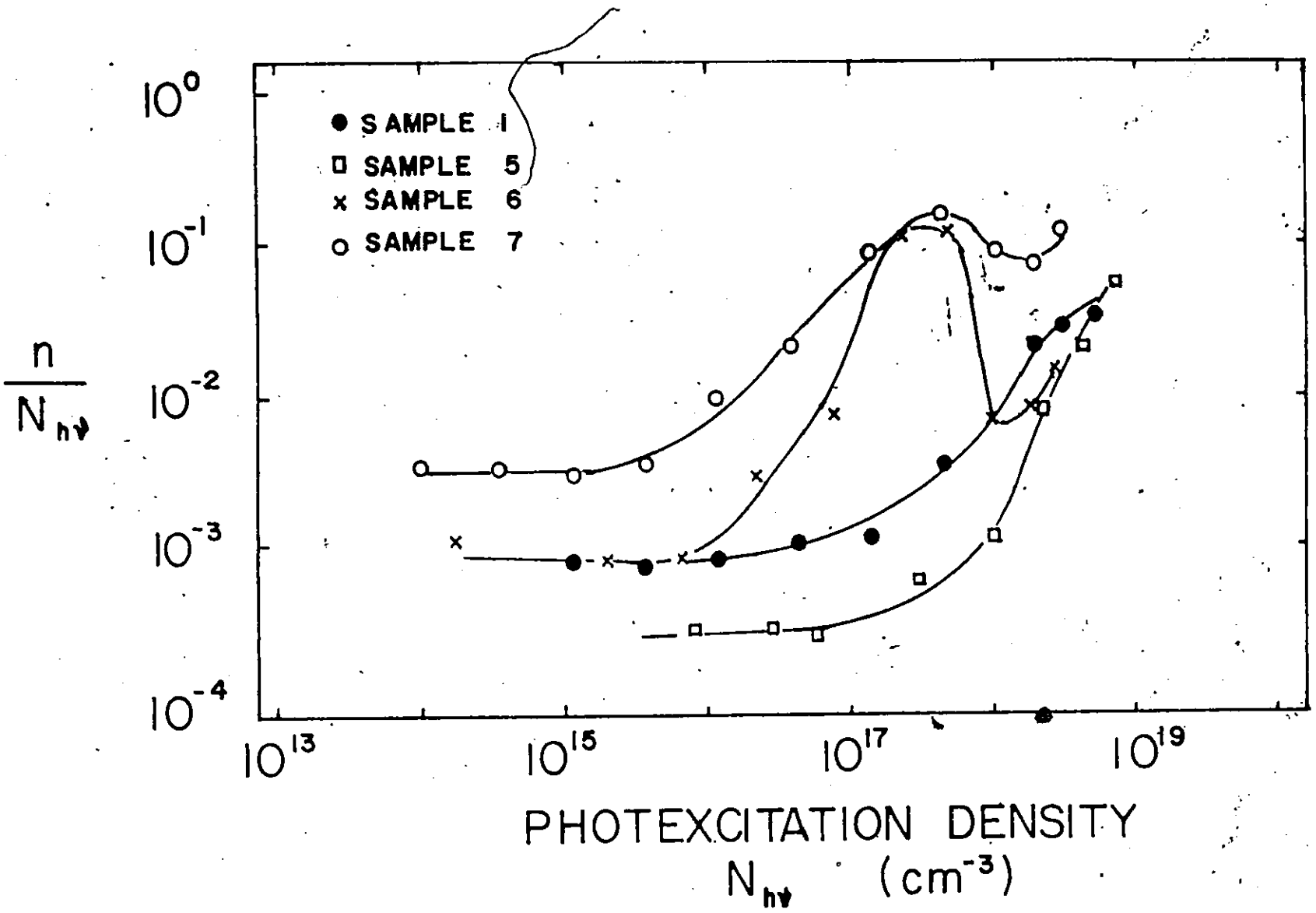

FIGURE 25
FRACTION OF PHOTOEXCITED ELECTRONS REMAINING IN CB
AT END OF LASER PULSE VERSUS PHOTOEXCITATION DENSITY (300K)

The ratio of 'n' to $N_{h\nu}$ is shown as a function of $N_{h\nu}$ at 300K in figure 25. Figure 25 is esentially another way of presenting the PC curve of figure 21. One sees in figure 25 that the fraction of photoexcited carriers that remain in the CB at the end of the laser pulse is approximately constant until $N_{h\nu}$ is between 10^{16} and 10^{17} cm^{-3} when the free electron lifetime begins to increase. Thus, the most important recombination process in $ZnIn_2S_4$ (which is probably d-a recombination as suggested by the correlation between the type(b) PC characteristic and the type (a) PL characteristic) becomes saturated for photoexcitation densities of the order of 10^{16} to 10^{17} cm^{-3}.

One also sees, for samples 6 and 7 that some sort of breakdown process is happening beginning at photoexcitation densities of approximately $10^{18} cm^{-3}$ since the ratio $(n/N_{h\nu})$ decreases there. It was noted that the photocurrent was very unstable (pulse to pulse variation of 100 per cent) at these excitation densities. This was also seen in sample 5 but the experiment was terminated before data collection. This instability is perhaps thermal in origin since, as has been noted, some of the samples were burned during the laser experiments.

Another interesting feature of the saturation phenomenon that begins for photoexcitation densities of around 10^{16} to 10^{17} cm^{-3} is shown in figure 26. In figure 26, the peak time which is defined as the time required for the PC transient to go from 0% to 100% of the peak PC value is plotted as a function of photoexcitation density. Figure 26 is remarkable in that the PC

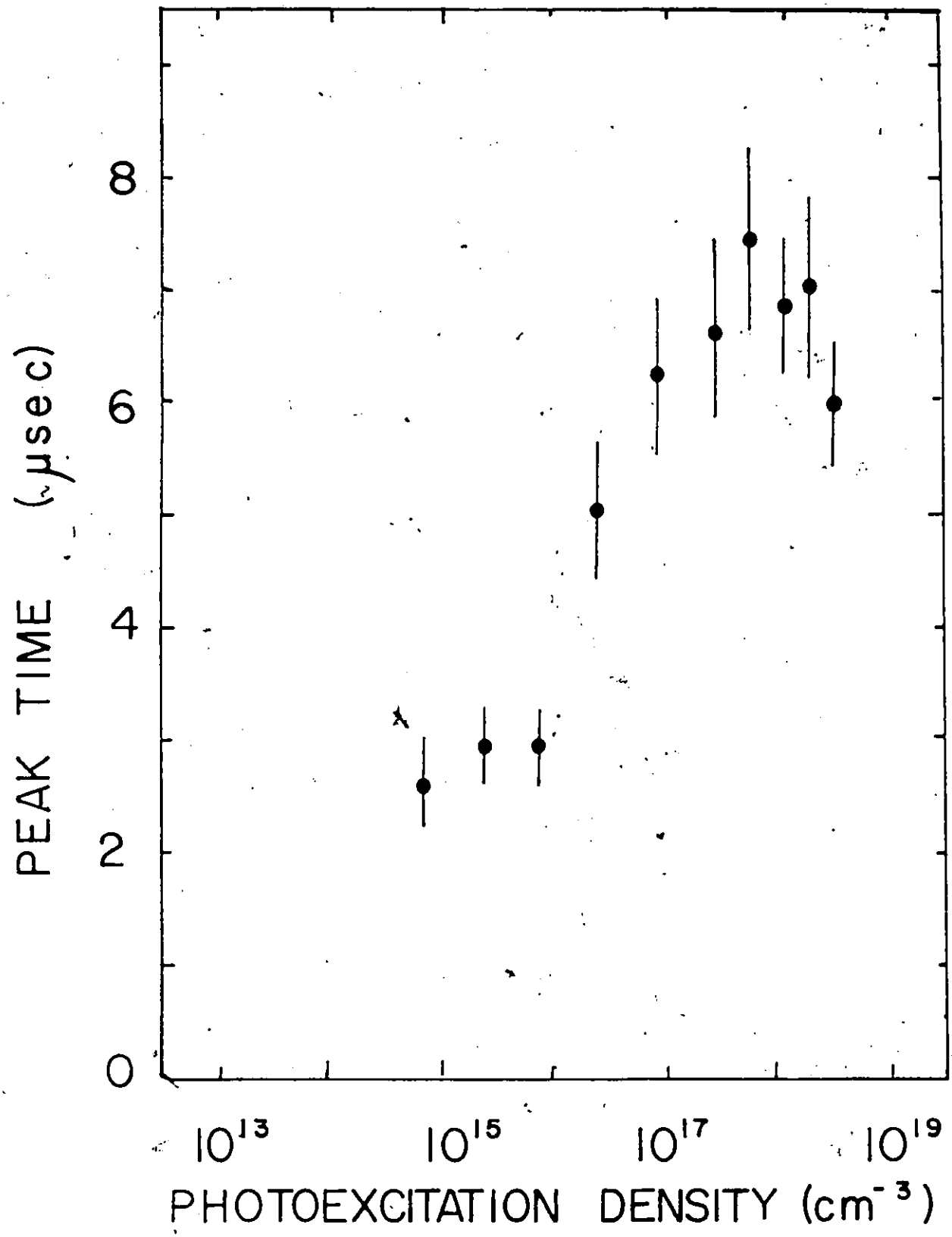

FIGURE 26
PEAK TIME VERSUS PHOTOEXCITATION DENSITY
(300K)

transient for photoexcitation densities greater than 10^{16} to 10^{17} cm^{-3}, the peak of the PC transient occurs after photoexcitation has ceased (the absolute laser pulse width - from 0% to 0% -. is 3.24 μsec). This means that detrapping is exceeding trapping. This could happen for at least two conceivable situations: first, if the traps are becoming completely filled then the probability of thermal excitation to the CB for the majority of trapped carriers could exceed the trapping probability; and second, figure 26 could be explained by a non-radiative Auger process.

Let us first consider the possibility that the probability of thermal excitation to the CB is exceeding the trapping probability. To a first approximation this should happen only when the traps are more than half filled. A comparison of the photoexcitation density when the lifetime increase begins (10^{16} to 10^{17} cm^{-3}) with the total trap densities listed in table VII (greater than 10^{18}cm-3) of section 2.4(b) shows that this is unlikely. The fact that 'τ_{eff}' increases (that is $n/N_{h\nu}$ increases before the traps are totally filled is consistent with the hypothesis that the d-a transitions are occuring between the '600 meV' donor and the 'A' levels of figure 1 if there are less '600 meV' levels than other levels close to the CB.

Let us now consider the possibility of non-radiative Auger recombination. A non-radiative Auger transition is a two body process whereby an electron is captured and the energy liberated is given to a second body[72]. The "Impurity Band Auger Effect"[54], which seems very likely in $ZnIn_2S_4$ because of the large 'T' level

density, could explain figure 26: If electrons are making non-radiative transitions to a deeper lying level and energy liberated excites an electron from the 'T' levels to the CB, detrapping could exceed trapping without the 'T' levels having to be more than half full.

Before turning to a summary and the end of the thesis, a few remarks should be made on the PL transients.

3.4(f) PL Transients

For a given sample and temperature, as the intensity increases, more donor acceptor decays happen during photoexcitation than after the laser pulse has finished. In other words, the ratio of the signal integrated between t=0 and t=3.74 μsec to the total time integrated signal increases with intensity. This has also been seen by Zhitar et al.[18] who noted that for times greater than 100 nsec after N_2 pulse excitation, the PL decays as t^{-n} where $0.5 < n < 1.2$ and where n increases with excitation intensity. The effect can be seen in figure 27.

It is due to the fact that as the photoexcitation density increases, the average d-a pair separation decreases (due to the increased density of non-ionized d-a pairs). Since an electron on a donor can make a transition to any nearby ionized acceptor and since the recombination probability increases with decreasing pair separation, the PL transient becomes faster. One should also note that the d-a band is more complex in $ZnIn_2S_4$ than in other compounds: a given pair separation cannot be correlated with a photon energy. Since E_d are spread in energy, various

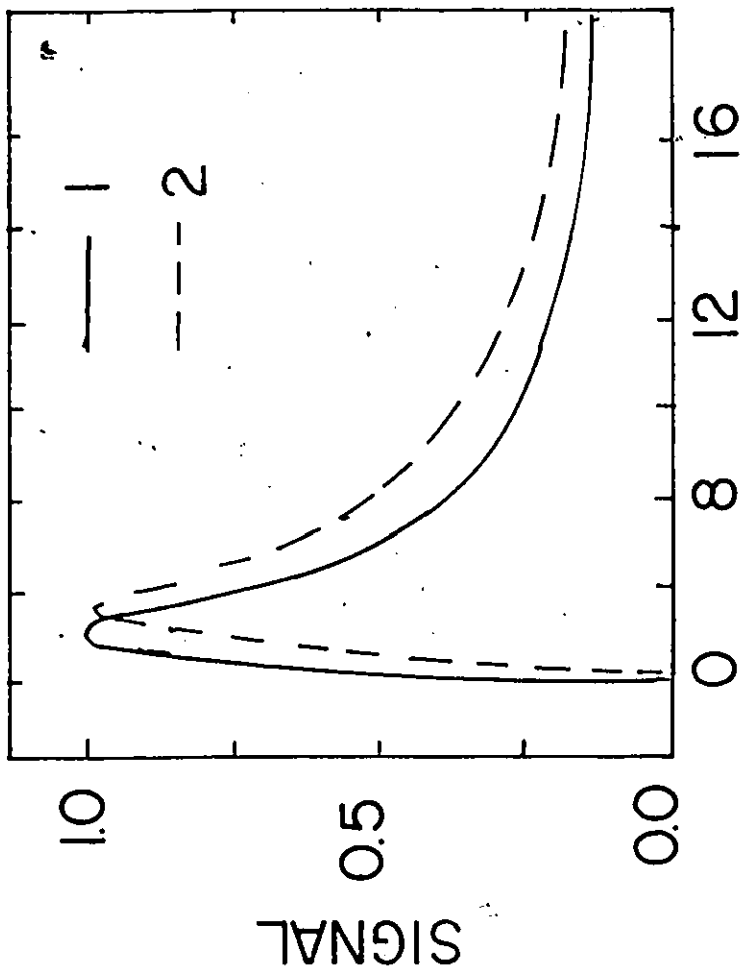

FIGURE 27
SAMPLE PL TRANSIENTS (84K)

1: Excitation Intensity= 500 MW/m^2

2: Excitation Intensity =0.5 MW/m^2

pair separations can give rise to the same photon energy (see equation 8).

We have now come to the end of our discussion of laser excited PC and PL in $ZnIn_2S_4$. Let us summarize the important facts that have been learned concerning the recombination kinetics in $ZnIn_2S_4$ and make some suggestions for further work.

CHAPTER 4 SUMMARY AND CONCLUSIONS

We set out to learn something about the influence of the 'A' and 'T' levels of figure 1 on the recombination kinetics of photoexcited electrons in $ZnIn_2S_4$ and a lot of interesting things have been learned along the way.

The first new discovery was the increase in trap density at about 600 meV below the CB (see section 2.4(b). It was assumed that the increase in trap density suggests a discrete donor which was called the '600 meV' donor. It was stressed in section 2.4(b) that the '600 mev' donor could help explain the discrepancy between the observed manximum of the PL emission band and the theoretical predictions of equation 8. Further work should be done to confirm the existence of the "600 meV" donor. The techniques of deep level transient spectroscopy (DLTS) or thermally stimulated current could be used.

Turning to the high intensity laser work, a number of important facts were uncovered. It appears that, at least in the four samples studied, donor-acceptor recombination is the dominant route by which electrons which have been excited from the 'A' levels of figure 1 to the conduction band can relax. The correlation between the saturation of donor-acceptor recombination and effective free electron lifetime increase is the major evidence for this hypothesis. The fact that the onset of the saturation of the d-a recombination mechanism occurs for photoexcitation density of 10^{16}-10^{17} cm^{-3} while the trap density

is greater than 10^{18} cm^{-3} also supports the idea that the d-a transitions occur between the '600 meV' donor and the 'A' levels rather than from the whole trap distribution and the 'A' levels.

Evidence for an impurity band Auger effect where the energy made available by non-radiative recombination excites electrons from the 'T' levels to the conduction band was also presented. More work could be done to try to assess the relative importance of this effect.

The fact that donor-acceptor recombination process is saturated suggests very interesting possibilities. Saturation is a necessary but not sufficient condition for population inversion between the A and the donor levels (which could be the '600 meV' trap). Stimulated emission was not observed in the PL vs. I characteristic. But a type (a) characteristic is not conclusive evidence that stimulated emission cannot occur. The geometry used was not optimal for the observation of stimulated emission.

Further work might be done to explore the possibility of lasing in $ZnIn_2S_4$. There are at least two techniques which can be used to demonstrate optical gain. Both involve looking at the luminescence using a different geometry than the one used in this work. The first technique[73] requires measuring the luminescence intensity resulting from exciting a rectangular section of a sample as a function of the length of the rectangular section. The exciting beam must be perpendicular to the rectangular section and the luminescence must be observed perpendicular to the exciting beam. If the emission intensity is an exponential

function[73] of the length of the rectangular section then stimulated emission is occuring and one can actually measure the optical gain.

The other technique involves the same beam geometry (that is, exciting beam perpendicular to sample and observation perpendicular to the exciting beam) and measuring the luminescence emission spectrum as a function of intensity of the exciting beam. If the spectrum begins to exhibit a spike at a certain wavelength, then stimulated emission is occuring[73].

The fact that the donor-acceptor luminescence in $ZnIn_2S_4$ occurs between donors that are spread in energy rather than from a highly localized donor makes the level structure look surprisingly like an organic dye. Conceivably, $ZnIn_2S_4$ and other ternary compounds may form solid state analogues of tunable organic dye lasers.

A tremendous amount of basic physics remains to be done to understand $ZnIn_2S_4$ before attempting to use it as the lasing medium in a tunable solid state laser.

APPENDIX - PC DETECTION CIRCUIT ANALYSIS

The following circuit analysis was performed in order to determine under what conditions the height of the voltage transient across the resistor in series with the sample (refer to the inset of figure 18) is proportional to the change in conductivity of the sample.

Define:

R_s = sample resistance between pulses

R_s' = sample resistance at the peak of the PC transient

$\Delta R_s = R_s - R_s'$

R_o = resistance is series with sample

V_o = power supply voltage

V_m = voltage across R_o

$\gamma = R_o/R_s$

$\beta = R_s'/R_s$

Since R_o and R_s for a voltage divider circuit give,

$$V_m = \frac{R_o}{R_o + R_s} V_o \qquad (A1)$$

When light is shone on the sample reducing R_s to R_s', the following voltage transient is measured:

$$V_m = R_o V_o \left[1/(R_0 + R_s') - 1/(R_o + R_s)\right] \qquad (A2)$$

Equation A2 can be rewritten as follows:

$$v_m = R_o V_o \ (R_s - R_s')/(R_0 + R_s')(R_o + R_s) \qquad (A3)$$

Using the definitions of 'γ' and 'β' listed above, equation A3 can be rewritten as:

$$\Delta V_m = \frac{R_o V_o}{R_s^2} \Delta R_s \, [1 + \gamma]^{-1} \, [\beta + \gamma]^{-1} \qquad (A5)$$

By definition (σ_s = sample conductivity, C = constant):

$$\sigma_s = \frac{C}{R_s} \qquad (A6)$$

An analysis (similar to the one for V_m above) gives:

$$\Delta\sigma_s = C \frac{\Delta R_s}{R_s R_s'} \qquad (A7)$$

Equation (A5) divided by (A7) gives:

$$\frac{\Delta V_m}{\Delta\sigma_s} = \frac{V_o R_o}{C} \frac{\Delta R_s}{R_s^2} [1+\gamma]^{-1} \, [\beta + \gamma]^{-1} \frac{R_s R_s'}{\Delta R_s} \qquad (A8)$$

which can be rewritten as follows:

$$\frac{\Delta V_m}{\Delta\sigma_s} = C' \, \beta(1+\gamma)^{-1} \, (\beta + \gamma)^{-1} \qquad (A9)$$

Let us now define $V_m/\sigma_s C'$ as equal to 'Z'. Figure A1 is a plot of 'Z' as a function of 'γ' for various values of 'β'. V_m is proportional to σ_s when 'Z' = 1. One can see that this is true when the following conditions are satisfied:

$$\gamma = \frac{R_o}{R_s} \leq 10^{-2} \qquad (A10)$$

$$\gamma = \frac{R_o}{R_s} \leq 10^{-2} \frac{R_s'}{R_s} = 10^{-2}\beta \qquad (A11)$$

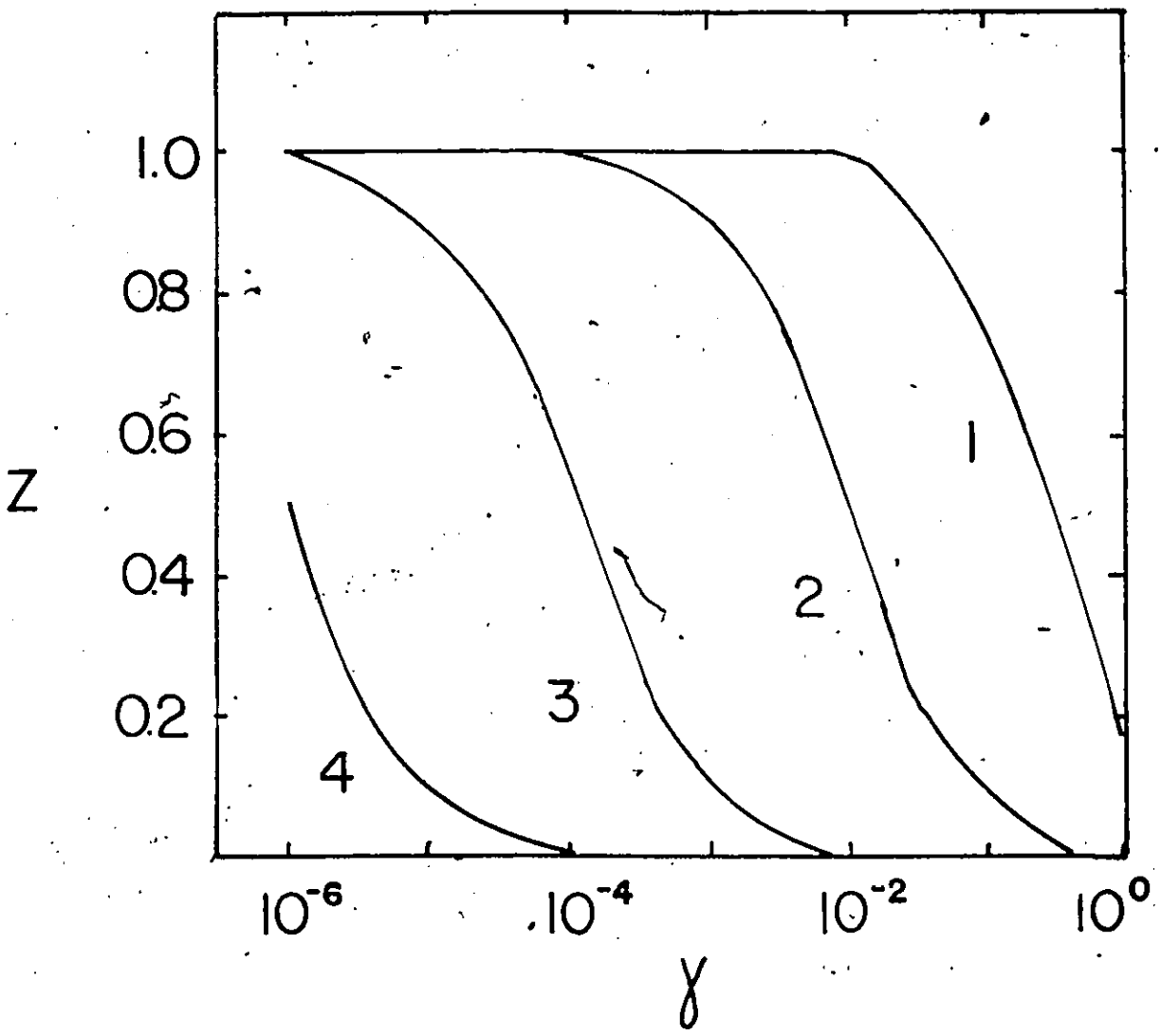

FIGURE A1

PC DETECTION CIRCUIT REQUIREMENTS

γ: R_o / R_s (R_o is resistance in series with sample; R_s is dark sample resistance)

β : R'_s / R_s (R'_s is sample resistance at peak of PC transient)

Z: when Z equals 1 the circuit is working properly

1: β equals 0.5; 2: β equals 10^{-2}; 3: β equals 10^{-4}; 4: β equals 10^{-6}

REFERENCES

1. H. Hahn, Z. Anorg. Chem., 263, 177 (1950).

2. J.A. Beun, R.Nitsche, Lichtensteiger, Physica, 26, 647 (1960).

3. S. Shionoya Y. Tamoto, J. Phys. Soc. Jpn., 19, 1142 (1964).

4. A. Cingolani, M. Ferrara, A. Minafra, F. Adduci, P. Tantalo, phys. stat. sol.(a), 23, 367 (1974).

5. A. Serpi, J. Phys. D., 9, 1881 (1976).

6. L. Hernandez, O. Vigil, F. Gonzales, phys.stat. sol.(a), 36, 33 (1976).

7. S. Mora, C. Paorici, N. Romeo, J. Appl. Phys., 42, 2061 (1971).

8. V.F. Zhitar', N.A. Moldovyan, S.I. Radautsan, Sov. Phys. Sem., 13, 495 (1979).

9. V.F. Zhitar', N.A. Moldovyan, S.I. Radautsan, Sov. Phys. Sem., 14, 353 (1980).

10. V.F. Zhitar', N.A. Moldovyan, S.I. Radautsan, Sov. Phys. Sem., 13, 1100 (1979).

11. A. Anagnostopolous, J. Spyredelis, phys. stat. sol.(a), 66, K127 (1981).

12. A. Anagnostopolous, C. Manolikas, D. Papadopolous, J. Spyredelis, phys. Stat. Sol.(a), 72, 731 (1981).

13. A. Anagnostopolous, C. Manolikas, D. Papadopolous, J. Spyredelis, phys. Stat. Sol.(a), 77, 595 (1983).

14. A. Anagnostopolous, B. Ploss, phys. stat. sol.(a), 73, 591 (1982).

15. A. Anagnostopolous, Ch. Lioutas, phys. stat. sol.(a), 79, 513 (1982).

16. M. Guzzi, G. Baldini, J. of Lum., 9, 514 (1975).

17. E. Grilli, M. Guzzi, phys. stat. sol.(a), 40, 69 (1977).

18. V.F. Zhitar', V.Ya. Ravvlan, S.T. Radautsan, Nuovo Cim. 2D, 6, 1919 (1983).

19. A. Bossachi, B. Bosachi, S. Franchi, L. Hernandez, Sol. St. Comm, 13, 1805 (1973).

20. M. Guzzi, E. Grilli, Mat. Chem. and Phys., 11, 295 (1984).

21. A. Rose, Concepts in Photoconductivity and Allied Problems, (New York: Wiley Interscience, 1964).

22. P.J. Dean, Prog. Sol. St. Chem., 8, 1 (1973).

23. E. Grilli, M. Guzzi, Nuovo Cimento 2D, 1927 (1983).

24. D.G. Thomas, J.J. Hopfield, W.M. Augustyniak, Phys. Rev. 140, A202 (1963).

25. J.J. Hopfield, D.G. Thomas, M. Gerzhenzon, Phys. Rev. Lett., 10, 162 (1963).

26. F. Lappe, A. Niggli, R. Nitsche, J.G. White, Z. fur. Kristall., 117, 146 (1962).

27. D.L. Greenaway and G. Harbeke, Optical Properties and Band Structure of Semiconductors (Oxford: Pergammon Press, 1968).

28. S. Shionoya, A. Ebina, J. Phys. Soc. Jpn., 19, 1150 (1964).

29. U. Giorgianni, V. Grasso, G. Mondio, G. Saitta, Phys. Lett., 68A, 247 (1978).

30. A. Anedda, L. Cugusi, E. Grilli, M. Guzzi, F. Raga, A. Spiga, Sol. St. Comm. 29, 829 (1979).

31. A. Anagnostopolous, K. Kambas, B. Ploss, phys. stat. sol.(b), 123, K155 (1984).

32. S. Logothetidis, S. Ves, J. Spyredelis, phys. stat. sol.(b), 122, 613 (1984).

33. R. Nitsche, W.J. Merz, Helv. Phys. Acta, 35, 274 (1962).

34. N. Romeo, O. Vigil, phys. stat. sol.(a),10, 447 (1962).

35. E. Gombia, N. Romeo, G. Sbverveglieri, C. Paorici, phys. stat. sol.(a), 34, 651 (1976).

36. S.I. Radautsan, V.F. Zhitar', V. Ya. Ravlyan, Sov. Phys. Sem. 9, 1476 (1976).

37. L. Baldasarre, V. Capozzi, G. Maggipinto, A. Minafra, phys. stat. sol.(a), 46, 589 (1978).

38. A. Anagnostopolous, A. Karoutis, phys. stat. sol.(a), 71, 543 (1982).

39. E. Zachs, A. Halperin, Phys. Rev. B. 6, 3072 (1972).

40. H.B. DeVore, Phys. Rev., 102, 86 (1956).

41. A. Rose, RCA Review, XII, 362 (1951).

42. E. Bhattacharya, K.L. Narasimhan, Phys. Rev B., 28, 2287 (1983).

43. H.A. Klasens, J.Phys.Chem.Solids, 7, 175 (1958).

44. R.H. Bube, G.A. Dussel, C.T. Ho, L.D. Miller, J.Appl.Phys., 37, 21 (1966).

45. R.A. Smith, Semiconductors, 2nd Ed., (Cambridge: Cambridge University Press, 1978).

46. R. Fivaz, E. Mooser, Phys. Rev., 163, 743 (1967).

47. C. Kittel, Introduction to Solid State Physics, 5th Ed., (New York: John Wiley and Sons, 1976).

48. J. Topping, Errors of Observation and their Treatment, 4th Ed.(London: Chapman and Hall, 1972).

49. A. Anedda, L.Garbato, F. Raga, A. Serpi, phys. stat. sol.(a), 50, 643 (1978).

50. N.N. Greenwood, Ionic Crystals, Lattice Defects and Non-Stoichiometry (London: Buttersworth, 1968).

51. W. Kohn, "Shallow Impurity States in Silicon and Germanium", in Solid State Physics, (eds. F. Seitz and D. Turnbull), 5, 258 (1957).

52. E. Fortin, A. Roth, S. Charbonneau, S. Meikle, J. Appl. Phys.,56, 1141 (1984).

53. M. Jaros, Deep Levels in Semiconductors (Bristol: Adam Hilger,1982).

54. P.T. Landsberg, phys. stat. sol. 41, 457 (1970).

55. F. Cardon, R.H. Bube, J. Appl. Phys. 35, 3344 (1964).

56. A. Rose, Phys. Rev., 97, 322 (1955).

57. K.L. Shaklee, R.F. Laheny, Appl. Phys. Lett., 18, 475 (1971).

58. R. Levy, J.B. Grun, J. of Lum., 5, 406 (1972).

59. S.S. Jayaraman, C.H. Lee, Appl. Phys. Lett. 20, 18 (1972).

60. R.H. Bube, C.T. Ho, J. Appl. Phys. 37, 4132 (1966).

61. G.K. Celler, S. Mishra, Ralph Bray, Appl. Phys. Lett., 27, 297 (1975).

62. G.A. Abdullaev, G.L. Belen'kii, S.M. Ryvkin, V.H. Salmonov, Yu. A. Sharanov, I.D. Yarosetskii, Sov. Phys. Sem. 5, 328 (1971).

63. J.E. Fouquet, A.E. Siegmann, R.D. Burnham, T.tl. Paoli, Appl. Phys. Lett. 46, 374 (1985).

64. Guy Bernier, Serge Jandl, Private Communication, Poster Session CAP Conference, 1985.

65. S. Charbonneau, E. Fortin, A. Anedda, Phys. Rev. B31, 2326 (1985).

66. C.C. Lee and H.Y. Fan, Appl. Phys. Lett. 20, 18 (1972).

67. I.A. Damaskin, S.L. Pyshkin. S.I. Radautsan, V.E. Tazlavan, Opto-Electronics, 5, 405 (1973).

68. G.B. Abdullaev. M. Kh. Alieva. B.R. Mirzoev, S.M. Ryvkin, V.H. Salmonov, I.D. Yaroshetskii, Sov. Phys. Sem., 4, 1187 (1971).

69. A.F. Gibson, C.B. Hatch, P.N.D. Maggs, D.R. Tilley, A.C. Walker, J.Phys. C, 9, 3259 (1976).

70. J.H. Yee, Phys. Rev. 186, 778 (1969).

CONTINUED

71. Orazio Svelto, Principles of Lasers, (New York: Plenum Press, 1976).

72. See reference 54 and references quoted therein.

73. K.L. Shaklee, R.E., Nahory, R.F. Leheny, J. of Lum. 7, 284 (1973).